

**Functional connectivity of layer II/III and V GABAergic Martinotti
cells in the primary somatosensory (barrel) cortex of mice**

Dissertation
for the award of the degree

“Doctor rerum naturalium”

Faculty of Biology
of the Georg-August-Universität Göttingen

within the doctoral program *Sensory and Motor Neuroscience*
of the Georg-August University School of Science (GAUSS)

submitted by

Florian Walker

from Papenburg, Germany

Göttingen 2015

Thesis Committee

Prof. Jochen Staiger, Institute of Neuroanatomy, University Medical Center
Göttingen

Prof. Swen Hülsmann, Experimental Neuroanesthesiology, University Medical
Center Göttingen

Prof. Tobias Moser, Department of Otolaryngology, University Medical Center
Göttingen

Members of the Examination Board

Referee: Prof. Jochen Staiger, Institute of Neuroanatomy, University Medical
Center Göttingen

2nd Referee: Prof. Swen Hülsmann, Experimental Neuroanesthesiology,
University Medical Center Göttingen

Further members of the Examination Board

Prof. Tobias Moser, Department of Otolaryngology, University Medical Center
Göttingen

Prof. Thomas Dresbach, Department of Anatomy and Embryology, University
Medical Center Göttingen

Camin Dean, Ph.D., Research group "Trans-synaptic Signaling", European
Neuroscience Institute Göttingen

Dr. Manuela Schmidt, Somatosensory Signaling and Systems Biology Group,
Max-Planck-Institute for Experimental Medicine

Date of oral examination: February 10th, 2016

I hereby declare that this doctoral thesis entitled “Functional connectivity of layer II/III and V GABAergic Martinotti cells in the primary somatosensory (barrel) cortex of mice” has been written independently with no other sources and aids than those quoted.

Florian Walker

December 21st, 2015

Göttingen, Germany

Table of contents

1 Summary	1
2 Introduction	3
2.1 The whisker-to-barrel pathway in rodents	4
2.2 The columnar structure of the rodent barrel cortex	7
2.3 Cortical inhibitory interneurons of rodents.....	10
2.3.1 PV-expressing interneurons	12
2.3.2 5HT3aR-expressing interneurons.....	15
2.3.3 SST-expressing interneurons.....	17
2.4 Martinotti cells.....	18
2.5 Outline of this thesis.....	22
3 Material & Methods	24
3.1 Animals.....	24
3.2 Slice preparation and solutions.....	25
3.3 Electrophysiology and data acquisition.....	27
3.4 Calibration of focal photolysis of caged compounds	30
3.5 Activation of presynaptic cells by focal photolysis of caged glutamate	35
3.6 Paired recordings.....	37
3.7 Histology	38
3.7.1 ABC-DAB and cytochrome oxidase staining	39
3.7.2 Immunohistochemical staining	40
3.8 Statistics	41
4 Results	42
4.1 L II/III and V GIN-cells show typical characteristics of Martinotti cells.....	42

4.2 Calibration of experimental set-up for focal photolysis of caged glutamate	48
4.3 Localisation of inhibitory cells presynaptic to L II/III and V Martinotti cells.....	54
4.4 Paired recordings of presynaptic INs and L II/III and V Martinotti cells.....	59
4.4.1 PV- and VIP-cells project onto L II/III Martinotti-cells.....	60
4.4.2 Identified unitary connections of PV- versus VIP-cells onto L II/III MCs differ in elementary synaptic properties and short-term plasticity	64
4.5 Paired recordings of presynaptic INs and L V Martinotti cells	69
4.5.1 Innervation of L V MCs by PV-cells	69
4.5.2 Innervation of L V MCs by VIP-cells	74
5 Discussion	78
5.1 Technical consideration of glutamate uncaging	80
5.2 Unique innervation of MCs by PV- and VIP-cells in S1	81
5.3 Differences in axonal targeting and/or synaptic architecture can explain differential elementary synaptic properties	83
5.4 Differential effect of short-term plasticity on MC activity.....	87
5.5 Disinhibition of cortical PCs depends on excitatory drive of VIP- and PV-cells.....	90
5.6 Functional aspects of reciprocal PV to MC connections in L II/III of S1.....	91
6 Outlook.....	93
7 Figures & Tables	95
8 Abbreviations	97
9 References.....	99
10 Curriculum Vitae.....	117
11 Publications related to this thesis	122

12 Acknowledgments.....	123
--------------------------------	------------

1 Summary

Although they represent only a small portion of cortical neurons, inhibitory interneurons take a major role in controlling the activity of cortical excitatory cells and, hence, cortical processing. The interaction of cortical inhibitory neurons, especially in the form of disinhibitory circuits, is the recent subject of scientific investigations. Disinhibition of cortical excitatory cells, for example, gates information flow through cortical columns. One of the key players in inhibiting excitatory neurons are Martinotti cells (MC). This specific cell type is known to receive inhibitory input and thus could be a main relay cell for disinhibitory connections affecting cortical pyramidal cells.

By means of glutamate uncaging we found that MCs in layer II/III of the primary somatosensory cortex receive inhibitory input from local sources, whereas layer V MCs receive local as well as interlaminar inhibitory input. Paired recordings revealed that the local inhibitory input of MCs in layer II/III and V is provided by parvalbumin-expressing (PV-) and vasoactive intestinal polypeptide expressing (VIP-) cells. Furthermore, layer V MCs receive interlaminar inhibitory input from layer II/III. PV-cells caused stronger synaptic input in layer II/III MCs as compared to VIP-cells. Additionally, these two unitary connections showed significant differences in elementary synaptic properties. Moreover, PV-cell input showed frequency-independent depression whereas VIP-cell input facilitated at high frequencies. This local connectivity scheme is also present in layer V of the primary

somatosensory cortex. There, PV-cells cause inhibitory input onto MCs with a similar strength and short-term synaptic plasticity. Although the local VIP to MC connection seems to be present as well in L V, further experiments are necessary to firmly establish this connectivity in terms of probability and effect. Furthermore, VIP-cells in layer II/III are likely the source of interlaminar inhibitory input of layer V MCs. In conclusion, the observed differences in the properties of the two unitary connections enable disinhibition of pyramidal cells (PC) with opposed spatial and temporal features. Viewed spatially, PV-cells might control spiking output of MCs, whereas VIP-cells might be able to control excitatory inputs to MCs. Furthermore, PV-cells may induce a transient release from MC inhibition, whereas VIP-cells may result in tonic disinhibition of PCs via MCs.

2 Introduction

To interact with the physical world biological organisms developed a variety of sensory systems to detect, process and respond adequately to changes in their environment. Specific functional systems evolved to process different sensory cues, e.g. auditory, visual, or somatosensory (touch) information.

In vertebrate sensory systems specific sensory input is perceived by specialized sensory receptors, e.g. eyes, ears and vibrissae, and transmitted to the central nervous system. There, this information is processed in subcortical and cortical brain areas dedicated to these specific inputs and merged with information from other sensory areas. Ultimately, certain motor output is generated causing a reaction to the sensory information perceived. Sensory information is often represented in a topographic manner in the neural pathway up to the six-layered cortex (Killackey et al., 1995; Kaas, 1997), which consist of the supragranular layers I to III, the granular layer IV and the infragranular layers V and VI (Brodmann, 1909). This means that information from neighboring sensory fields is also represented in neighboring cortical areas. A typical example of topographic organization is the primary somatosensory cortex (S1) which has been intensively investigated in rodents (Fox, 2008). Within this part of the rodent cortex information of the large facial whiskers is processed in an area related to as barrel cortex, named according to the barrel-like anatomical structures in layer (L) IV (Figure 2.1a, b) (Woolsey and Van

der Loos, 1970; Cooper and Steindler, 1986; Koralek et al., 1990; Agmon and Connors, 1991; Bennett-Clarke et al., 1993; Schlaggar et al., 1993; Boylan et al., 2000). In the barrel cortex thalamic fibers, conveying tactile information from the main facial whiskers, mainly project to L IV cells, where they are involved in forming the above mentioned barrel-like structures, which closely represent the organization of the facial whiskers (Figure 2.1a, b) (Woolsey and Van der Loos, 1970; Welker and Woolsey, 1974; Woolsey et al., 1975; Killackey and Belford, 1979).

2.1 The whisker-to-barrel pathway in rodents

A large part of the cortex in rodents, like mice and rats, is dedicated to process somatosensory information, especially of the facial whiskers, or vibrissae, which have been specialized to function as touch receptors. With these whiskers rodents are able to explore their surrounding and for example discriminate the texture of objects (Prigg et al., 2002). The vibrissae are located on the snout of the animal and organized in several rows (A-E) and arcs (1-7) (Figure 2.1a). Their deflection is detected by mechanoreceptors located in the follicle of each individual whisker (Rice et al., 1993; Ebara et al., 2002).

This tactile information is transferred via the infraorbital nerve to the principal trigeminal nuclei in the brainstem (Figure 2.1a), called the principal (principalis), interpolar (interpolaris), caudal (caudalis) and oral

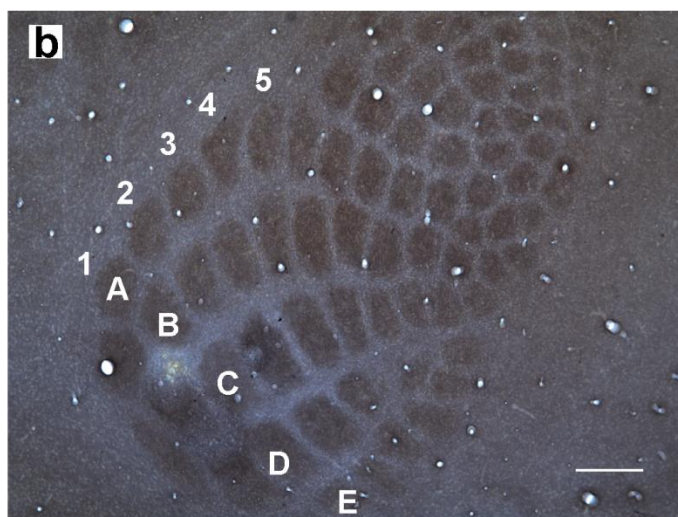
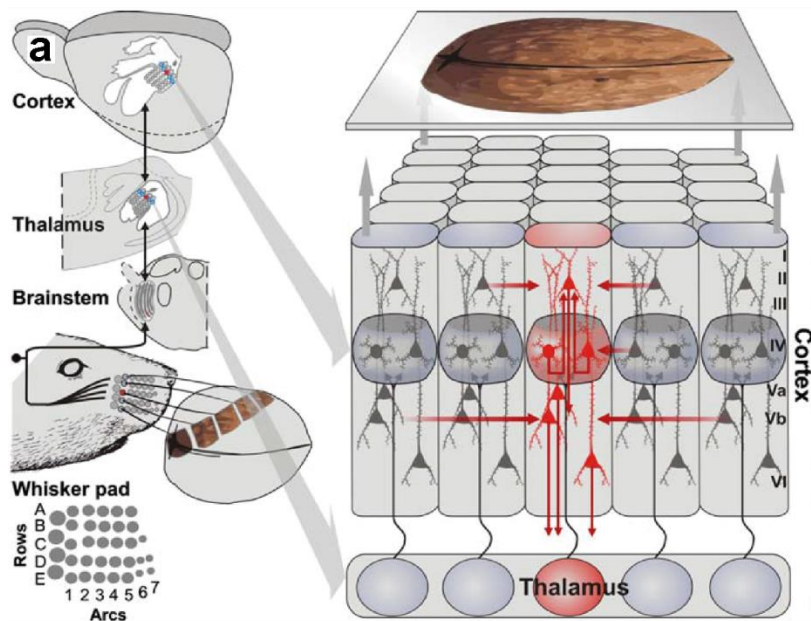


Figure 2.1: The rodent whisker-to-barrel pathway (modified after Schubert et al., 2007)

a) The main facial whiskers on the snout of rodents are organized in rows (A-E) and arcs (1-7). Sensory information introduced by movement of the whiskers (surface structure of walnut) is transferred to the primary somatosensory cortex. On all levels of this pathway a somatotopic representation of the whisker pad can be found. These are called barrelettes in the primary trigeminal nucleus of the brainstem, barreloids in the thalamus, and barrels in the primary somatosensory cortex, hence it is named barrel cortex. Within the cortex sensory information is processed in a canonical way within barrel-related columns (vertical arrows). Additionally, sensory information is distributed to neighboring columns and information from these columns is integrated (horizontal arrows). This flow of information allows object identification.

b) Shown is the cytochrome oxidase staining of a tangential section through layer IV of the primary somatosensory cortex. Obvious is the somatotopic arrangement of intensely stained barrel-structures. Barrels are labeled according to standard nomenclature (Photo provided by Julien Guy). Scale 200µm

nucleus (oralis). Already at this level a highly ordered arrangement of whisker representation is obvious (Ma, 1991; Chiaia et al., 1992; Jacquin et al., 1993). In these nuclei the afferents from the trigeminal ganglion form anatomical well defined modules known as barrelettes (Belford and Killackey, 1979; Ma and Woolsey, 1984; Ma, 1991). Furthermore, these modules are arranged in a somatotopic fashion, meaning that the barrelettes reflect the organization of the whisker pad on the snout of the animals (Figure 2.1a) (Ma, 1991; Chiaia et al., 1992; Jacquin et al., 1993).

From the brainstem sensory information is forwarded to the thalamus (Figure 2.1a). The main input from the brainstem is supplied by the principalis and the interopolaris (Fox, 2008). The principalis mainly projects to the ventroposterior medial thalamic nucleus (VPM) (Chiaia et al., 1991), forming the main pathway for somatosensory information, also known as lemniscal pathway (Figure 2.1a) (Diamond and Armstrong-James, 1992; Bureau et al., 2006). The somatotopic representation of tactile information is maintained in the thalamus, and single whiskers are represented by barreloids (Van Der Loos, 1976), analogous to barrelettes in the brainstem (Figure 2.1a).

Thalamic fibers of the lemniscal pathway project to the primary somatosensory (barrel-) cortex (Diamond, 1995; Ahissar et al., 2000). The lemniscal efferences heavily target L IV (Koralek et al., 1988; Chmielowska et al., 1989; Lu and Lin, 1993), being involved in forming the barrel like structures in this layer (Figure 2.1b). Like in the brainstem

and thalamus, the barrels in S1 represent the organization of the main facial whiskers. Each row and column of barrels corresponds to the rows and columns formed by the vibrissae on the snout of rodents (Figure 2.1a, b). Therefore, barrels are named according to the main whiskers on the snout of the animal, by rows (A-E) and columns (1-7) (Simons and Woolsey, 1979; Petersen, 2007).

2.2 The columnar structure of the rodent barrel cortex

Mountcastle and colleagues (Mountcastle et al., 1955) proposed a columnar structure of sensory processing in the cortex. While investigating the somatosensory cortex of cats, they found that cells with similar receptive field properties are aggregated in clusters vertically spanning all six cortical layers and extending horizontally by ~500 μm . This led to the hypothesis that the cortex consists of many repeated fundamental units with a common architecture of neuronal circuitry, the cortical column (Figure 2.1a). Neurons located within a specific column receive the same information, for example they all react to the same specific orientation of a visual cue as shown by Hubel and Wiesel (Hubel and Wiesel, 1962, 1968). Furthermore, each column receives differential thalamic input (Mountcastle, 1957; Mountcastle et al., 1957). In principle this would lead to a common scheme of information-processing within the column independent of its specific

area location. Already the existence of a cortical division into several layers, each containing a specific set of neuronal subtypes, hints to a common architecture of neuronal circuits within the cortex (Molyneaux et al., 2007).

Although the concept of the cortical column is lively debated in the scientific community (Nelson, 2002; Horton and Adams, 2005), the somatotopically structured barrel cortex of rodents speaks in favor of the columnar hypothesis. As mentioned, within S1 thalamic fibers project to L IV in separated aggregations, called barrels. In mouse these barrels spread horizontally about 100 – 200 μm and contain ~2000 cells (Pasternak and Woolsey, 1975). The cell density is low within the barrel hollow and increased in the barrel wall (Woolsey and Van der Loos, 1970). This leads to the eponymous structure in L IV and can already be observed in preparations without further staining (Figure 2.1, Figure 3.2) (Agmon and Connors, 1991; Petersen and Sakmann, 2000). Barrel-related columns, vertically covering all layers, are defined by the horizontal spread of each barrel in L IV and neurons within these receive their input primarily from a single whisker (Welker, 1971; Simons, 1978; Armstrong-James and Fox, 1987; Brecht and Sakmann, 2002).

Furthermore, a general scheme for the flow of information through the cortical column has been described, the canonical pathway of cortical processing (Figure 2.1a) (Douglas et al., 1989; Douglas and Martin, 2004; Harris and Mrsic-Flogel, 2013). As mentioned before, thalamic

input enters the cortex via L IV, is relayed via the supragranular layers II and III (Laaris et al., 2000; Feldmeyer et al., 2002; Petersen et al., 2003) to infragranular layers V and VI (Armstrong-James et al., 1992; Schubert et al., 2001; Schubert et al., 2007). So far, no clear cytoarchitectonic border between layer II and III has been identified in rodents. Thus, with regard to rodents the area containing L II and III is referred to as L II/III. From L II/III sensory information is forwarded horizontally to other cortical areas (Laaris et al., 2000; Brecht et al., 2003; Petersen et al., 2003). In L V and VI the processed information leaves the cortex via pyramidal cells (PC), which give rise to corticothalamic projections (Zhang and Deschenes, 1997)..

In summary, each barrel-related column in S1 processes information received by a single vibrissa within a universal canonical pathway, as proposed by the hypothesis of a cortical column. Nevertheless, the architecture of the neuronal circuits within the cortex and especially within the cortical column is not fully understood and seems to be slightly changed between cortical areas and surprisingly even between individual barrel-related columns (DeFelipe, 1993; Meyer et al., 2013). An important part in these circuits seems to play the interaction of excitatory and inhibitory interneurons (IN) and especially the balance between excitation and inhibition (Anderson et al., 2000; Wehr and Zador, 2003; Wilent and Contreras, 2004; Okun and Lampl, 2008; Atallah and Scanziani, 2009; Taub et al., 2013).

2.3 Cortical inhibitory interneurons of rodents

Within the cortex many different cell types are involved in processing tactile information, which can be divided in several subgroups. Cortical neurons either express glutamate, therefore being excitatory, or gamma-aminobutyric acid (GABA), which is the main inhibitory neurotransmitter in the cortex (Markram et al., 2004).

As the main focus of this thesis was based on the interconnection of INs, the main excitatory subtypes of cortical neurons are just introduced shortly. The majority of cortical cells (~80 - 90%) are indeed excitatory neurons (Harris and Mrsic-Flogel, 2013; Hu et al., 2014), which can be divided into spiny stellate, star pyramidal cells and PCs. These three groups differ in several aspects, e.g. in morphology and cortical location. Spiny stellate cells exhibit a round or ellipsoid soma and can be found in granular layer IV (Lubke et al., 2000; Staiger et al., 2004b). Star pyramidal cells also occur in L IV, and, in correspondence to their morphology, seem to be the intermediate form between spiny stellate and PCs. They have an irregularly shaped soma with a prominent apical dendrite pointing to L I (Lubke et al., 2000; Staiger et al., 2004b). PCs can mostly be found in L II/III and V and typically have a triangular-shaped soma and an apical dendrite, which reaches L I (De No Lorente, 1949; Larkman and Mason, 1990). These excitatory cells are the main relay units for sensory information, while their response properties are under the control of inhibitory interneurons (Xiang et al., 2002; Spratling and Johnson, 2003; Isaacson and Scanziani, 2011). Inhibitory synapses

onto PCs can be found on soma, dendrites, and axon (Markram et al., 2004; Huang, 2006), which enables a differential spatiotemporal influence onto excitatory in- and output (Somogyi et al., 1998).

Although excitatory neurons represent the vast majority of cortical neurons, recent research has been focused on inhibitory interneurons. INs only make up 10 to 20% of the cortical neurons (Harris and Mrsic-Flogel, 2013; Hu et al., 2014), nevertheless, they have a major impact on cortical sensory processing (Lee et al., 2013; Pfeffer et al., 2013; Pi et al., 2013; Hangya et al., 2014). It has been shown that INs are involved in learning, cortical rhythmic activity patterns, i.e. gamma oscillations, feedforward and feedback inhibition and integration of information from other brain areas (Silberberg and Markram, 2007; Sohal et al., 2009; Buzsaki and Wang, 2012; Donato et al., 2013; Lee et al., 2013; Pi et al., 2013; Fu et al., 2014; Li et al., 2014; Chen et al., 2015; Kuki et al., 2015). Furthermore, dysfunction of cortical INs is linked to neurological or psychiatric pathologies like schizophrenia, bipolar disorder or epilepsy (Powell et al., 2003; Cobos et al., 2005; Levinson et al., 2007; Rogasch et al., 2014). These inhibitory cells show a huge variety of electrophysiological and morphological characteristics (Ascoli et al., 2008). An ongoing scientific discourse concentrates on the classification of INs in several subgroups and their specific function (Ascoli et al., 2008; DeFelipe et al., 2013; Kepecs and Fishell, 2014). As an example, in case of the hippocampus at least 21 distinct classes of INs seem to be present (Klausberger and Somogyi, 2008) whereas for

the neocortex, recently, only 6 types were proposed (Staiger et al., 2015).

A first possibility to distinguish subtypes of INs is the expression of specific molecular markers. Three non-overlapping groups of INs have been identified in correspondence to the expression of parvalbumin (PV), the serotonin receptor 3a (5HT3aR) and somatostatin (SST). Overall, ~40% of INs are PV-expressing (PV-) cells, whereas 5HT3aR-expressing (5HT3aR-) and SST-expressing (SST-) cells each represent ~30% (Figure 2.2a) (Rudy et al., 2011; Staiger et al., 2015). Although there might be a huge diversity of IN subtypes within these three defined groups only the most common ones will be described here.

2.3.1 PV-expressing interneurons

Within the cortex PV-cells are distributed through cortical layers II to VI (Ren et al., 1992). PV-expression in INs is often associated with a fast-spiking pattern. This means that these cells are able to produce high frequency non-adapting trains of action potentials (AP) while a strong depolarizing current is applied (Kawaguchi et al., 1987; Cauli et al., 1997; Kawaguchi and Kubota, 1997; Gibson et al., 1999; Rudy and McBain, 2001; Ascoli et al., 2008; Xu and Callaway, 2009; Hu et al., 2014). Furthermore, PV-cells have a low input resistance (~90 M Ω) and, in relation to other INs, a fast membrane time constant (~4 - 7 ms) (Galarreta and Hestrin, 2002; Doischer et al., 2008). Due to their

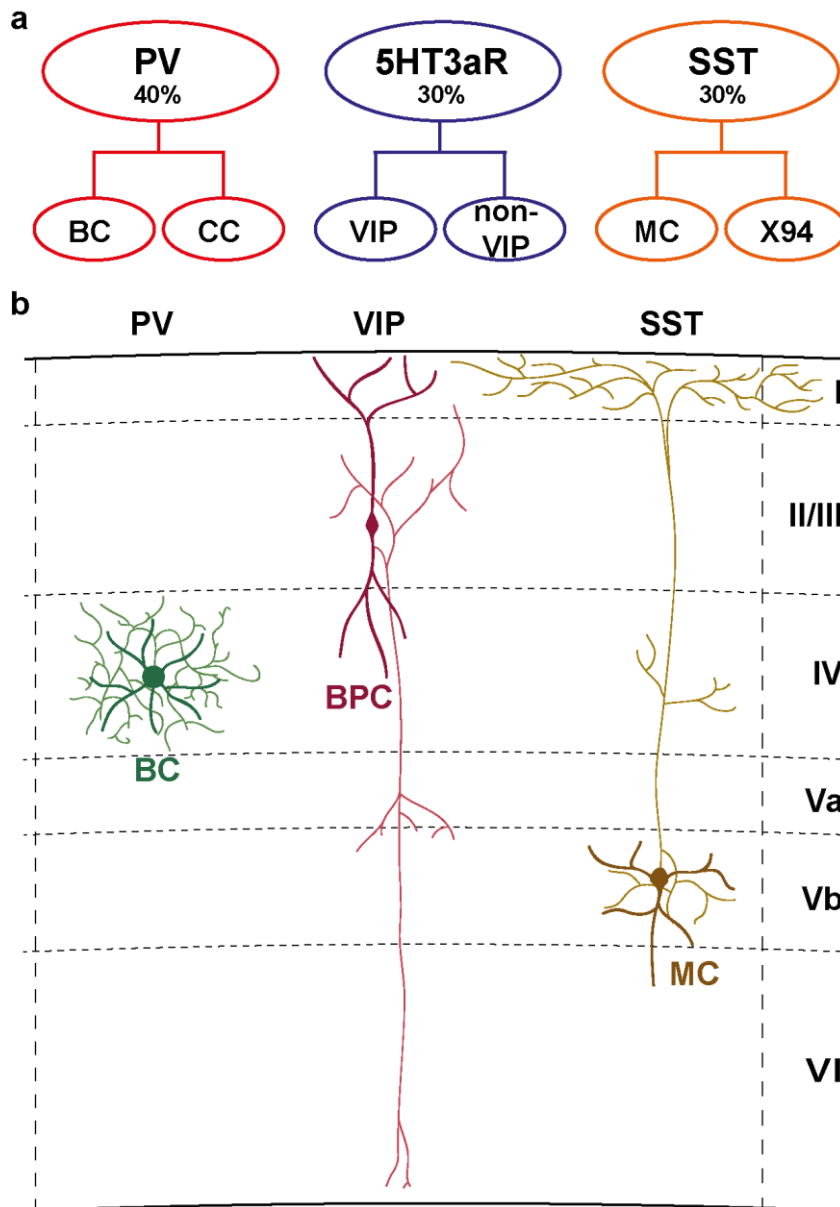


Figure 2.2: Three non-overlapping groups of INs and the corresponding morphology of their main subtypes (modified after Rudy et al., 2011, Staiger et al., 2015)

a) The three non-overlapping groups of cortical INs can be distinguished by their expression of parvalbumin (PV), the serotonin-receptor 5HT3a (5HT3aR), or somatostatin. The PV-expressing cells can be subdivided in basket cells (BC) and chandelier cells (CC), the 5HT3aR-expressing cells in vasoactive intestinal polypeptide (VIP)-expressing and non-VIP-expressing cells, and the somatostatin expressing cells in Martinotti cells (MC) and X94-cells (X94). Given are the percentages of the three main IN-subgroups accounting for the whole population of cortical INs.

b) Schematic morphological representation of the main subclasses of the three non-overlapping IN subgroups shown in a). Thick lines represent the somatodendritic configuration, whereas the axonal arborization is indicated by finer lines. PV-expressing cells show a locally defined basket-like axonal arborization and have, therefore, been described as basket-cells (BC). VIP-cells in L II/III often show a bipolar somatodendritic configuration and, hence, are called bipolar cells (BPC). MCs are the main subgroup of somatostatin expressing cells and can be identified due to an ascending axon branching in L I. Cortical layers are labelled by I-VI.

electrophysiological characteristics, these cells are able to maintain a fast response to presynaptic excitatory cells and they can cause a fast and powerful inhibition of postsynaptic cells (Rudy et al., 2011).

On a morphological level, these fast-spiking cells often show an oval-shaped soma, giving rise to multipolar dendrites. The axonal arborization pattern is locally confined and has been described to form basket-like structures around the somata and proximal dendrites of other neurons (Figure 2.2b) (Lemkey-Johnston and Larramendi, 1968; Somogyi et al., 1983; Jones and Hendry, 1984; Kisvarday, 1992; Wang et al., 2002). Thus, these cells are known as basket cells. Moreover, basket cells are known to target the somatic and perisomatic areas of postsynaptic cells (Freund and Katona, 2007). These cells are the main IN subgroup receiving thalamic input in L IV and are involved in several cortical processing steps, e.g. feedforward inhibition, gamma-oscillation and experience-dependent plasticity (Hensch et al., 1998; Swadlow, 2003; Fagiolini et al., 2004; Cardin et al., 2009).

Another group of PV-expressing cells are the so called Chandelier (or axo-axonic) cells (Szentagothai and Arbib, 1974; Szentagothai, 1975). These cells can be identified due to the candelabra-like axonal projection and preferentially target the axonal initial segment of PCs (Somogyi, 1977). Nevertheless, recent findings argue if these cells are probably excitatory, although these cells release GABA (Woodruff et al., 2010).

2.3.2 5HT3aR-expressing interneurons

As mentioned, a heterogeneous group of GABAergic interneurons expresses the 5HT3a-receptor (Figure 2.2a). Although the subdivision of this group is the substrate for an ongoing scientific discussion, the most common neurons, which express this specific 5HT3a-receptor are the vasoactive intestinal polypeptide-expressing (VIP-) cells. This cell type makes up ~40% of the 5HT3aR-cell population (reviewed by Rudy et al., 2011). The highest number of cells of this subgroup can be found in cortical layer II/III and often show a bipolar or bitufted somatodendritic configuration (Figure 2.2b) (Prönneke et al., 2015). The dendritic branches of VIP-cells can be found in all layers but especially in L I and II/III. The majority of VIP-cells give rise to a descending axon, in some cases innervating all cortical layers from II to VI, with a vertically restricted branching pattern (Figure 2.2b). Nevertheless, several different types of morphologies have been described for this cell type (Prönneke et al., 2015). As reviewed by Thomson and Bannister (Thomson and Bannister, 2003), VIP-cells have been proposed to preferentially target dendrites of other inhibitory interneurons.

Besides being morphologically heterogeneous, also differential electrophysiological properties of VIP-cells have been described. Although VIP-cells generally have a high input resistance it varies between ~300 and ~900 MOhm. The AP firing-pattern in response to high current injections can be continuous adapting, irregular, bursting or even high threshold bursting (Prönneke et al., 2015). The burst spiking

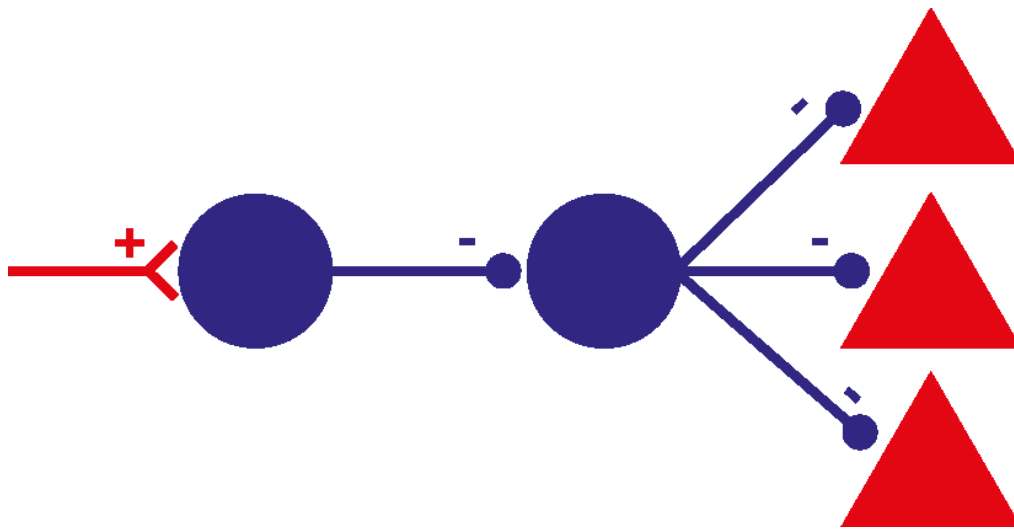


Figure 2.3: Schematic of a disinhibitory circuitry (modified after Roux and Buszaki, 2015)

Shown is the connection scheme of a disinhibitory circuit. Within this kind of circuitry, activation of an IN ultimately leads to release from inhibition of other neurons via an intercalated GABAergic interneuron. This might result in an overall higher excitability of cells, for example pyramidal cells, targeted by a disinhibitory connection. INs are labelled in blue, Excitatory input and pyramidal cells are labeled red. Excitatory and inhibitory synapses are marked by + or -, respectively.

behavior might also be influenced by preceding membrane depolarization, probably in response to other neuronal transmitters like serotonin, acetylcholin or noradrenalin (Porter et al., 1999; Ferezou et al., 2002; Fu et al., 2014; Prönneke et al., unpubl).

VIP-cells are considered to be specialized in controlling other inhibitory interneurons (Staiger et al., 2004a). In recent optogenetic studies of the primary visual and somatosensory cortex it has been shown that VIP-cells are a part of a neuronal circuit motif known as “disinhibition” (Figure 2.3) (Lee et al., 2013; Pi et al., 2013; Fu et al., 2014; Roux and Buzsáki, 2015). Within this pathway, information from the motor cortex is integrated to sensory cortices via VIP-cells. Activation of VIP-cells, via motor cortex input, leads to inhibition of other INs, especially SST-

cells, and releases excitatory neurons from the inhibitory influence of these cells. Ultimately, the excitability of excitatory neurons is enhanced. Therefore, VIP-cells are estimated to be integrators for information of other cortical areas (Lee et al., 2013; Pi et al., 2013; Fu et al., 2014). At least for the visual cortex, VIP-cells have been described to target almost exclusively SST-cells (Pfeffer et al., 2013).

2.3.3 SST-expressing interneurons

SST-cells have come to attention of the scientific community because of their unique interconnection within cortical circuits. For example, these cells seem to take over a key role in so called disinhibitory circuits. The main subpopulation of SST-cells consists of Martinotti cells (MC). As the subject matter of this thesis was the inhibitory innervation of MCs, this specific cell type will be described in greater detail in chapter 2.4. In mice, these cells can be easily distinguished from the smaller subgroup of SST-expressing interneurons, defined as X94-cells (Ma et al., 2006), due to specific differences in laminar location as well as morphological and electrophysiological characteristics.

The X94-cells have been investigated by Xu and colleagues using the X94 mouse line (Xu et al., 2013). Within this line, SST-expressing interneurons, predominantly located in L IV, are labeled by expression of green fluorescent protein (GFP) (Ma et al., 2006). These cells only receive sparse thalamic input and are rather targeted by local excitatory

cells within L IV. X94-cells show an axonal arborization pattern mostly confined to L IV. There, fast spiking PV-cells are the main target of these cells. Due to this circuitry, activation of X94-cells leads to inhibition of fast-spiking cells and ultimately local excitatory cells are released from the inhibition of PV-cells. Thus, SST-cells in L IV, in cooperation with fast-spiking cells, are specialized in controlling the overall activity of excitatory cells in the same layer. Furthermore, besides their specific location and morphology, X94-cells can be distinguished by their intrinsic electrophysiological characteristics. Additionally, analysis of L IV SST-expressing cells, which did not express GFP, showed that these cells inherit the same morphological and electrophysiological characteristics of X94-cells. Hence, in mice SST-cells in L IV seem to belong to a homogenous group. As these cells are almost exclusively located in L IV and show unique morphological and electrophysiological characteristics (Xu et al., 2013), they can be easily distinguished from the most common SST-expressing cells, the Martinotti cells.

2.4 Martinotti cells

Martinotti cells (MC) were first discovered by Carlo Martinotti in 1889 and named after him a few years later in 1891 by Ramon y Cajal (Martinotti, 1889; y Cajal, 1891; Wang et al., 2004). MC can be found throughout cortical layers II to VI (Wang et al., 2004) and can be easily identified due to their very unique morphology. Commonly their oval-

shaped soma bears bitufted or multipolar dendrites and an ascending axon branching extensively in layer I (Figure 2.2b) (Fairén et al., 1984). This cell type has been reported to exist in several cortical areas, e.g. in prefrontal, frontal, cingulate, visual and somatosensory cortices, of many different species, e.g. mouse, rat, monkey and even human (y Cajal, 1911; de Nó, 1922; Marin-Padilla, 1970; Ruiz-Marcos and Valverde, 1970; Valverde, 1976; Vogt and Peters, 1981; Luth et al., 1994; Gabbott and Bacon, 1996; Kawaguchi and Kubota, 1998; Berger et al., 2009; Berger et al., 2010). Thus, MCs occur to be a common building block for cortical circuitry architecture, likely taking a key role in cortical processing. Indeed, dysfunction of this specific cell type has been linked to diseases like epilepsy and schizophrenia (Beneyto et al., 2011; Tai et al., 2014). Furthermore, MCs seem to play an important role in introducing and maintaining theta- or beta-oscillations, respectively (Li et al., 2013).

Due to their relatively small input resistance and therefore small rheobase, these cells have also been known as low-threshold spiking cells (Kawaguchi, 1995; Goldberg et al., 2004). Further typical characteristics of MCs is the adapting firing pattern during high depolarizing current injections and, on rare occasions, even burst spiking patterns (Kawaguchi and Kubota, 1997; Silberberg and Markram, 2007).

Martinotti cells can be further subdivided in respect to the expression of calretinin (CR). Xu and colleagues (Xu et al., 2006) discovered that

MCs, coexpressing SST and CR, had more primary processes (number of primary processes: MC/CR+: 6.1 ± 0.3 ; MC/CR-: 5.0 ± 0.2) and a dendritic field extending more horizontally. Furthermore, these cells had broader action potentials width (CR+: 1.23 ± 0.04 ms, Cr-: 1.11 ± 0.03 ms) and a slower afterhyperpolarization (CR+: 21.49 ± 0.91 ms, Cr-: 13.36 ± 1.46 ms) (Xu et al., 2006).

Martinotti cells are known to receive excitatory input from neighboring PCs (Figure 2.4), whereas repetitive spiking of these presynaptic cells can lead to generation of APs in MCs (Silberberg and Markram, 2007). Additionally, MCs themselves target PCs via their apical dendrite (Figure 2.5) (Thomson et al., 1995; Kawaguchi and Kubota, 1997; Thomson and Bannister, 2003; Wang et al., 2004; Ascoli et al., 2008). Therefore, activity of a presynaptic PC leads to activation of MCs and this in turn causes inhibition of other postsynaptic PCs. Hence, MCs are known to effectively mediate disynaptic lateral inhibition between nearby excitatory cells (Silberberg and Markram, 2007).

Recently, it was hypothesized that MCs are a major target for inhibitory input from other GABAergic neurons. Gentet and colleagues (Gentet et al., 2012) could show that SST-expressing cells of S1 receive inhibitory input while the corresponding whisker was touched. In contrast, all other recorded cells, excitatory as well as inhibitory neurons, received excitatory input. Furthermore, these SST-expressing cells were described to show typical features of MCs (Gentet et al., 2012). Using an optogenetic approach, VIP-cells have been identified to be a major

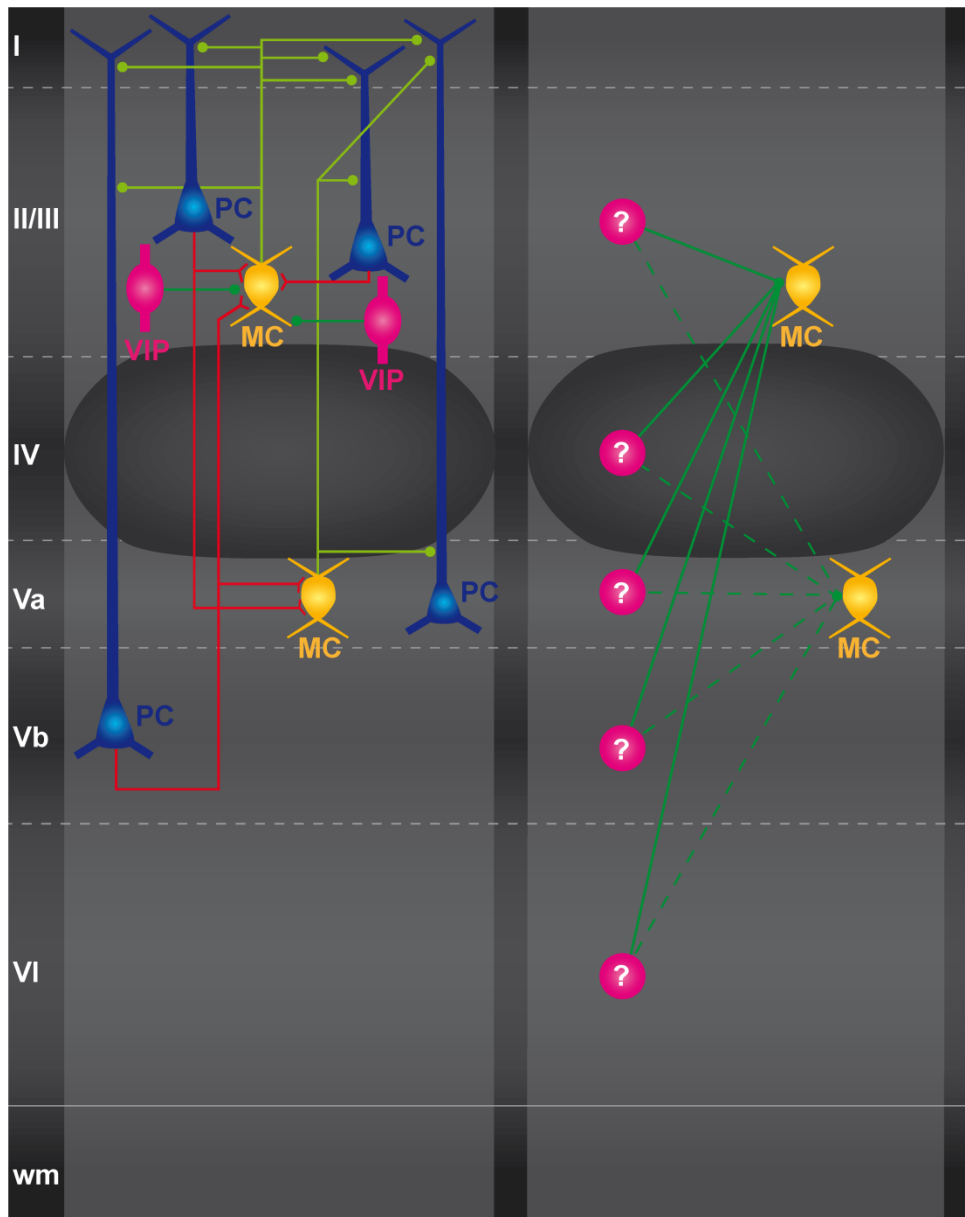


Figure 2.4: Known connectivity of Martinotti cells in the primary somatosensory cortex and working hypothesis

Left: Martinotti cells in L II/III as well as L V receive excitatory input from neighboring PCs. In turn, MCs inhibit these cells via their apical dendrite. Additionally, MCs in L II/III receive inhibitory input from VIP-cells. MCs: orange, VIP-cells: pink, PCs: blue, excitatory input: red, inhibitory input green, Cortical layers are labeled I – VI, wm: white matter

Right: Are the other cell types involved in the inhibition of MCs and might inhibitory input differ between L II/III and V MCs? To answer this questions the goal of this thesis was to locate, identify and analyze local inhibitory input to MCs in L II/III and V. MCs: orange. Probable location (pink circles) and possible connections of presynaptic INs (green) are shown.

group giving rise to inhibitory input to SST-cells (Lee et al., 2013; Pi et al., 2013; Fu et al., 2014). In these experiments, activation of fibers coming from the motor-cortex triggered spiking in VIP-cells, leading to inhibition of SST-cells. This caused a higher excitability of excitatory cells, which is known as disinhibitory circuit (Figure 2.3). Hence, like X94-cells, also MCs seem to be involved in disinhibitory circuits, although being engaged at different levels of this specific circuitry. In case of the mouse visual cortex it has been shown that only VIP-cells target SST-cells (Pfeffer et al., 2013). Nevertheless, the question arises if this is also true for other cortical areas or if more inhibitory subpopulations might be involved in the inhibition of Martinotti cells (Figure 2.4).

2.5 Outline of this thesis

As mentioned, disinhibitory circuits have a major impact on cortical processing. This circuit motif has been shown to integrate information from other cortical areas and can precisely control the activity of excitatory cells. Within disinhibitory circuits activity of an inhibitory IN causes inhibition of one or even more GABAergic cells. The excitability of these target-cells is therefore reduced and subsequent postsynaptic cells are released from inhibition. In the visual and somatosensory cortex information from the motor cortex is integrated via the activity of VIP-cells, which leads to the inhibition of SST-cells and ultimately releases excitatory cells from SST-cell inhibition. Hence, especially

SST-cells seem to play a key role in disinhibitory circuits. So far, many of the findings on disinhibitory circuits rely on population data derived from optogenetic experiments. Only in the visual cortex inhibitory to inhibitory connections have been investigated on a single cell level. There, it was shown that VIP-cells exclusively target SST-cells.

Considering the results of Gentet and colleagues (Gentet et al., 2012) it is likely that within S1 especially Martinotti cells receive inhibitory input. Hence, these cells seem to be the main relay for disinhibitory circuits. Since Martinotti cells represent the largest group of somatostatin-expressing cells and due to their connection pattern onto neighboring PCs we focus on the inhibitory input to these specific cell types in L II/III and V of the barrel cortex. Especially, with regard to inhibitory control of L V MCs, information is lacking.

First, we locate presynaptic inhibitory cells within acute brain slices of the barrel cortex using a combination of whole-cell patch-clamp recordings of MCs in L II/III and V and focal photolysis of caged glutamate. With this method it is possible to contain the localization of presynaptic INs in respect to layers and barrel-related columns. Afterwards, we identified presynaptic inhibitory cells by means of paired recordings. We hypothesized that besides VIP-cells other GABAergic subpopulations are involved in targeting MCs in the barrel cortex. Further analysis was then focused on the elementary synaptic properties of identified unitary inhibitory connections and their short-term plasticity.

3 Material & Methods

3.1 Animals

All experiments were performed in accordance with the German Law on the Protection of Animals. PV-cre (Pvalb^{tm1(cre)Arbr}/J), VIP-cre (VIP^{tm1(cre)Zjh}), SST-cre (SST^{tm2.1(cre)Zjh}), Ai9 mice (B6.Cg-Gt(ROSA)26Sor^{tm9(CAG-tdTomato)Hze}/J) and GIN mice (FVB-Tg(GadGFP)45704Swn) were obtained from the Jackson Laboratory (The Jackson Laboratory, Bar Harbor, USA) and kept under standard housing conditions.

Homozygous Ai9 mice were crossbred with homozygous PV-cre, VIP-cre or SST-cre mice to create PV-cre / VIP-cre / SST-cre::tdTomato mice. These mice were further crossed with homozygous GIN mice to create the triple transgenic mouse lines PV-cre::tdTomato::GIN, VIP-cre::tdTomato::GIN and SST-cre::tdTomato::GIN. Within the GIN-line, GFP-expressing cells are found primarily in cortical layers II to V (Xu et al., 2006) and seem to be almost exclusively Martinotti cells within L II/III and V (Ma et al., 2006; Fanselow et al., 2008; McGarry et al., 2010).

Using the triple transgenic mouse lines PV-expressing (PV-cell), VIP-expressing (VIP-cell), SST-expressing (SST-cell) and GIN-cells in cortical layers I to IV could be identified due to their specific fluorescent label (PV-/ VIP-/ SST-cells: tdTomato fluorescence, GIN-cells: GFP fluorescence) (Figure 3.1a, b).

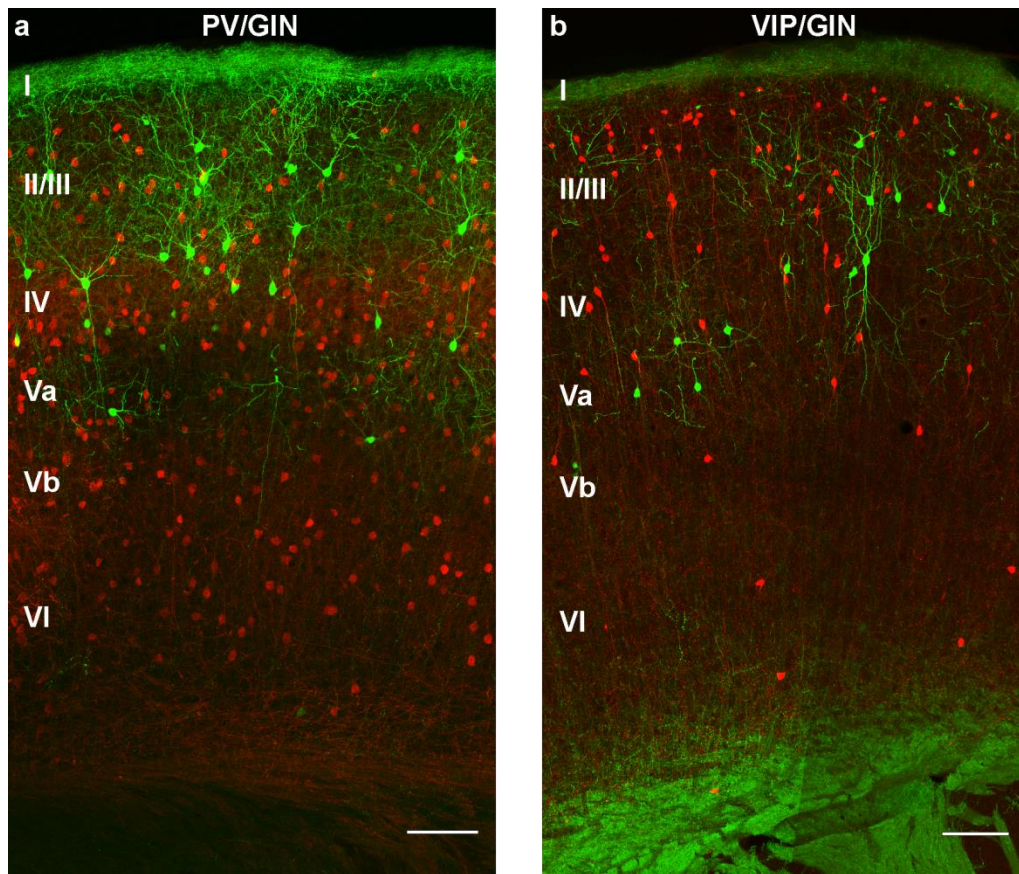


Figure 3.1: Transgenic mice used for experiments

a, b) Immunohistochemical staining of a 50 μm thick section of a PV-cre::tdTomato::GIN- (PV/GIN) **(a)** or a VIP-cre::tdTomato::GIN-mouse (VIP/GIN) **(b)** containing the barrel cortex. Cre-expressing PV- or VIP-cells are labelled by tdTomato, respectively, and GIN-cells are labelled by GFP. Cortical layers are labelled I-VI. Scale: 100 μm

3.2 Slice preparation and solutions

To obtain acute brain slices including the barrel cortex (Figure 3.2), mice (postnatal day (P) 21-36, median: P 28) were deeply anesthetized with isoflurane and decapitated. The brain was removed, the hemispheres separated and kept in cold (4°C), oxygenated (Carbogen: 95 % O₂ / 5 % CO₂) preparation solution used for cutting (in mmol: 75 sucrose, 87 NaCl, 2.5 KCL, 0.5 CaCl₂, 7.0 MgCl₂, 26 NaHCO₃, 1.25 NaH₂PO₄ and 10 glucose; pH: 7.4). Thalamo-cortical slices of 300 μm

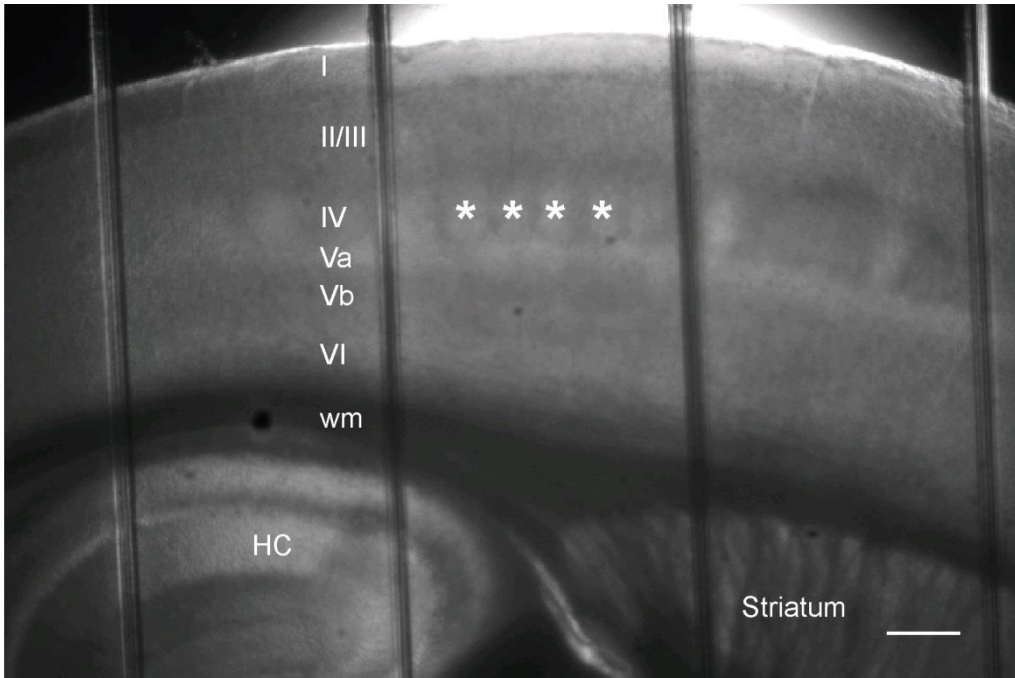


Figure 3.2: Acute brain slice used for electrophysiological experiments

Depicted is a 300 μm thick acute brain slice in the recording chamber (2.5x objective). Note the barrel-like structures, marked by asterisks, in LIV of the primary somatosensory cortex. Hence, this area is called barrel cortex. Cortical layers are labeled I – VI, wm: white matter, HC: Hippocampus, Scale: 100 μm

thickness from mouse barrel cortex were prepared according to Porter and colleagues (Porter et al., 2001) using a vibratome (Vibratome Leica VT 1200 S, Leica, Wetzlar, Germany). Slices were incubated in oxygenated artificial cerebrospinal fluid (ACSF) (in mmol: 125 NaCl, 2.5 KCL, 2 CaCl₂, 1 MgCl₂, 26 NaHCO₃, 1.25 NaH₂PO₄ and 25 glucose; pH: 7.4) at 32°C for 30 min and later kept at room temperature until further processing. Thalamo-cortical slices were used because the morphology of included cells and laminar connections are best preserved in this cutting plane.

3.3 Electrophysiology and data acquisition

Slices were transferred to a submerged recording chamber (ACSF flow rate of 2 ml/min at 32°C) in an upright microscope (Axio Examiner, Zeiss, Germany) (Figure 3.3a). For photostimulation a 405 nm laser (DL-405, Rapp OptoElectronic, Wedel, Germany) was coupled via a 200 µm liquid-fiber to the epifluorescence path of the microscope and guided into the 40x objective. Whole-cell recordings from PV-, VIP-, SST-, GIN- and excitatory cells in layers II/III to VI of the barrel cortex were performed in current clamp. Although L V can be subdivided into L Va and Vb (Zilles and Wree, 1995), we did not differentiate between cells located in these sublayers. Therefore we address cells as L V cells, regardless of their position in L Va or Vb. In case of glutamate uncaging experiments GIN-cells were recorded in voltage clamp. During paired recordings presynaptic cells were recorded in current clamp and postsynaptic cells in voltage clamp. Borosilicate patch pipettes were made using a micropipette puller (P-1000, Sutter Instruments, Novato, USA) and had a resistance of 5-8 MΩ. Patch pipettes contained a potassium-based intracellular solution (in mmol: 135 K-gluconate, 5 KCl, 0.5 EGTA, 10 HEPES, 4 Mg-ATP, 0.3 Na-GTP, 10 Na-phosphocreatine phosphate; pH: 7.4) for current clamp recordings and a cesium-based solution (in mmol: 135 CsMeSO₄, 5 CsCl, 0.5 EGTA, 10 HEPES, 4 MG-ATP, 0.3 Na-GTP, 10 Na-phosphocreatine phosphate; pH: 7.4) for voltage clamp recordings. Internal solutions always contained 0.3-0.5 % biocytin for subsequent morphological visualization. Depolarizing and hyperpolarizing current pulses were

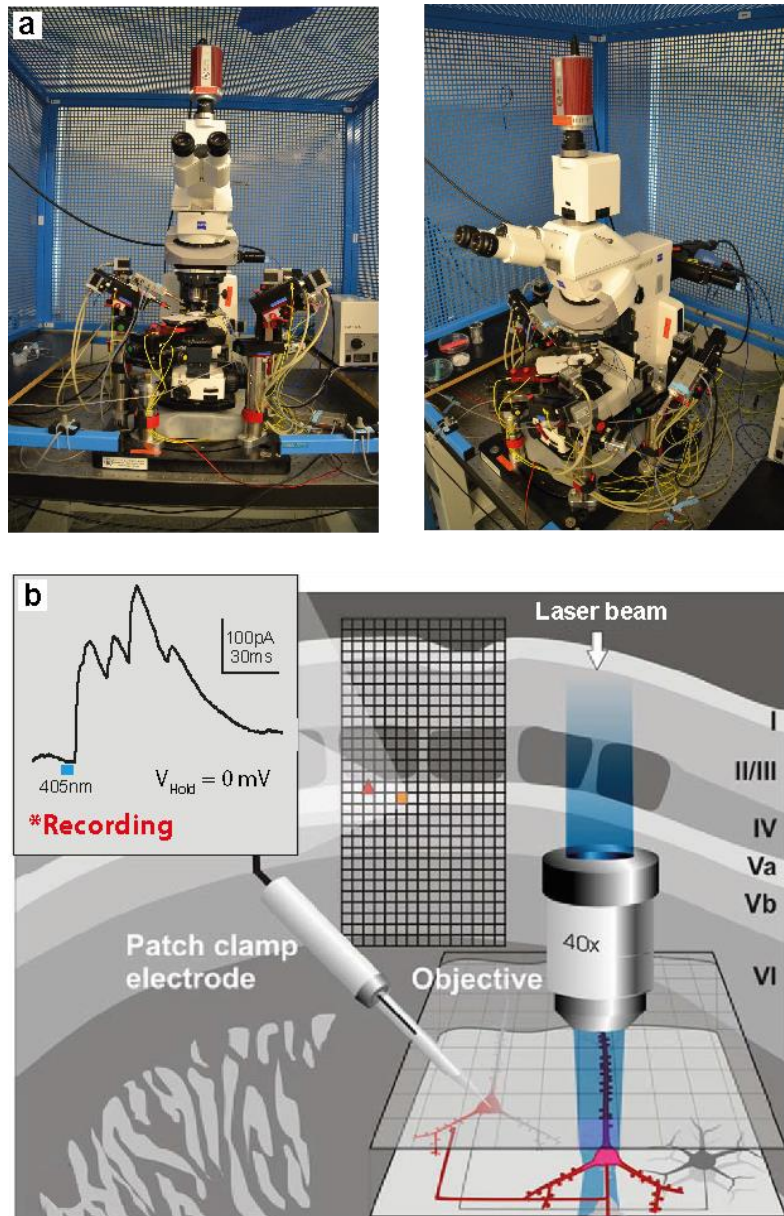


Figure 3.3: Electrophysiological set-up and experimental approach for uncaging experiments (modified after Schubert et al., 2007)

a) The set-up consists of an upright microscope, two recording electrodes and a 405 nm laser for glutamate uncaging. For details see material & methods.

b) Schematic representation of the uncaging experiments. Foreground: a patch clamp electrode records from a visually defined target cell (red triangle in L Va in the background). At the same time the laser beam is focused on a 50x50 μ m-large area (orange square). Here, caged components can be released. In case of mapping experiments using caged glutamate, this excites presynaptic INs, which causes an inhibitory postsynaptic current in the target cell (inset recording). After three repetitions of laser stimulation the objective could be moved to the adjacent field. In case of caged GABA experiments, release of GABA directly evokes inhibitory responses in the recorded cell. A drawing of a slice including its layers and barrels is shown in gray. The map (black grid) could be varied in its dimensions from single field stimulations used for somatic release of caged components, to maps consisting of 7 x 7 fields (soma centered in the middle) for direct activation of cell compartments by glutamate release, to maps consisting of 9 x 9 fields (soma centered in the middle) for release of GABA and to maps covering all cortical layers and three barrel related columns for the mapping experiments to define inhibitory input to Martinotti cells.

used to characterize PV-, VIP- and GIN-cells during initial current clamp recordings. Therefore, these cells were recorded in current clamp at V_{Rest} using a potassium-based internal solution. A 1 s depolarizing current pulse was applied and increased manually in steps of 1 pA until threshold for eliciting a single spike was reached. Recordings were repeated at least five times using this specific current with a stimulus interval of 3.6 s to obtain the rheobase for each individual cell. Afterwards, tenfold repetitions of hyperpolarizing currents (-10 pA and -50 pA) were applied with a stimulus interval of 1.5 s. This was done to evaluate the input resistance and the membrane time constant, whereas only the average response to the -50 pA stimulus was used for further analysis. Using another protocol, non-repetitive hyperpolarizing currents with a stimulus interval of 5 s were applied starting from -10 pA to -100 pA in steps of -10 pA. Subsequently, depolarizing currents were applied ranging from +10 pA to +300 pA in steps of +10 pA. If it was not possible to elicit a series of spikes with a current stimulus of +300 pA the current was further increased in steps of +10 pA. Hence, the U/I relationship could be analyzed as well as the firing behavior during high current injections. Following passive and active electrophysiological characteristics were analyzed: resting membrane potential (V_{Rest}), membrane time constant for highest deflection (τ), input resistance at highest deflection (R_{in}), Rheobase (Rheo), action potential amplitude at firing threshold (AP amp) and action potential width at firing threshold (AP width).

To investigate inhibitory postsynaptic currents (IPSC) in all following experiments, GIN-cells were kept close to AMPA-receptor equilibrium potential in voltage clamp (E_{AMPA} : ~0 mV). This was done to increase the driving force for chloride hence the amplitude of inhibitory postsynaptic currents and minimize contamination by excitatory postsynaptic currents. Data were acquired using a SEC-05L amplifier (npi electronics, Tamm, Germany) in discontinuous mode with a switching frequency of 50 kHz. The signals were filtered at 3 kHz and digitized at 10-25 kHz using a CED Power 1401 (CED Limited, Cambridge, England). Data were collected, stored and analyzed with Signal 5 (CED Limited, Cambridge, England).

3.4 Calibration of focal photolysis of caged compounds

To locate presynaptic INs projecting onto GIN-cells we used a combination of whole-cell patch-clamp recordings of GIN-cells and focal photolysis of caged glutamate. This was done in order to trigger APs in presynaptic INs by release of glutamate. When these cells were synaptically coupled to the recorded GIN-cell inhibitory postsynaptic responses could be detected. To test whether (i) inhibitory inputs can be detected even elicited at distant dendritic compartments of GIN-cells, and (ii) specifically INs can be activated by focal photolysis of caged

glutamate in a layer-specific manner, we set up a series of calibration experiments.

Laser calibration for focal photolysis of caged compounds.

Before and after each uncaging experiment the intensity of laser output at the level of the recording chamber was measured, with a probe positioned according to the later used acute brain slices. Therefore, the 405 nm laser beam was set to a size of 50 x 50 µm by a customized rectangular shutter (Luigs & Neumann, Ratingen, Germany) (Figure 3.3b). This configuration was used for all subsequent uncaging experiments. Afterwards, the laser intensity was increased in steps of 10%, ranging from 0 to 100% (Tab. 3.1). The corresponding laser intensity was measured in mW with a laser power detector (PowerMax-USB WAND UV/IS Quantum Sensor, Coherent Deutschland GmbH, Germany) and displayed on a PC using the PowerMax software (Coherent Deutschland GmbH). Only if these values did not differ before and after experiments the recorded data was accepted and further evaluated.

Table 3.1 Constant laser intensity before and after uncaging experiments

Table containing the laser intensity at the level of the slice chamber in response to increasing laser power before and after an uncaging experiment. Note that the laser intensity stays the same for the different laser settings before and after experiments. Furthermore, an intensity of ~20 mW was reached at 75% laser power.

Laser intensity (%)	10	20	30	40	50	60	70	80	90	100
Output at slice chamber, before (mW)	2.7	5.3	8.0	10.7	13.3	16.0	18.8	21.4	24.1	26.8
Output at slice chamber, after (mW)	2.6	5.4	8.0	10.7	13.4	16.1	18.8	21.5	24.1	26.9

Calibration of experimental set-up for focal photolysis of caged glutamate

Mapping of direct inhibitory inputs

Dendrites act as electrical filters (Rall, 1977), therefore IPSCs elicited at distant dendritic parts might degrade while being transmitted to the soma of GIN-cells (Figure 3.4), which are very likely Martinotti cells (see results in chapter 4.1). Furthermore, with somatic voltage clamp recordings, voltage is not uniformly controlled across the whole dendritic tree of a cell, which is known as space clamp error (Williams and Mitchell, 2008). This potentially introduces errors in measurement of dendritic synapses by somatic voltage clamp. To test the possibility of detecting dendritically evoked inhibitory currents, we performed voltage-clamp recordings of GIN-cells using a holding potential (V_{Hold}) of 0 mV and a cesium-based internal while releasing caged GABA (O-CNB-caged GABA, Molecular Probes, Carlsbad, USA) with laser light. The laser beam was focused on an area including the soma of the recorded cell. Caged GABA was added to the ACSF perfusion with a final concentration of $\sim 315 \mu\text{M}$. Afterwards, GABA was released by a short laser stimulus (1ms) repeated every 10 s while gradually increasing laser intensity, in steps of 10%, as described above. This will cause an immediate, directly evoked inhibitory response with gradually increasing amplitude, if the recorded cell contains GABA-receptors. Only deflections passing the threshold of mean baseline + $3 \cdot \text{SD}$ of the baseline were accepted as direct inhibitory responses. If the patched

cell responded to GABA-release and no further change in amplitude of this inhibitory response was observable the corresponding laser energy was noted.

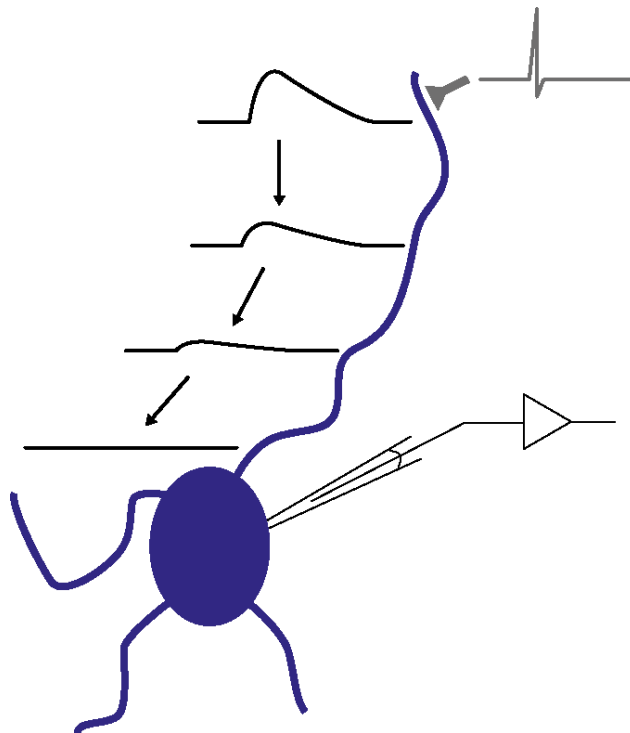


Figure 3.4: Dendritic cable properties interfere with detection of dendritic events

Shown is the effect of dendritic cable properties, known as the space clamp problem. Events (schematic black traces) elicited by incoming APs (gray) at synapses located at distant dendritic sites (presynaptic terminal in gray, dendrite and soma of postsynaptic cell in blue) degrade while being transferred to the soma. In theory this means that these events might remain undetected at somatic recording sites.

This energy was used to release GABA on dendritic parts of the recorded cell. Therefore, a 450 x 450 μm large area, parallel to the surface of the acute brains slice, was defined with the soma centered.

This was done to cover all, or at least most, of the dendritic parts of the recorded cell. This area was separated in 81 (9x9) non-overlapping fields with the size of 50 x 50 μm corresponding to the size of the laser illumination spot, similar to the procedure shown in figure 3.3. In each of these fields GABA was released by short laser pulses (1ms) repeated three times per field at an interval of 3 s. Successive scanning of all fields was done systematically (50 μm and 10 s per step) along rows, starting with the pial facing one, with alternating directions controlled by Morgentau M1 software (Morgentau Solutions GmbH, Munich, Germany).

Detection of spiking-threshold with somatic release of caged glutamate

In order to define the laser energy needed to drive cortical neurons to spiking we performed glutamate-uncaging experiments while focusing on the soma of recorded cells. Therefore, we tested five groups of cortical neurons, PV-, VIP-, SST-, GIN- and excitatory cells. As soon as stable whole-cell current clamp recordings at V_{Rest} of PV-, VIP-, SST-, GIN- or excitatory cells throughout layers II/III to VI were achieved, somatic activation via focal photolysis of caged glutamate was carried out. The laser beam was focused on an area of 50 x 50 μm surrounding the recorded cell soma. Caged glutamate (CNB-caged-L-glutamate, Molecular Probes) was added to the ACSF perfusion with a final concentration of $\sim 379 \mu\text{M}$, which was used as a standard for all

following glutamate-uncaging experiments. Glutamate was released with a short (1 ms) laser light pulse repeated every 10 s and the laser intensity gradually increased in steps of 10%, ranging from 10% to 100%. This was done to achieve a graded, immediate excitatory potential, due to activation of glutamate receptors, finally reaching threshold for triggering a single spike. If this threshold was not reached the stimulus length was elongated to 3 ms, 6 ms or 10 ms and the laser intensity was increased correspondingly.

3.5 Activation of presynaptic cells by focal photolysis of caged glutamate

Immediately after stable whole-cell voltage clamp recordings of L II/III or V GIN-cells were achieved ($V_{\text{hold}} = 0$ mV), focal photolysis of caged glutamate with a 405 nm laser light was carried out to activate presynaptic inhibitory interneurons. This method was modified from Schubert et al. (Figure 3.3b) (Schubert et al., 2007). To reduce detection errors of IPSCs, laser stimulus was repeated three times per field at an interval of 3 s. The laser stimulus had a length of 6 ms and an intensity of ~20mW and hence a laser energy of 120 μ J (see results for calibration experiments in section 4.2.2 and figure 4.5b). IPSCs were only accepted as stimulus evoked if: (i) their amplitude exceeded the mean baseline + 3*SD of the baseline, (ii) they were detected in at least two out of three stimulus repetitions, and (iii) they appeared within a

10 ms time window after stimulus offset and, therefore, were accounted as monosynaptic input. The laser was moved over an area stretching over three adjacent barrel-related columns, whereas the middle one contained the recorded MC, and the entire cortical depth either from pia to white matter or vice versa. Scanning was done systematically (50 μm and 10 s per step) along rows with alternating directions controlled by Morgentau M1 software, as described before. Thus up to 364 different fields were stimulated without any intermittent gaps. In every slice containing a recorded MC, layer and column borders were estimated from DAPI stainings and aligned with the scanned cortical area. Once individual fields were assignable to specific columns and layers, maps were created representing the average IPSC amplitude in fields containing sources of inhibitory input (inhibitory fields). These maps were then converted into binary ones by assigning the greyscale value 0 (black) to each inhibitory field, irrespective of the corresponding amplitude of the average inhibitory response, and the value 255 (white) to the remaining fields. In addition, the number of inhibitory fields containing one or more presynaptic INs was counted per layer and column. Individual binary maps were then aligned in relation to the barrel-like structure in L IV of the home column and converted into an average map depicting the confidence level for the position of inhibitory fields by means of a customized Matlab script (The MathWorks GmbH, Ismaning, Germany).

3.6 Paired recordings

To investigate if PV- or VIP-cells target GIN-cells, simultaneous whole-cell patch-clamp recordings of presynaptic PV- or VIP-cells and GIN-cells were carried out. During paired recordings PV- and VIP-cells remained at resting membrane potential (V_{rest}) in current clamp. Postsynaptic GIN-cells were kept at $V_{hold} = 0$ mV in voltage clamp. Consecutive brief current injections (5 ms per pulse, 20-650 pA, 10-20 sweeps, 10 s sweep interval) to presynaptic inhibitory neurons caused single spikes leading to IPSCs in GIN-cells, if the recorded cells were synaptically connected. All measurements were done on averages of individual sweeps. Prior to averaging, all individual IPSCs of a connected pair were aligned with respect to the spike peak of the presynaptic AP. This was done to prevent disturbance of the average IPSC waveform due to spike jitter. For responses from single spike stimulations we analyzed the following parameters: latency (time from presynaptic spike peak to IPSC onset), time to peak (time from IPSC onset to peak amplitude), amplitude (difference from baseline to peak) and mean slope of the ascending phase of the IPSC.

Short-term plasticity was tested by applying a train of five spikes with frequencies of 1, 8 and 40 Hz in the presynaptic cell (paired train experiments). As mentioned before, all measurements were done on averages of individual sweeps. Here, we only measured the peak amplitudes of the average IPSCs and calculated the response ratio for each IPSC relative to the amplitude of the first response

(n^{th} -response/ 1^{st} -response). If consecutive IPSCs overlapped, the amplitude of single responses was measured in this case by fitting the decay phase of preceding IPSCs (Figure 3.5). This fit was extrapolated to baseline level. Response amplitude was then calculated as the difference between the peak of the response and the fit value at that point in time.

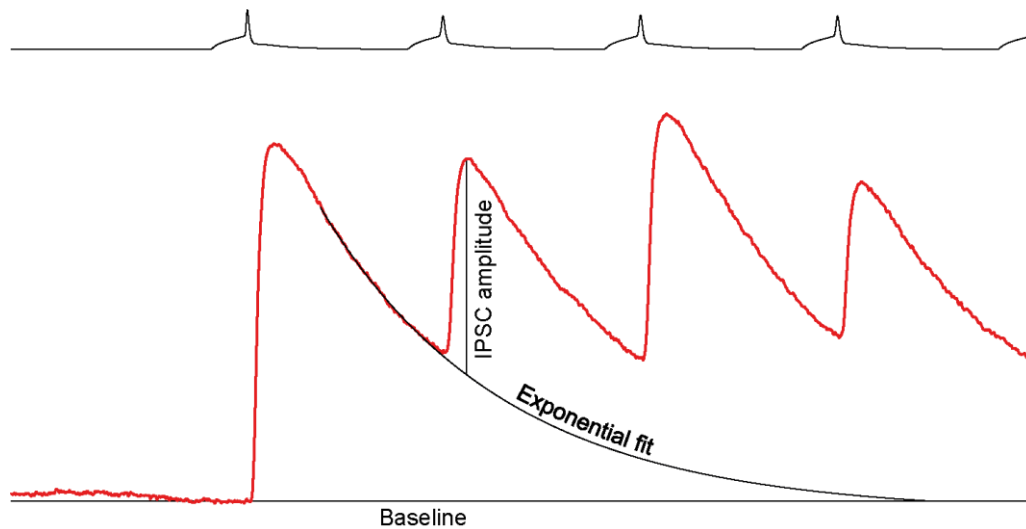


Figure 3.5: Fitting procedure to determine the amplitude of overlapping IPSCs in response to a 40 Hz spike train

To exclude the postsynaptic summation effect on the amplitude of overlapping IPSCs the descending phase of the preceding IPSC was exponentially fitted and elongated until reaching baseline level. Afterwards, the amplitude the IPSC was measured between the peak of the response and the fit value at that point in time.

3.7 Histology

After experiments, slices were fixed with 4% paraformaldehyde in 0.1 M phosphate buffer (PB) + 15 Vol% picric acid at 4°C overnight. Afterwards, slices were stained either histochemically using the avidin-

biotin complex (ABC)-diaminobenzidine (DAB) and cytochrome oxidase staining method or immunohistochemically. The stainings were used to verify the identity of recorded cells by means of their morphological identity.

3.7.1 ABC-DAB and cytochrome oxidase staining

To obtain the morphology of recorded GIN-cells used for initial characterization experiments (chapter 4.1) ABC-DAB and Cytochrome-oxidase staining was carried out according to a published protocol (Staiger et al., 2004b). Slices were rinsed in PB (pH: 7.4) three times for 15 min and incubated for 1.5 h in 25% saccharose + 10% glycerol in PB-buffer, for cryprotection. Afterwards, they were freeze-thawed three times over liquid nitrogen and rinsed in 1% H₂O₂ (in PB) to block endogenous peroxidase activity. Slices were washed in PB and incubated overnight with Avidin-Biotin Complex (ABC; 1:200; Vector, Burlingame, CA) at 4 °C. After 10 min of preincubation with 1 mg/ml 3,3' diaminobenzidine (DAB; Sigma, Deisenhofen, Germany) the peroxidase was revealed by starting the reaction with 0.01% H₂O₂. Rinsing with PB stopped the reaction.

Cytochrome oxidase (CO) histochemistry was used to visualize the barrellfield. For this purpose, slices were rinsed in PB and then incubated (at 39°C in a water bath) in a solution of 6 mg cytochrome C, 5 mg DAB and 444 mg saccharose in 10 ml PB, including 0.3%

catalase (all from Sigma, Deisenhofen, Germany). When sufficient staining was achieved, the reaction was stopped by rinsing with PB. Finally, slices were mounted on glass slides and coverslipped in Aqua Poly/Mount (Polysciences, Inc., Warrington, USA) and pictures were taken with an upright microscope (AxioImager.M2, Zeiss, Jena, Germany).

3.7.2 Immunohistochemical staining

To visualize biocytin-filled neurons as well as GFP and tdTomato expressing cells, slices were processed as described by Gentet and colleagues (Gentet et al., 2012). In summary, slices were rinsed three times (3 x 15 min) with phosphate-buffer saline (PBS), and incubated with primary antibodies: rabbit anti-red fluorescent protein (RFP; 1:500, Rockland, Limerick, PA, USA) and goat anti-GFP (1:2000, Abcam, Cambridge, UK) in blocking solution (0.25% bovine serum albumin (BSA), 10% normal donkey serum and 0.5% Triton X-100, pH 7.6, in PBS) for 48-72h at 4°C. Afterwards, slices were washed in PBS (5 x 10 min), followed by 4h of secondary antibody incubation at room temperature, again washed in PBS (6 x 10 min) and DAPI-stained (1:1000, Molecular Probes). Donkey anti-goat AF488 (1:500, Invitrogen, Carlsbad, CA, USA) and donkey anti-rabbit AF546 (1:500, Invitrogen) were used as secondary antibodies. Streptavidin-conjugated AF633 (1:500, Life Technologies, Carlsbad, CA, USA) was used for biocytin-labelling. Slices were mounted in AquaPolyMount and fluorescent

images were taken using a Leica SP2 confocal microscope (40x objective; voxel size: 0.18 x 0.18 x 0.80 μm), controlled by arivis software (arivis AG, Unterschleißheim, Germany).

3.8 Statistics

For statistical comparisons, data were tested for normality (Shapiro-Wilk test) and equal variance using SigmaPlot (SigmaPlot Version 13.0, Systat Software, Inc., Erkrath, Germany). If both passed, a one-way student *t*-test was used. If one or both failed, a Mann-Whitney rank sum test was used. Results were given as P values. $P < 0.05$ was interpreted as significantly different. Mean \pm S.E.M. are given for all other values, if not stated otherwise. Graphs showing statistical analysis were created using SigmaPlot and Origin (Origin 8.5.0G SR0, OriginLab Corporation, Northampton, USA).

4 Results

4.1 L II/III and V GIN-cells show typical characteristics of Martinotti cells

We used the GIN-mouse line to investigate inhibitory input onto L II/III and V MCs. In this specific line, a subpopulation of SST-expressing cells in the cortex is labelled by GFP (Oliva et al., 2000) (Figure 4.1a', b') and it has been shown that most of these cells show typical characteristics of Martinotti cells (Ma et al., 2006; Fanselow et al., 2008).

To make sure that GIN-cells in L II/III and V are indeed MCs we carried out preliminary studies. Therefore, we performed whole-cell patch-clamp recordings of GIN-cells with a potassium-based internal. Additionally, recorded cells were filled with biocytin. This was done to obtain an electrophysiological and morphological characterization of GIN-cells in L II/III and V. Following passive and active electrophysiological properties were observed for L II/III (n = 20) and V GIN-cells (n = 7), respectively: V_{Rest} : -61.65 ± 0.89 mV, -64.63 ± 1.60 mV; Tau: 16.70 ± 2.01 ms, 23.20 ± 3.08 ms, R_{In} : 222.05 ± 18.11 MOhm, 256.39 ± 41.42 MOhm, Rheobase: 82.80 ± 9.07 pA, 90.85 ± 29.77 pA, AP amp: 68.00 ± 2.15 mV, 71.93 ± 5.13 mV, AP width: 0.49 ± 0.02 ms, 0.56 ± 0.06 ms (Figure 4.1c). These values are in agreement with results for MCs in juvenile rats and juvenile GIN-mice (Table 4.1) (Wang et al., 2004; Ma et al., 2006; McGarry et al., 2010).

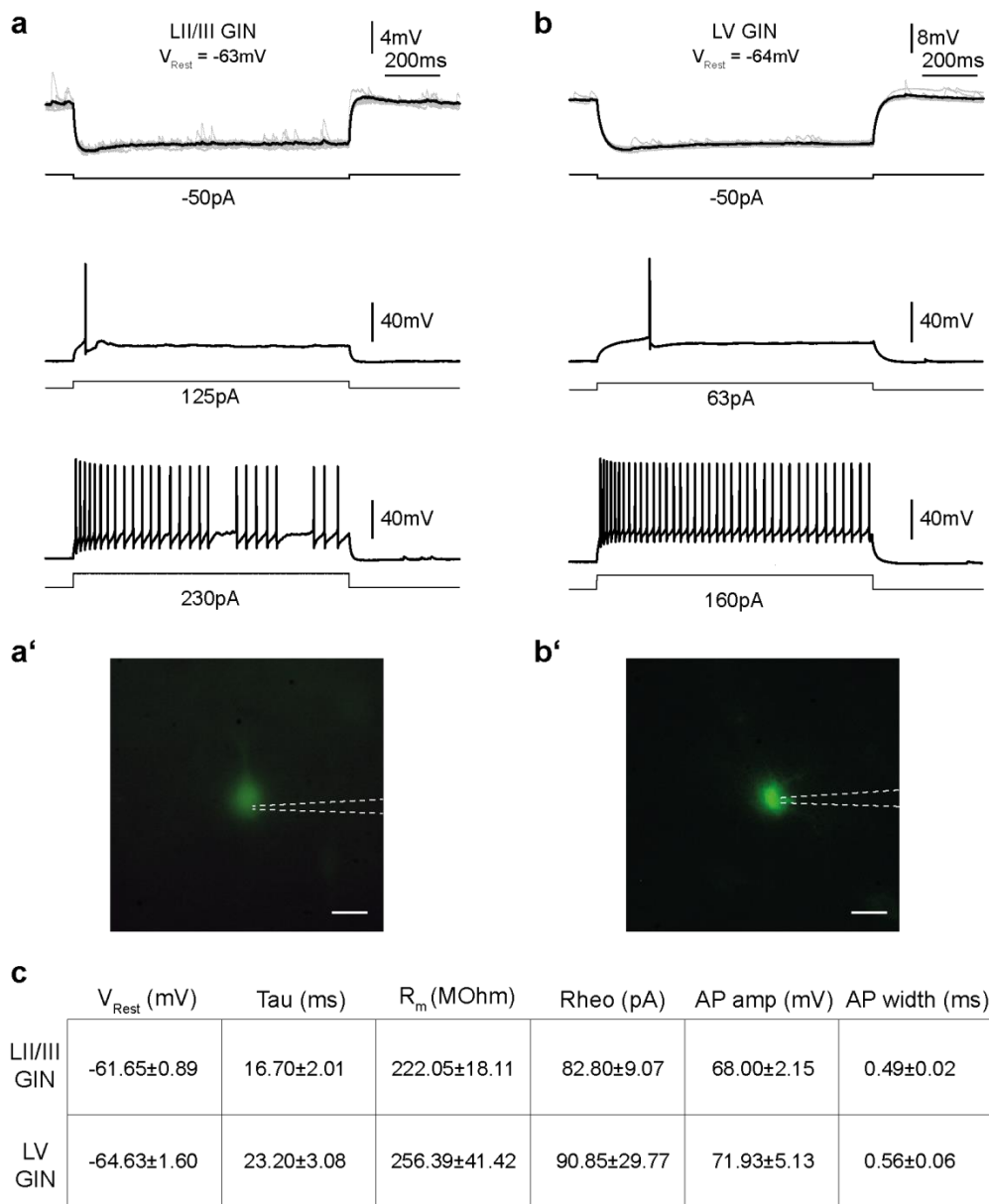


Figure 4.1: L II/III and V GIN cells show electrophysiological characteristics of MCs

a, b) *Top:* average response to a hyperpolarizing current of -50 pA, individual reponses are shown in gray. *Middle:* Minimum depolarizing current to elicit a single action potential (rheobase). *Bottom:* Response to a depolarizing current ~100 pA above rheobase. Note the adapting firing pattern typical for MCs.

a', b') Native brain slice showing widefield GFP fluorescence of GIN-cells recorded in **a** and **b**. Patch pipettes are delineated by dashed lines. Scale: 20 μm

c) Table showing quantification of electrophysiological parameters of L II/III and V MCs. Given are the values for the resting membrane potential (V_{Rest}), membrane time constant (Tau), membrane resistance (R_{Mem}), Rheobase (Rheo), action potential amplitude at firing threshold (AP amp) and action potential width at firing threshold (AP width). L II/III GIN: n = 20, L V GIN: n = 7. Given are mean \pm S.E.M.

Differences can be explained by the use of different model systems (rat vs. mice), differences in age (juvenile vs. adult) and differences in recording conditions (recordings at room temperature vs. recordings at 32°C). Due to the observed relatively low rheobase, the recorded cells are classified as low-threshold spiking cells. Furthermore, recorded cells exhibited a prominent “voltage sag” during application of hyperpolarizing currents and a rebound depolarization after this type of current injection (Figure 4.1a, b; top). During high depolarizing current injections an adapting firing pattern was observed in recorded GFP-expressing cells (Figure 4.1a, b; bottom). As MCs are described as low-threshold spiking cells with a high input resistance, prominent “voltage sag”, rebound depolarization and adapting firing pattern our results were in agreement with already known properties for this cell type (Kawaguchi and Kubota, 1996; Kawaguchi and Kondo, 2002; Goldberg et al., 2004; Wang et al., 2004).

Furthermore, MCs can be easily identified by an ascending axon and a broad axonal arborization within L I (Ma et al., 2006). In our case all GIN-cells, which could be morphologically recovered after biocytin labeling and ABC-DAB staining showed this specific axonal branching pattern. Examples of the somatodendritic and axonal configuration are shown as reconstructions of a L II/III and a L V cell in figure 4.2. Further examples of stained cells in L II/III and L V are given in figure 4.3 and figure 4.4, respectively. Although there seems to be a heterogeneity of somatodendritic and axonal configurations for L II/III cells, especially in axonal targeting of L II/III, the prominent feature of MCs, axonal

branches in L I, was always observed. The somatodendritic and axonal configuration of recorded L V cells seems to be homogenous, with vertically distributed arbors, local axonal innervation areas in L V and a few or even just one ascending axonal arbors branching in L I. Hence, as all GIN-cells in L II/III and V could be identified as MCs, on an electrophysiological as well on a morphological level, we will use the term Martinotti cell for all GIN-cells recorded in following experiments.

Table 4.1: Comparison of observed electrophysiological properties of L II/III and V MCs with data from literature

Table showing observed values for resting membrane potential (V_{Rest}), membrane time constant (τ), input resistance (R_{in}), Rheobase (Rheo), action potential amplitude (AP amp) and action potential width (AP width) of L II/III and V MCs in comparison to data for MCs from known literature. ¹Own observations from recordings of adult mice at 32°C, ²recordings from juvenile mice at room temperature (McGarry et al., 2010), ³recordings from juvenile mice at 32°C (Ma et al., 2006), ⁴recordings from juvenile rats at room temperature (Wang et al., 2004). Although values differ at some point between data sets, our observations are in general agreement with published data. Differences can be explained by differences in age, recording conditions and model system.

	V_{Rest} (mV)	τ (ms)	R_{in} (MOhm)	Rheo (pA)	AP amp (mV)	AP width (ms)
P21-36 GIN-mice L II/III¹ (n=20)	-61.65±0.89	16.70±2.01	222.05±18.11	82.80±9.07	68.00±2.15	0.49±0.02
P21-36 GIN-mice L V¹ (n=7)	-64.63±1.60	23.20±3.08	256.39±41.42	90.85±29.77	71.93±5.13	0.56±0.06
P10-18 GIN-mice L II/III & V² (n=24)	-65.34±0.44	/	469±35.84	36.04±6.36	55.41±2.55	1.65±0.08
P16-24 GIN-mice L II/III & V³ (n=33)	-67.1	20.09	282	51	58.1	0.55
P13-16 Wistar-rats L II/III⁴ (n=30)	-54.63±5.06	22.77±6.78	287.63±99.18	/	65.99±7.96	1.57±0.23
P13-16 Wistar-rats L V⁴ (n=14)	-54.57±6.57	25.59±12.06	371.98±156.52	/	66.26±7.12	1.64±0.23

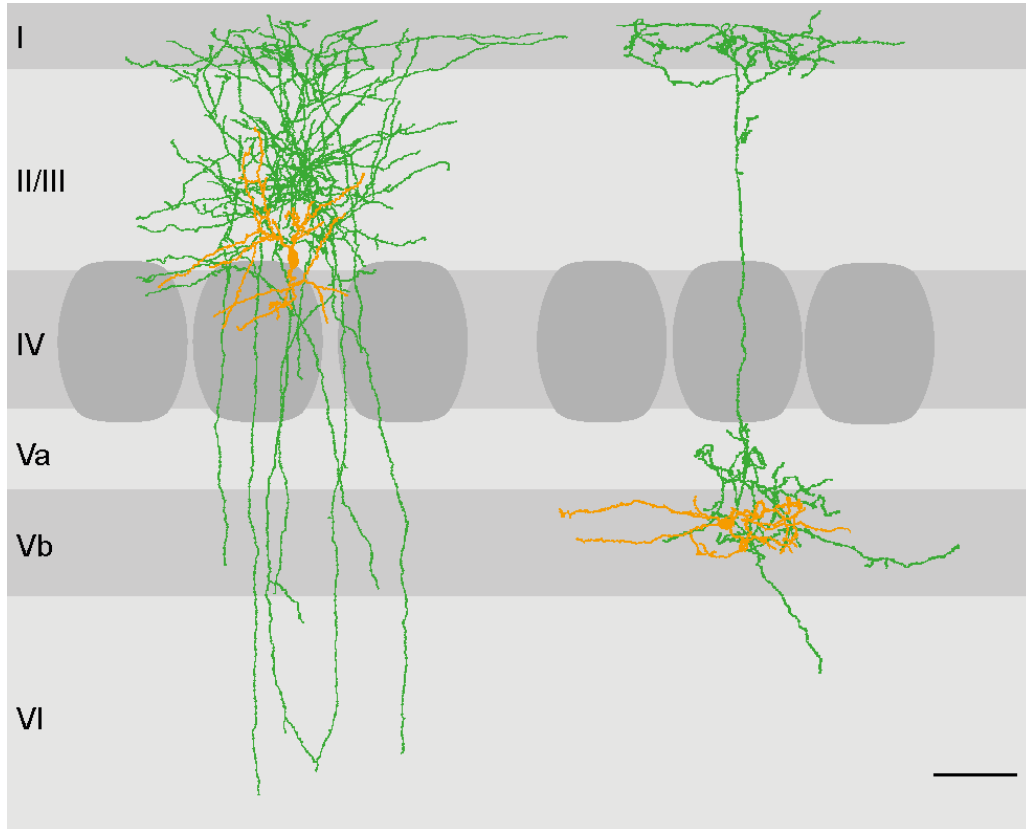


Figure 4.2: Morphological characteristics of MCs in L II/III and V

Reconstructions of L II/III GIN-cells with somatodendritic compartments in orange and axonal arborizations in green. Note the dense axonal branching in L I, which is indicative for MCs. These data were taken from experiments using potassium-based internal solution for whole cell recordings (shown in **figure 4.1**). Layers are labeled I-VI. Scale bar, 100 μm

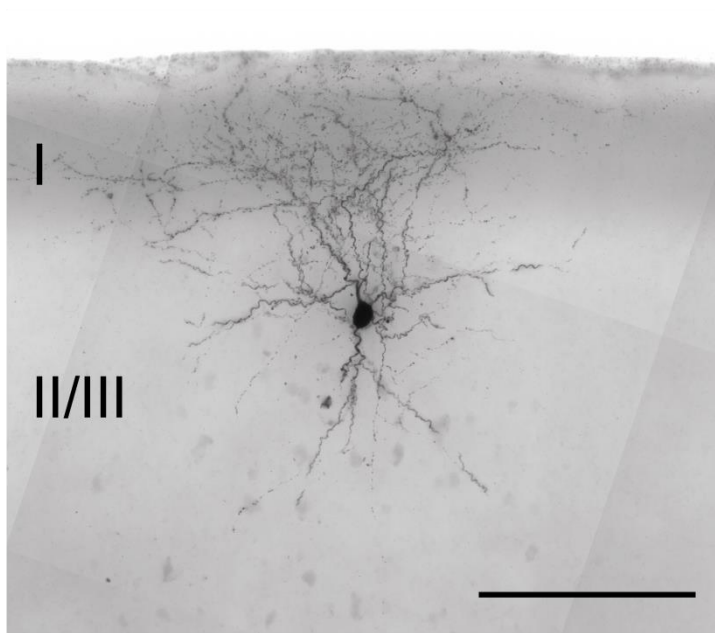
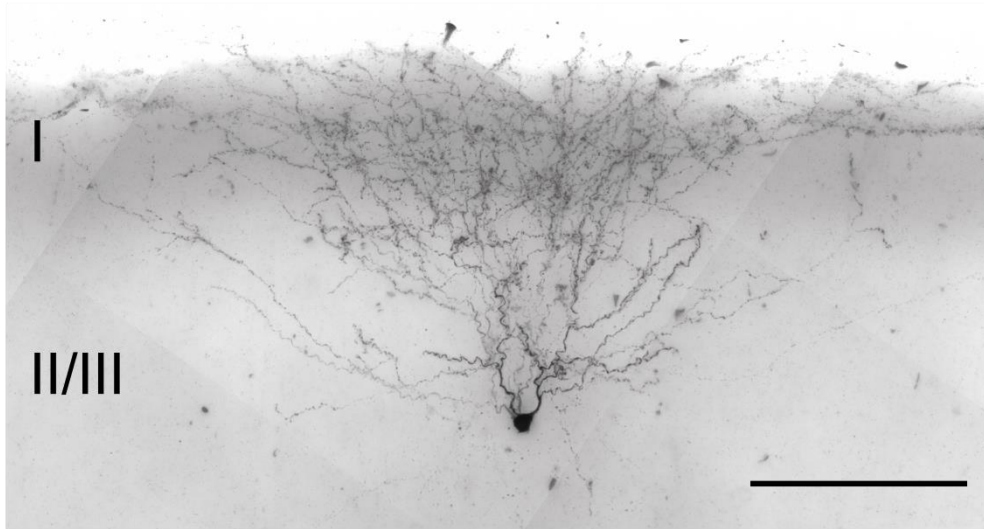


Figure 4.3: Layer II/III GIN cells show typical morphology of Martinotti cells

Shown are brightfield images (25x objective, minimum intensity projection) of biocytin filled and ABC-DAB stained GIN-cells. Note that both cells exhibit an ascending axon with axonal arborizations in LI, typical for MCs. Layer I and II/III are labeled, scale: 100µm

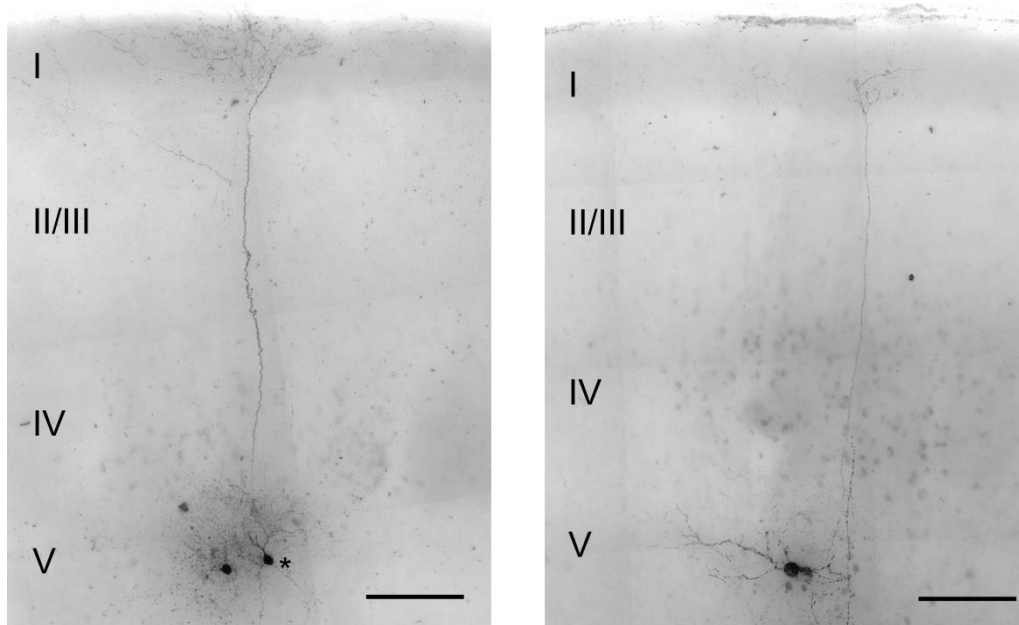


Figure 4.4: L V GIN cells show typical morphology of Martinotti cells

Shown are brightfield images (25x objective, minimum intensity projection) of biocytin filled and ABC-DAB stained GIN-cells. Note that both cells exhibit an ascending axon with axonal arborizations in L I, typical for MCs. Lower left: Asterisks indicates the soma of the recorded MC in L V. Layer I to V are labeled, scale: 200 μ m

4.2 Calibration of experimental set-up for focal photolysis of caged glutamate

One of the main topics of this work was to locate presynaptic inhibitory neurons projecting onto MCs in S1. We were especially interested in MCs located within barrel-related cortical columns, as within these the main processing of sensory information takes place. Thus, we used a combination of whole-cell patch-clamp recordings of MCs in L II/III and V and focal photolysis of caged glutamate to activate presynaptic INs and thereby defining their location in acute brain slices. We set up a series of calibration experiments to test whether (i) all probable presynaptic cells, i.e. different subtypes of IN, can be detected

independently of their projection pattern, e.g. dendritic versus somatic targeting, (ii) photolysis of caged glutamate can be used to specifically activate INs, and (iii) the resolution of this method was high enough to define the position of presynaptic INs within layers and columns.

GABA induced direct inhibitory responses can be detected independently of release site

Due to the so called space clamp problem, inhibitory currents elicited at dendritic sites might not be detectable with somatic recordings of MCs (Figure 3.4). To test whether those responses can be recorded with an electrode placed at the soma we used focal photolysis of caged GABA to cause inhibitory currents at different parts, soma as well as dendrites, of the recorded MC. Release of GABA, the main inhibitory transmitter in the nervous system, reliably caused direct inhibitory responses in both L II/III (n = 7) and V MCs (n = 4) on both somatic and dendritic levels (Figure 4.5a, a', b, b'). The amplitude of these responses at somatic levels ranged from 78.52 pA to 227.36 pA and was on average $143,189 \pm 12.84$ pA (n = 11). The amplitudes ranged from 6.49 pA to 227.36 pA, including values from dendritic and somatic release sites.

The highest amplitudes of responses in individual cells could always be detected at somatic release sites (Figure 4.5a, a', b, b'). The amplitudes of inhibitory responses decreased with the distance of the GABA release site from the soma (Figure 4.5a, a', b, b'). Nevertheless, in

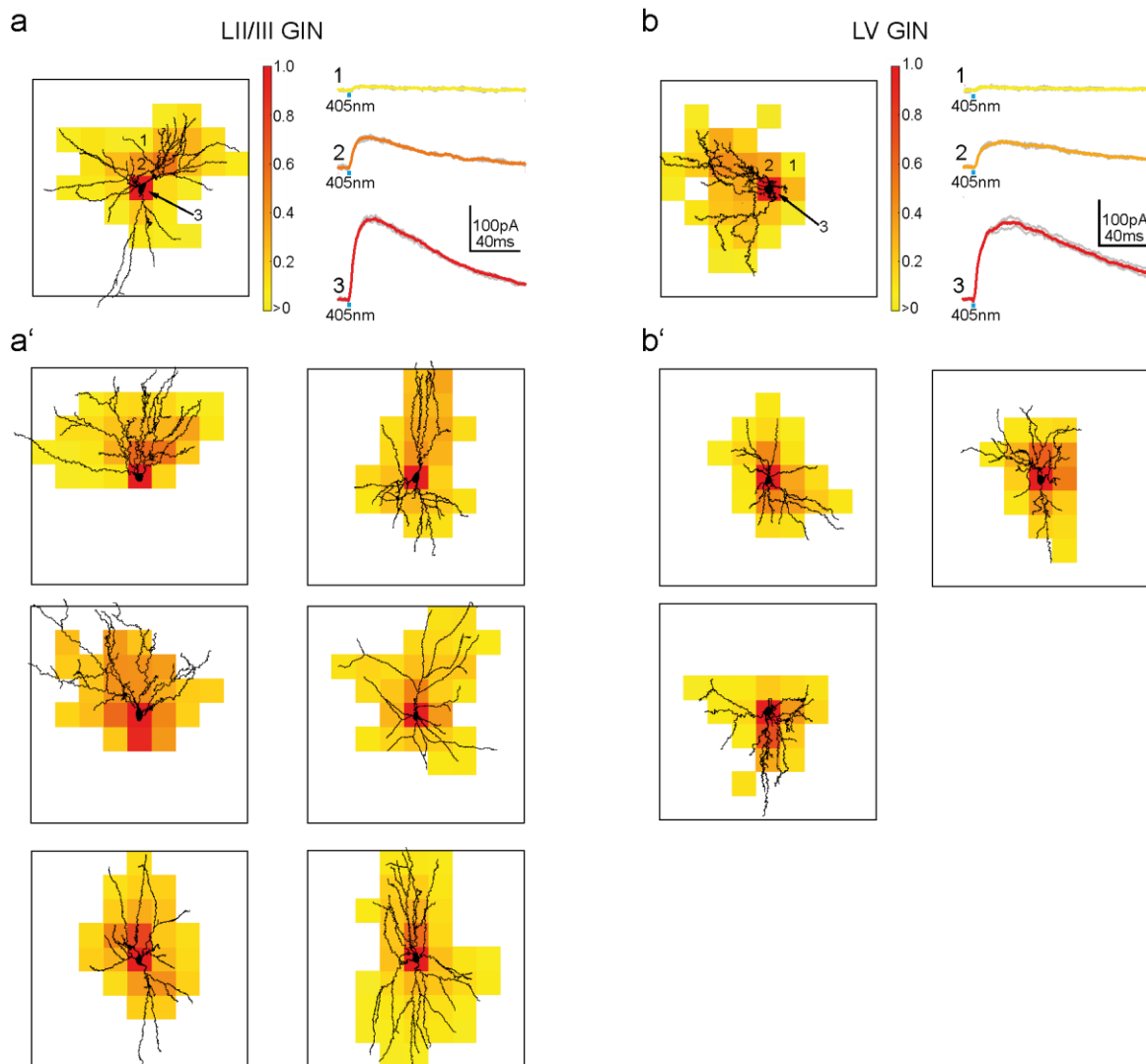


Figure 4.5: GABA-evoked IPSCs can be detected in all compartments of recorded GIN-cells

a, b) Example map of a GABA uncaging experiment while recording from a L II/III (**a**) or a L V GIN cell (**b**), which were somatodendritically reconstructed after ABC-DAB staining (left). The maps consist of 81 fields ($50 \times 50 \mu\text{m}$) and the soma of the recorded cell was centered. The color code depicts the average amplitude of direct IPSCs evoked by GABA release. The amplitudes were normalized to the average somatic IPSC. Example traces of direct IPSCs in fields labeled by 1-3 are given on the right. Average IPSCs, in response to GABA release via three repetitions of a 6 ms long laser (405 nm) stimulus (blue bar), are color coded in correspondence to their field. Individual responses are shown in gray.

a', b') GABA uncaging maps of six L II/III and three L V GIN cells. Note that fields including direct IPSCs cover almost the entire somatodendritic part of the recorded cells. The color code is according to the one in **a** and **b**.

many cases inhibitory events elicited even at distant dendritic parts (distances up to 250 μm) could be detected with a recording electrode placed at the soma (Figure 4.5a, a', b, b'). Although in some cases inhibitory responses could be elicited in fields seemingly not including dendritic parts this can be explained by an incomplete morphological recovery of recorded and biocytin-labelled cells. Nevertheless, the GABA release sites causing inhibitory responses covered almost all parts of the recorded cells and closely represent the somatodendritic configuration of individual cells (Figure 4.5a, a', b, b').

We are aware that focal photolysis of caged GABA is not directly applicable to synaptic GABA release but in principle we could show that it is possible to record inhibitory currents evoked by GABA release even at distant dendritic parts. Hence, it is less likely to miss inhibitory input of presynaptic INs, which might only target distant dendritic parts of MCs.

Focal photolysis of caged glutamate can directly induce spiking predominantly in inhibitory interneurons

In principle, all types of neurons can be activated by focal photolysis of caged glutamate. Although MCs were kept close to AMPA-receptor equilibrium potential ($\sim 0\text{mV}$), hence driving force for excitatory inputs should be low, activation of presynaptic excitatory neurons can lead to interference with the detection of inhibitory postsynaptic currents.

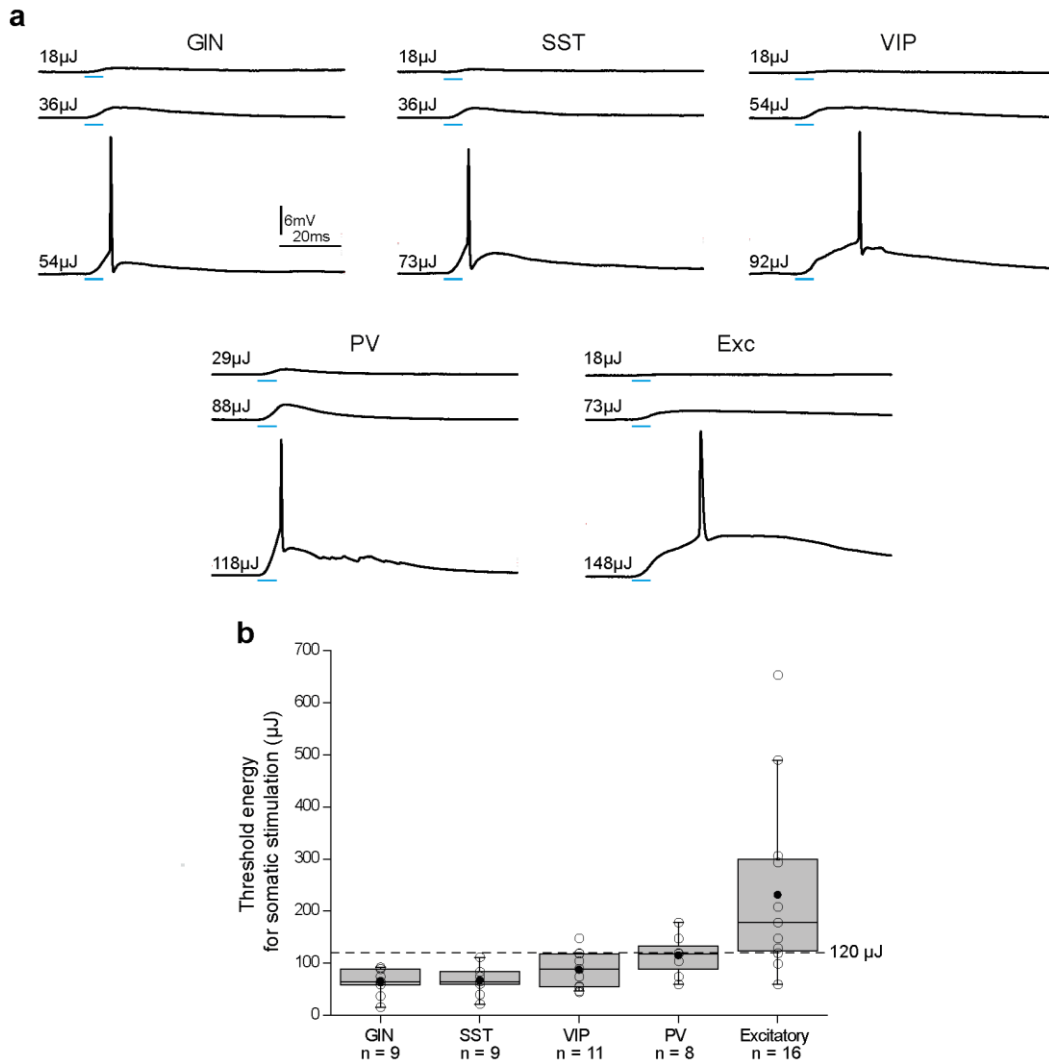


Figure 4.6: Different laser energies are needed to activate inhibitory and excitatory neurons by glutamate uncaging

a) Examples of direct activation of inhibitory (GIN, SST, VIP, PV) and excitatory neurons (Exc) in response to somatic glutamate release during uncaging experiments with increasing laser intensities. Laser stimulus is indicated by blue bar.

b) AP-threshold by glutamate uncaging. Box plots show the mean (filled circle), the median, and the interquartile range of laser energy necessary to pass firing threshold for inhibitory (GIN-, SST-, VIP-, and PV-cells) and excitatory cortical neurons at somatic locations. Whisker boundaries are the 10th and 90th percentile. Individual thresholds for recorded cells are depicted as open black circles. The dashed line marks the laser energy used during subsequent uncaging experiments (120 μ J). Note that under these conditions, ~86% of INs, but only ~25% of excitatory neurons were driven to threshold.

Hence, a series of experiments was set up to determine a laser energy (with the laser beam centered on the soma) generating spikes due to laser-induced glutamate release in as many inhibitory neurons as possible without activating a substantial proportion of excitatory ones. Therefore, PV-, VIP-, SST-, GIN-cells and excitatory neurons were recorded in current clamp at V_{Rest} . At least two cells of each neuronal type were recorded per layer ranging from layer II/III to VI. Afterwards, glutamate was released on the soma with increasing laser intensity.

Increasing laser energies caused increasing directly-evoked excitatory responses, very likely due to increased glutamate release (Figure 4.6a). In all cell types spiking could be induced with a certain laser energy used for somatic glutamate release (Figure 4.6a, b). This specific laser energy depended on stimulus length and the specific laser intensity could be calculated by using following formula: $J = W \cdot s$. On average this threshold laser intensity was $64.6 \pm 25.5 \mu\text{J}$ (Mean \pm SD) for GIN-cells ($n = 9$), $66.8 \pm 26.1 \mu\text{J}$ for SST-cells ($n = 9$), $86.7 \pm 34.6 \mu\text{J}$ for VIP-cells ($n = 11$), $114.5 \pm 37.7 \mu\text{J}$ for PV-cells ($n = 8$) and $230.9 \pm 159.3 \mu\text{J}$ for excitatory cells ($n = 16$). Furthermore, quantification of somatic threshold energy for spiking showed that a laser energy of $\sim 120 \mu\text{J}$ triggered APs in $\sim 88\%$ of all types of inhibitory cells located throughout all cortical layers (Figure 4.6b). Only 1 out of 11 VIP-cells and 2 out of 8 PV-cells showed a threshold above $120 \mu\text{J}$. With this specific laser energy spikes could be evoked in only $\sim 25\%$ of excitatory cells. Therefore, a laser energy of $\sim 120 \mu\text{J}$ was used in following experiments to localize presynaptic INs by focal photolysis of caged glutamate.

4.3 Localisation of inhibitory cells presynaptic to L II/III and V Martinotti cells

With the initial calibration experiments we were able to show (i) that focal photolysis of caged glutamate with a laser energy of 120 μ J is able to specifically activate INs and only a small proportion of excitatory ones and (ii) that we were able to detect inhibitory currents independently of their corresponding dendritic triggering site (caged-GABA experiments). As a first approach we wanted to test where presynaptic INs projecting onto MCs are located within different layers and columns of the barrel cortex.

We localized sources of monosynaptic inhibitory input to L II/III and V MCs by scanning specific areas including at least all cortical layers of the home column (containing the recorded MC) and the two neighboring columns with focal photolysis of caged glutamate while recording from MCs in acute thalamocortical slices (see methods in chapter 3.5). With this method we were able to specifically activate INs under certain conditions (see calibration experiments in chapter 4.2). In figure 4.7 the results of such scanning experiments are shown for a L II/III (Figure 4.7a) and a L V MC (Figure 4.7a'). In case of the L II/III MC, activation of presynaptic GABAergic cells in several fields located in L I and II/III led to IPSCs with amplitudes ranging from 13.43 pA to 69.81 pA, as indicated by the color code of the corresponding fields. Local inhibitory input, primarily from L Va and Vb, as well as interlaminar input, emanating from L II/III, was observed in case of the L V MC with

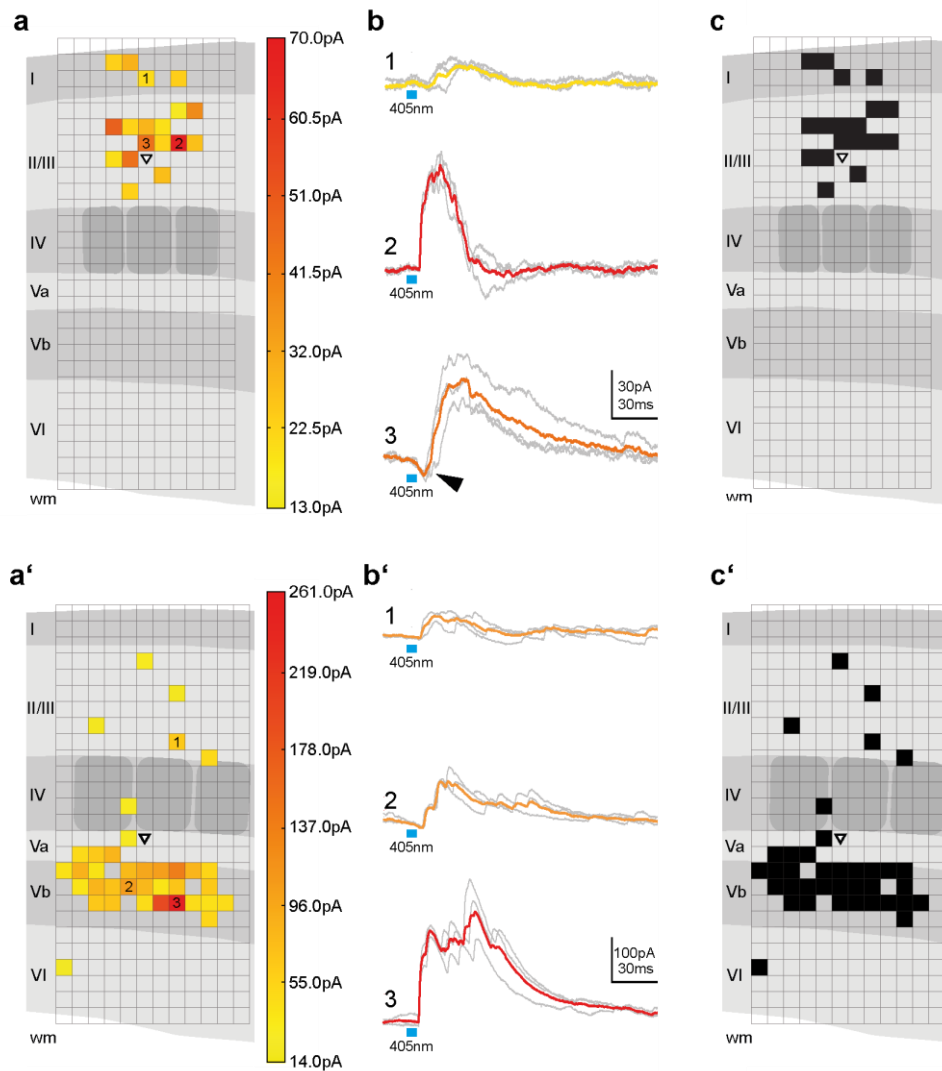


Figure 4.7: Mapping inhibitory input to L II/III and V MCs using glutamate uncaging

a, a') Example of a glutamate uncaging map of an MC (soma location: ∇) in L II/III (**a**) and L V (**a'**) of S1. Monosynaptic inhibitory responses were evoked in color-coded fields. These fields were located only in LI and II/III for L II/III MC. For L V MC, fields could be in LI and II/III for L II/III MC. The color code depicts the average IPSC amplitude per field. IPSC amplitudes seem not to correlate with distance from MC soma. Average responses evoked from numbered fields (1 - 3) are shown in **b, b'**. Layers are labeled I – VI, wm: white matter. Columns are indicated by schematic “barrels” in LIV (**a, a', c, c'**).

b, b') Average (color-coded) and individual (gray) compound IPSCs in response to three successive laser-stimulations (blue bar: 6 ms, 405 nm; laser energy: 120 μ J) of fields marked in **a, a'**. These examples show the typical range of amplitudes and waveforms. Note that example 3 in **b** consists of fast direct excitatory input (arrowhead) followed by strong monosynaptic inhibitory input.

c, c') Examples of binary glutamate uncaging maps. In binary maps, fields containing presynaptic INs are colored black regardless of the amplitude of the corresponding IPSC. The binary map here corresponds to the amplitude-coded example shown in **a, a'**. These maps ($n = 10$) were used to calculate: (i) the distribution of inhibitory fields with respect to layers and columns shown in **figure 4.8**, and (ii) the average confidence level map shown in figure 4.9. Layers are labeled I-VI, wm: white matter.

amplitudes ranging from 14.23 pA to 260.83 pA. Similar experiments were, overall, carried out with ten L II/III and V MCs, respectively. Considering all experimental data, IPSC amplitudes ranged from 6.25 pA to 260.83 pA. Interestingly, the average IPSCs often exhibited variable waveforms and several peaks. Examples of such compound IPSCs are shown in Figure 4.7b and b'. Variable waveforms might be explained by the activation of different subgroups of presynaptic INs. Multiple peaks can be explained by activation of several presynaptic INs within the field of glutamate release, triggering a series of spikes in a single presynaptic cell or a combination of both. In a few cases, responses consisting of fast direct excitatory input followed by strong monosynaptic inhibitory input could be detected (Figure 4.7b bottom). As the main focus was on the location of inhibitory inputs and not primarily on their precise amplitude, no measures to compute the true IPSC amplitude were taken in these cases. Interestingly, in case of the L V MC, IPSCs could also be evoked by glutamate release in fields located up to L II/III (Figure 4.7a'). This indicated a possible interlaminar connection between presynaptic INs and L V MCs.

For quantification of the amplitude-coded fields, shown as examples in Figure 4.7a and a', were converted into binary ones (Figure 4.7c, c'). In these cases fields containing presynaptic INs are colored black regardless of the amplitude of the corresponding average IPSC. These maps (L II/III MCs: n = 10, L V MCs: n = 10) were then used to calculate the distribution of inhibitory fields with respect to layers and columns. For L II/III MCs the distribution shows that the majority of these fields

	LII/III MCs				LV MCs		
	average field distribution (%)				average field distribution (%)		
	NC	HC	NC		NC	HC	NC
I	7.6	9.2	4.9	I	0	2.9	1.2
II/III	17.3	44.9	14.1	II/III	2.5	13.2	4.1
IV	0	1.1	0.5	IV	2.9	4.1	0.8
Va	0	0	0	Va	4.1	9.1	4.5
Vb	0	0.5	0	Vb	10.7	24.7	13.7
VI	0	0	0	VI	0	2.1	0

Figure 4.8 Distribution of inhibitory fields

a, b) Tables showing the layer- and column-specific distribution of inhibitory fields for the entire sample (L II/III MCs: n = 10, L V MCs: n = 10). We calculated the relative proportion of inhibitory fields for all layers in the home column (HC) of the recorded MCs as well as the two adjacent neighboring columns (NC). For **a**, note that the highest percentage of inhibitory fields (~45%) is found in L II/III of the home column. In case of L V MCs highest numbers of inhibitory fields can be found in L Vb of the home and neighboring columns and in L II/III of the home column.

(~45%) can be found within L II/III of the home column (Figure 4.8a). Furthermore, inhibitory fields could be found to a certain degree in L II/III of the neighboring columns (~14%, ~17%) and L I of all columns (home columns: ~9%; neighboring columns: ~4%,~8%). In case of L V

MCs the distribution is more widespread and inhibitory fields could be found in almost all parts of the scanned areas (Figure 4.8b). Nevertheless, the highest value could be found in L Vb of the home column (~25%), minor numbers especially in L II/III of the home column (~13%) and in L V of the neighboring columns (~11%, ~14%).

Next, we generated average maps for L II/III and V MCs across the entire sample (L II/III MCs: n = 10, L V MCs: n = 10) illustrating the confidence level for the position of inhibitory fields (Figure 4.9a, b). For L II/III MCs confidence levels above 90% are mainly found in the upper part of L II/III of the home column (Figure 4.9a). As mentioned, the highest proportion of inhibitory fields was found in this area (Figure 4.8a). In case of L V MCs, confidence levels above 90% are found in L Va and Vb of the home column and also in the same layers of the neighboring columns (Figure 4.9b). Interestingly, another area with a similar high confidence level (>90%) was found in L II/III of the home column (Figure 4.9b).

In summary, L II/III receive inhibitory input from local INs only, whereas L V MCs receive inhibitory input from local INs and additionally interlaminar input from INs located in L II/III. Furthermore, the variable waveforms of IPSCs indicate the involvement of several IN subtypes in the inhibition of MCs.

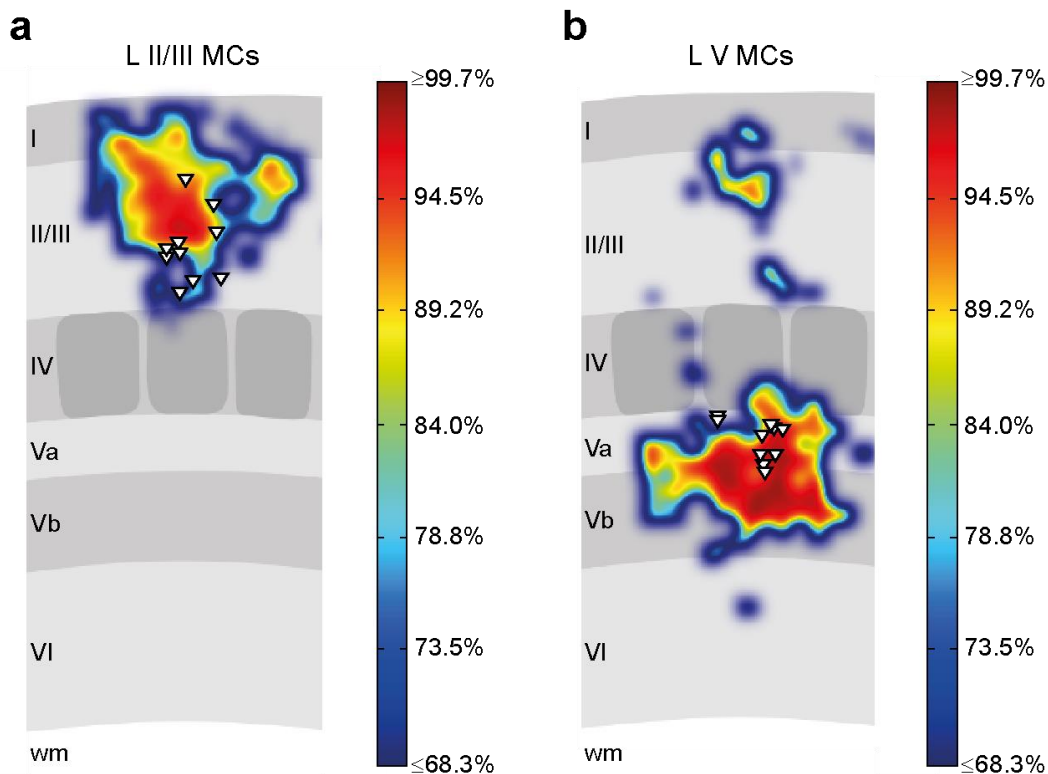


Figure 4.9: Localization of presynaptic inhibitory cells to L II/III and V MCs

a, b) Average maps (L II/III MCs: $n = 10$, L V MCs: $n = 10$) illustrating the confidence level for the distribution of monosynaptic inhibitory input. Note that for L II/III MCs confidence levels $\geq 90\%$ are predominantly found in L II/III of the home column and neighboring columns, but also extend to some degree into L I. For L V MCs, confidence levels $\geq 90\%$ are predominantly found in L Va and Vb of the home column and neighboring columns and to some degree in L II/III. Confidence levels ($\leq 68.3\%$ to $\geq 99.7\%$) are color-coded. Layers are labeled I-VI, wm: white matter.

4.4 Paired recordings of presynaptic INs and L II/III and V Martinotti cells

The results of the previous experiments showed a distinct localization of presynaptic INs to L II/III and V MCs and, considering the variable waveforms of induced IPSCs by glutamate release, indicated the involvement of several IN subtypes. Yet, the precise cellular identity of these cells remained to be established. As mentioned, PV- and VIP-

expressing cell are two major IN subpopulations not including SST-expressing cells and hence, were probable presynaptic candidates projecting onto L II/III and V MCs. The triple transgenic mouse lines PV-cre::tdTomato::GIN and VIP-cre::tdTomato::GIN were created to investigate if PV- and VIP-cells target MCs, respectively. Paired recordings of presynaptic INs located in areas defined by glutamate uncaging experiments (Figure 4.9a, b) and postsynaptic MCs in L II/III and V were used to test for unitary connections.

4.4.1 PV- and VIP-cells project onto L II/III Martinotti-cells

At first, we investigated the local inhibitory input to MCs located in L II/III of the cortex. In tested pairs 12 out of 21 PV-cells projected onto MCs, but only 11 out of 31 VIP-cells. Hence, the connection probability of PV-cells (~58%) was substantially larger than the one of VIP-cells (~35%) (Figure 4.10b). In both identified unitary connections repetition of single presynaptic spikes caused IPSCs with slightly variable amplitudes (Figure 4.10a). It was shown that this variability can be accounted for by deviant amounts of transmitter released in response to a single presynaptic spike (Liu, 2003; Biró et al., 2006). Nevertheless, the synaptic transmission was highly reliable (PV to MC: ~90%, n = 12; VIP to MC: ~80%, n = 11) (Figure 4.10b). Even though the connection probability of the two unitary connections was substantially different, the highly reliable synaptic transmission was indicative of very specific roles in inhibition of MCs for both cell types. If recordings were still stable

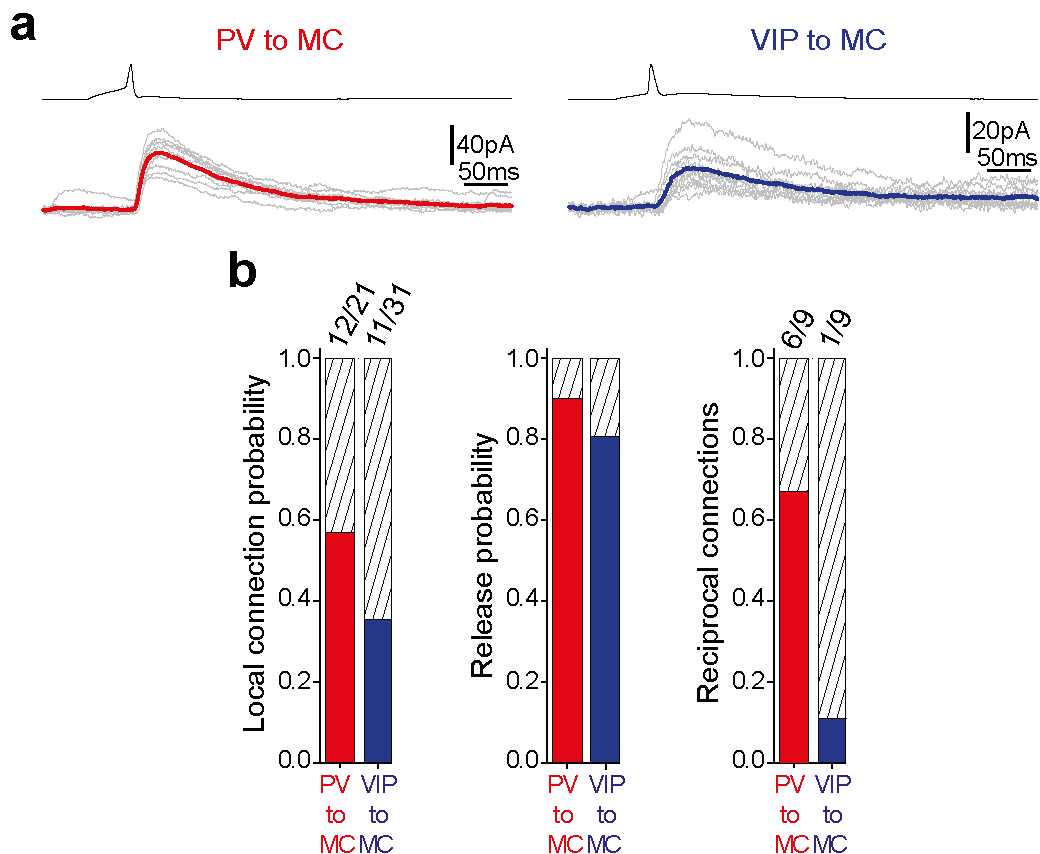


Figure 4.10: Connection properties of presynaptic PV- and VIP-cells and postsynaptic L II/III MCs

a) Connected pairs in L II/III of presynaptic cells (PV or VIP) and postsynaptic MCs. Presynaptic spikes reliably evoked IPSCs in both cases (gray traces). The average IPSCs of ten stimulus repetitions are shown in color (PV to MC: red, VIP to MC: blue).

b) Connection (left), release probability (middle), and amount of reciprocally connected pairs (right) of the two different kinds of unitary connections. Note that the connection probability of PV-cells (~58%, 12/21) is substantially larger than the one of VIP-cells (~35%, 11/31). In connected pairs, synaptic transmission is highly reliable independently of the type of the presynaptic cell. Furthermore, note that a reciprocal connection was more likely in case of connected pairs of PV-cells and MCs (~67%, 6/9) than in case of the VIP to MC connection (1/9, ~11%).

after preceding experiments to investigate PV- and VIP-inputs onto MCs, connected pairs were also tested for a reciprocal connection. A substantial difference was observed for the two identified unitary connections, whereas 6 out of 9 (~67%) pairs of PV-cells and MCs were reciprocally connected, only 1 VIP to MC pair out of 9 (~11%) showed a

reciprocal connection (Figure 4.10b). Unfortunately, due to the recording conditions, i.e. the drastic effect of cesium-based internal on AP shape in MCs, reciprocal connections could not be investigated for further comparisons.

With paired recordings we could show that nearby (distances up to 200 μm) PV- and VIP-cells target L II/III MCs. Presynaptic PV- and VIP-expressing INs showed electrophysiological and morphological characteristics, as described before (Lee et al., 2010; Prönneke et al., 2015). PV-cells exhibited a fast spiking pattern, whereas VIP-cells showed high-threshold bursting or a continuous adapting pattern (examples in Figure 4.11a). Also morphologies typical for PV- respectively VIP-cells were observed, an example of a PV- and a VIP-cell are shown in figure 4.11b. Whereas PV-cells in almost all cases had the appearance of basket-like cells, VIP-cells showed the configuration of bipolar cells.

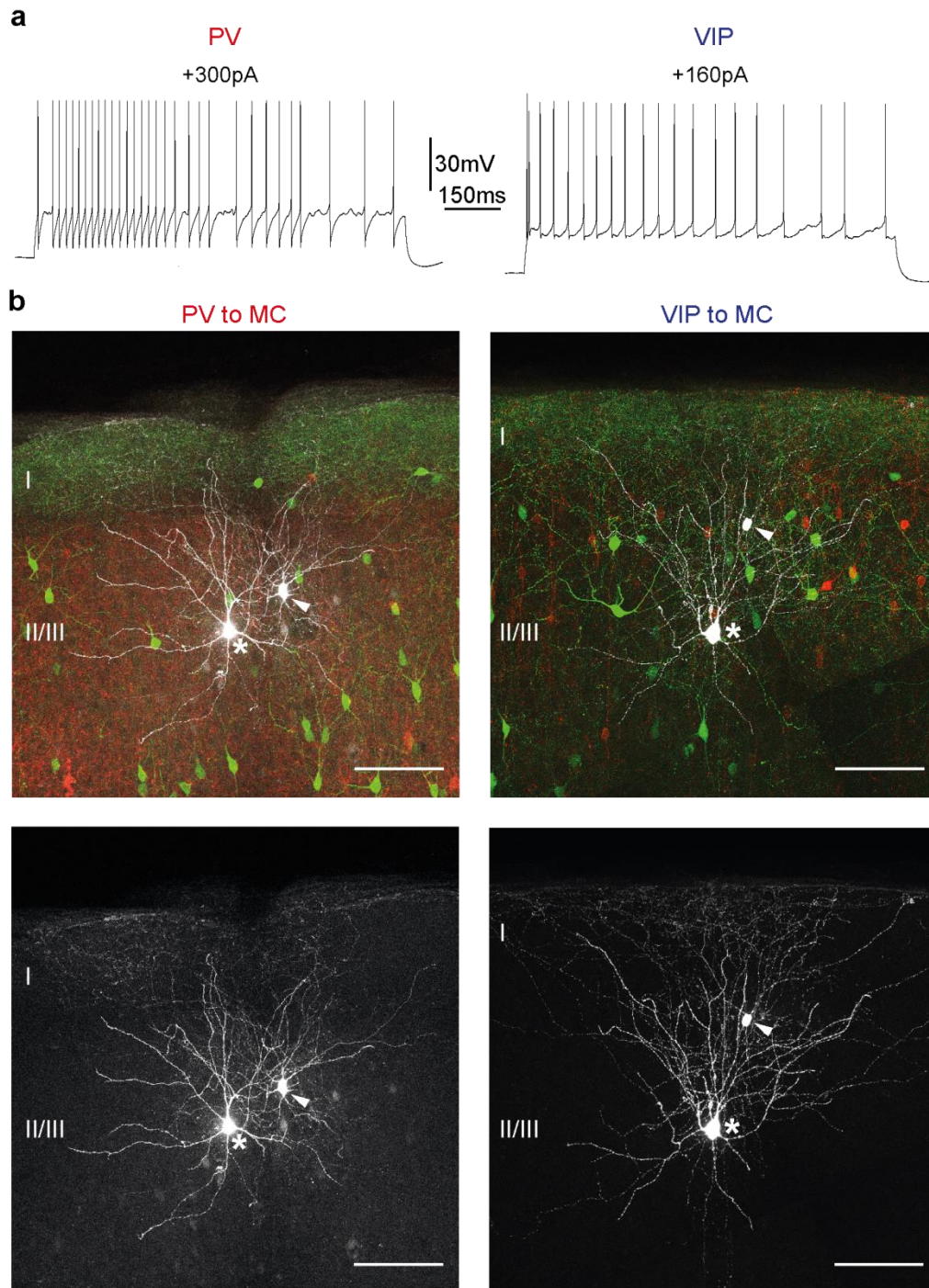


Figure 4.11: Morphology and electrophysiology of L II/III PV-MC and VIP-MC pairs

a) Whole cell recordings of a presynaptic PV- (left) and a VIP-cell (right), both connected to a recorded postsynaptic MC. During depolarizing current injections, the PV-cell shows a fast spiking pattern, whereas the VIP-cell shows a high-threshold bursting pattern.

b) Staining of acute brain slices containing synaptically connected and morphologically recovered pairs (left: PV to MC, right: VIP to MC). The connected cells are shown in white (pseudo-colored). Asterisks mark MC somata and arrowheads somata of presynaptic cells. GIN-cells are labeled green and the corresponding presynaptic population (PV or VIP) is labeled red (tdTomato-fluorescence). For clarity, connected cells are shown separately as gray-scale images at the bottom. The recorded PV-cell exhibits a multipolar dendritic morphology and an axon that is directed toward the pia, as described for basket cells. The VIP-cell shows an atypical tripolar dendritic configuration and an axon descending toward the white matter. Layers are labeled I-III. Scale bars, 100 μ m

4.4.2 Identified unitary connections of PV- versus VIP-cells onto L II/III MCs differ in elementary synaptic properties and short-term plasticity

After identifying PV- as well as VIP-cells as being presynaptic to L II/III MCs, the synaptic properties of these unitary connections were analyzed. As mentioned above, repetitive triggering of single presynaptic APs reliably caused IPSCs in MCs of both unitary connections. To investigate the elementary synaptic properties of these IPSCs, ten successfully elicited inhibitory responses by presynaptic APs were used to calculate an average IPSC per individual connected pair. These average IPSCs were then used to produce a grand average of inhibitory responses for both the PV to MC (n = 12) and VIP to MC (n = 11) connections (Figure 4.12a). Figure 4.12b shows the direct comparison of the grand average IPSCs of the two unitary connections. These seem to differ in several aspects like amplitude and latency. Indeed, quantification of IPSC kinetics showed that the average IPSC evoked by PV-cells had a significantly larger amplitude (PV to MC: 49.74 ± 12.97 pA, VIP to MC: 12.13 ± 3.57 pA), shorter latency (PV to MC: 0.60 ± 0.07 ms, VIP to MC: 1.39 ± 0.12 ms), shorter time to peak (PV to MC: 3.58 ± 0.38 ms, VIP to MC: 8.17 ± 1.34 ms), and steeper slope (PV to MC: 15.87 ± 4.61 pA/ms, VIP to MC: 2.09 ± 1.00 pA/ms) in comparison to VIP-cell evoked IPSCs (Figure 4.12c). These results could be explained by differences in subcellular targeting of MCs by PV- and VIP-cells, where PV-cells might target the perisomatic part and VIP-cells the dendritic part of MCs. Another explanation for different

IPSC kinetics might be corresponding to a differential subunit composition of postsynaptic GABA_A-receptors or a combination of both (Figure 5.1).

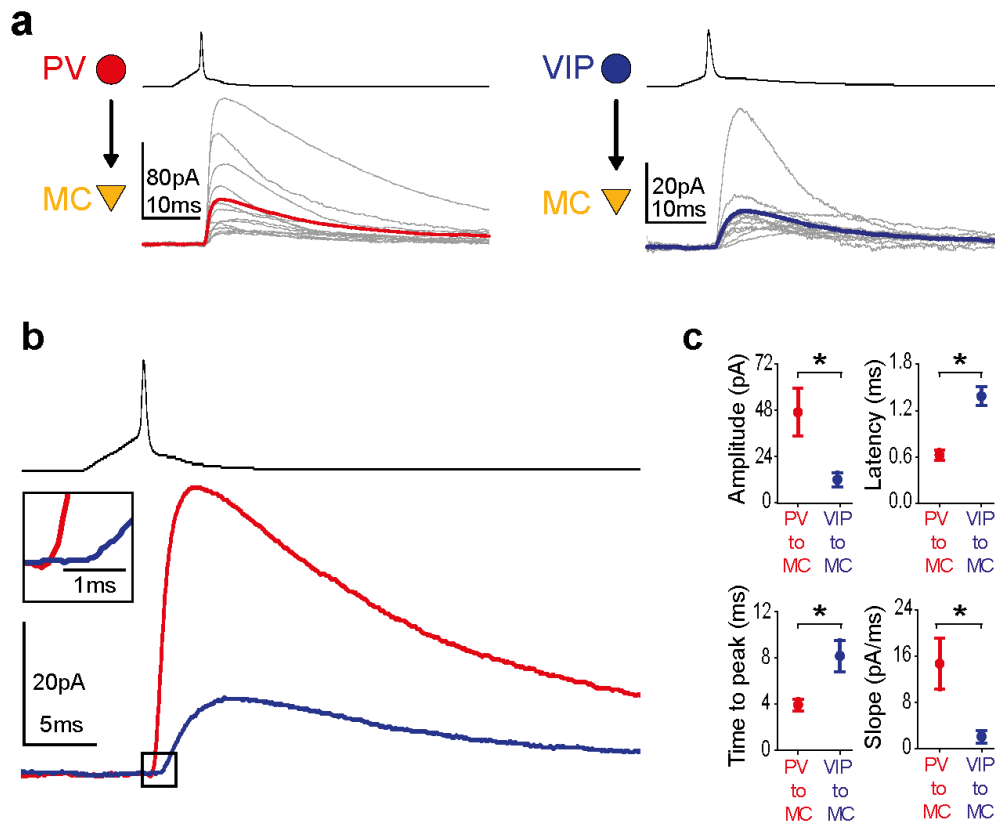


Figure 4.12: Unitary connections of PV- and VIP-cells onto L II/III MCs differ in their elementary synaptic properties

a) Grand average of unitary IPSCs (red: PV to MC, n=12; blue: VIP to MC, n=11) in MCs in response to a single spike repeatedly evoked in presynaptic INs. Averages of individual pairs are shown in gray

b) Overlay of grand averages (from **a**) aligned with respect to presynaptic spike peaks. IPSCs evoked by PV- and VIP-cells differ substantially in size and kinetics. For clarity, the boxed initial phase of both responses is shown at higher resolution as inset.

c) Quantification of unitary IPSCs. Amplitude, latency, time to peak, and slope were analyzed based on averages of each individual connected pair (PV to MC: red; VIP to MC: blue). Mean \pm S.E.M was then calculated for each group separately. Asterisks (* $p < 0.05$) indicate significant differences for all parameters.

Information processing is subject to short-term dynamic changes in synaptic transmission (Citri and Malenka, 2008; Fioravante and Regehr, 2011). Therefore, we triggered trains of presynaptic spikes at different frequencies (1, 8, 40 Hz) to investigate short-term plasticity for both types of pairs, PV to MC and VIP to MC (Figure 4.13a). The two examples in figure 4.13a show the typical average response of a single MC in response to five consecutive spikes in a presynaptic PV- or VIP-cell at 1, 8 and 40 Hz. Here the postsynaptic MCs responded reliably in case of every stimulus condition. The differences in IPSC amplitudes, (PV-cells on average induce IPSC with higher amplitudes) were still obvious. The spiking PV-cell caused on average a depressing inhibitory input already with a 1 Hz spike train. Also for the 8 and 40 Hz spike train a depressing input was observable. With a 40 Hz stimulus a postsynaptic summation effect of the consecutive IPSCs occurred. Nevertheless, this summation did not antagonize the depressing presynaptic component. On the other hand, no obvious change of the average IPSC could be observed with an evoked 1 and 8 Hz spike train of a presynaptic VIP cell. But with a 40 Hz stimulus the inhibitory responses clearly facilitated. On average, at low stimulus frequencies of 1 and 8 Hz the PV-input exerts higher amplitudes than the VIP-cell input even at depressed states (Figure 4.13d). Using a 40 Hz stimulus, only the first response to the spike train was significantly larger for the PV to MC connection as compared to the VIP to MC connection. The difference for the following IPSCs were not significantly different.

Furthermore, the responses to the fifth spike even had similar amplitudes in both unitary connections (Figure 4.13d)

Comparison of the average IPSC amplitude change showed that already with a presynaptic AP frequency of 1 Hz the PV to MC connection showed significant depression in IPSC amplitude (Figure 4.13b, c). In this case the IPSC amplitude changed significantly from 1st to 2nd response with an average drop of $19.20 \pm 4.07 \%$ ($n = 11$). The following three IPSCS remained at a similarly reduced amplitude level. With an 8 and 40 Hz AP frequency the amplitude change between 1st and 2nd IPSC further increased (8 Hz: $33.37 \pm 5.42 \%$, $n = 10$; 40 Hz: $42.75 \pm 4.11 \%$, $n = 10$) and showed a tendency to further declining amplitudes of the following responses was observable (Figure 4.13b, c). By contrast, repetitive firing in VIP-cells caused neither synaptic depression nor facilitation of inhibitory inputs to MCs with a 1 and 8 Hz stimulus. But a significant increase of IPSC amplitudes could be observed at 40 Hz causing a facilitating response with an amplitude increase of $87.74 \pm 24.82 \%$ from the first to the last response (Figure 4.13b, c).

In conclusion, our results show that PV-cells exert inhibitory input to L II/III MCs with higher amplitudes, shorter latency and faster kinetics than local VIP cells. Furthermore, PV-cells cause depressing inhibitory input to MCs already at low firing rates, whereas VIP-cells cause facilitating input only at higher frequencies.

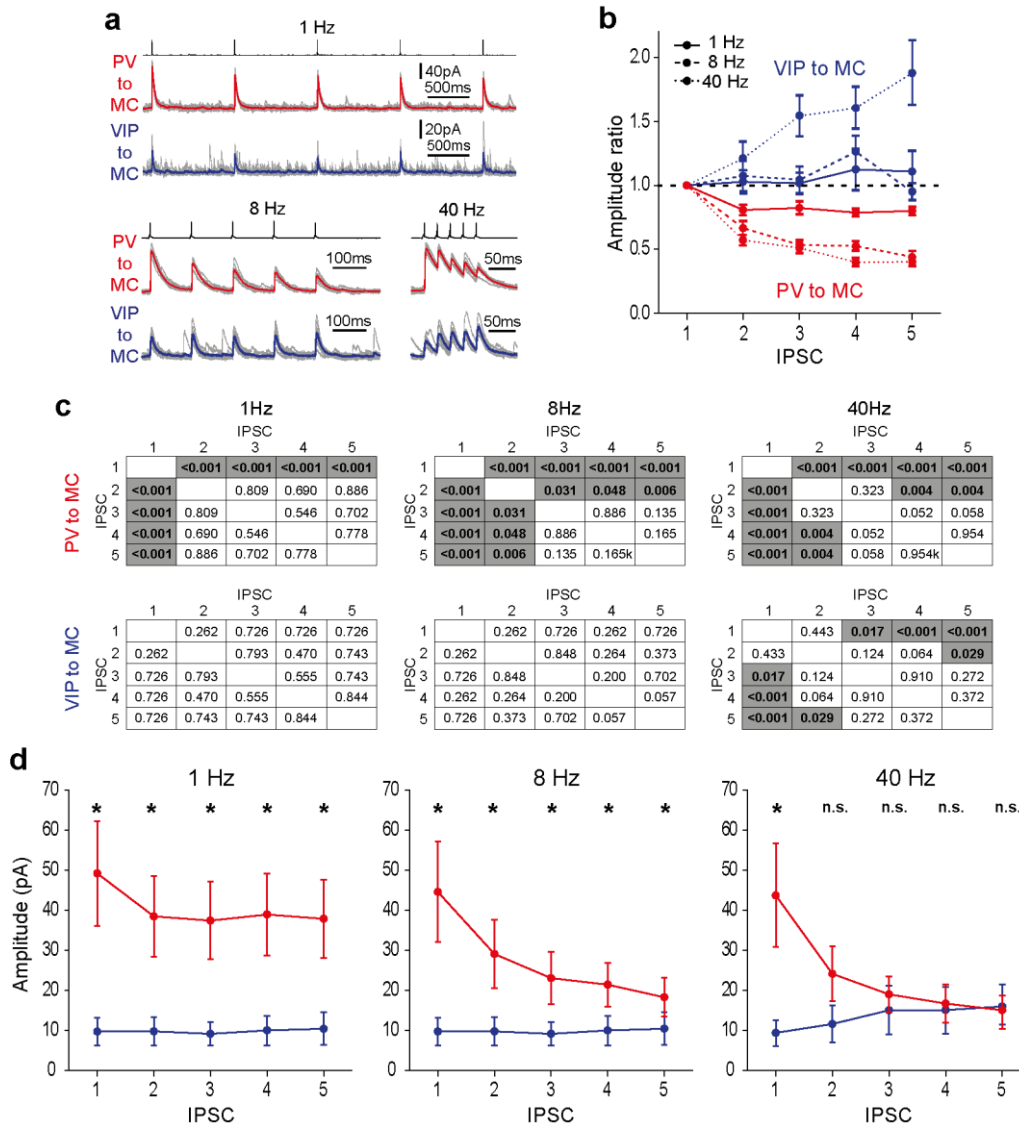


Figure 4.13: Unitary connections of PV- and VIP-cells onto L II/III MCs differ in short-term plasticity

a) Individual examples of averaged IPSCs in MCs in response to trains of five spikes (1, 8 and 40 Hz) in a presynaptic IN (PV to MC: red trace; VIP to MC: blue trace). Individual traces are shown in gray. Quantification is shown in b.

b) Quantitative analysis of short-term plasticity at different frequencies. Amplitude-ratio (n^{th} response/ 1^{st} response) of consecutive IPSCs plotted versus successive IPSCs. At the population level, PV to MC responses show synaptic depression under all stimulus conditions, whereas VIP to MC responses show no significant changes in amplitude at low frequencies but facilitate at 40 Hz.

c) Tables containing p-values of the statistical analysis of normalized IPSC amplitudes for both PV to MC (top row) and VIP to MC connections (bottom row) and for the different stimulus frequencies (1, 8, and 40 Hz). Amplitude ratios (n^{th} -response/ 1^{st} -response) were calculated and compared among each other. Significant differences ($P < 0.05$) are indicated by gray shading. Under all stimulus conditions, short-term plasticity was observed for the PV to MC connection. With a 1 Hz stimulus there is a significant difference between the 1^{st} and the four subsequent IPSCs, which remain at a similarly depressed amplitude level. Higher frequencies (8 and 40 Hz) induce further change in amplitude. For the VIP to MC connection synaptic plasticity was absent during 1 Hz and 8 Hz stimuli. With a 40 Hz-stimulus, a significant facilitation of the IPSC amplitude was observed for the last three responses with respect to the 1^{st} IPSC. →

d) Shown are the average IPSC amplitudes in MCs in response to a train of five spikes in presynaptically coupled INs (PV to MC: red trace; VIP to MC: blue trace) at different frequencies (1 Hz: PV to MC, n = 11; VIP to MC, n = 11; 8 Hz: PV to MC, n = 10; VIP to MC, n = 11; 40 Hz: PV to MC, n = 10; VIP to MC, n = 10). Note that during 1 and 8 Hz stimulation PV-cells cause on average IPSCs with higher amplitudes even at depressed states in comparison to the VIP-input. Only with a 40 Hz stimulus the amplitudes of PV- and VIP-inputs converge and reach a similar amplitude level in response to the 5th presynaptic spike.

4.5 Paired recordings of presynaptic INs and L V

Martinotti cells

We were able to show that L II/III MCs receive inhibitory input from local PV- as well as VIP-cells with different elementary synaptic properties and short-term plasticity. Next, we focused on inhibitory input to MCs in L V of the barrel cortex. There, this specific cell type is targeted by nearby L V and more distant L II/III INs, as shown by the preceding experiments using focal photolysis of caged glutamate (Figure 4.9b).

4.5.1 Innervation of L V MCs by PV-cells

As PV-cells are the most common inhibitory interneurons (Figure 2.2), we first focused on this cell type as probable presynaptic cells. Like in L II/III, we found locally connected pairs of presynaptic PV-cells and postsynaptic MCs (distances up to 200 μm) (Figure 4.14). These presynaptic PV-cells also exhibited the typical fast spiking pattern and basket-like morphology as described above (Figure 4.15a, b). An

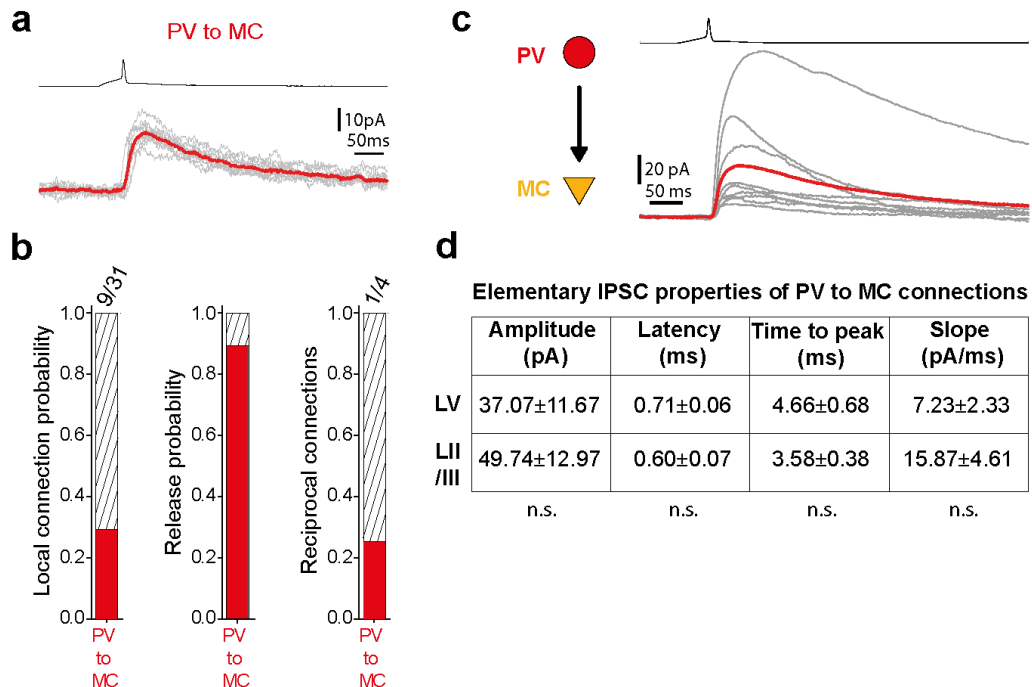


Figure 4.14: The local unitary connection of PV-cells onto L V MCs shows similar properties than the L II/III PV to MC connection

a) Connected pair in L V of presynaptic PV-cell and postsynaptic MC. Presynaptic spikes reliably evoked IPSCs (gray traces). The average IPSCs of ten stimulus repetitions are shown in color (red).

b) Connection probability (left), release probability (middle), and proportion of reciprocally connected pairs (right) in case of PV to MC paired recordings in L V. In contrast to L II/III, the connection probability is considerably smaller (~29%). In connected pairs, Synaptic transmission between coupled cells is highly reliable. Although the amount of reciprocal seems to be different, the actual number of tested pairs is too low for a reliable comparison.

c) Grand average of unitary IPSCs (red) in MCs in response to a single spike repeatedly evoked in presynaptic PV-cells. Averages of individual pairs are shown in gray.

d) Table showing the elementary IPSC properties of local PV to MC connections in L V (n = 9) and II/III (n = 12). Compared are the amplitude, latency, time to peak and slope of IPSCs. Note that no significant difference could be observed between the given values (shown as mean ± S.E.M.).

example of a local PV to MC connection in L V is given in figure 4.14a. In this case repetitive stimulation using a single presynaptic spike reliably caused an inhibitory response in the postsynaptic MC. In general, the release probability of L V PV to MC connections was highly reliable (~89%) (Figure 4.14b). The connection probability of PV to MC connections was ~29% (Figure 4.14b). Additionally, only 1 out of 4 tested pairs was reciprocally connected (Figure 4.14b). But the number of tested pairs was too small to make a general assumption.

Investigation of synaptic properties of PV to MC connections in L V showed that IPSCs had on average ($n = 9$) an amplitude of 37.07 ± 11.67 pA, a latency of 0.71 ± 0.06 ms, a time to peak of 4.66 ± 0.68 ms, and a slope of 7.23 ± 2.33 pA/ms (Figure 4.14c, d). As described before a train of five spikes was triggered in presynaptic PV-cells with frequencies of 1, 8 and 40 Hz to observe short-term plasticity. The example of an individual pair in figure 4.16a shows a slightly depressing postsynaptic inhibitory input while applying a 1 Hz stimulus, whereas on average the first IPSC shows the highest amplitude and the four following IPSCs had similar decreased amplitudes. Using an 8 Hz stimulus this depressing input became more obvious. With a presynaptic spike train of 40 Hz a summation effect occurred, causing overall increased amplitudes of the consecutive responses. However, the amplitude of individual responses decreased despite of the postsynaptic summation effect. Indeed, quantification of IPSC amplitudes showed a depressing input with a 1 Hz stimulus (Figure 4.16b). On average the IPSC amplitude decreased significantly from the

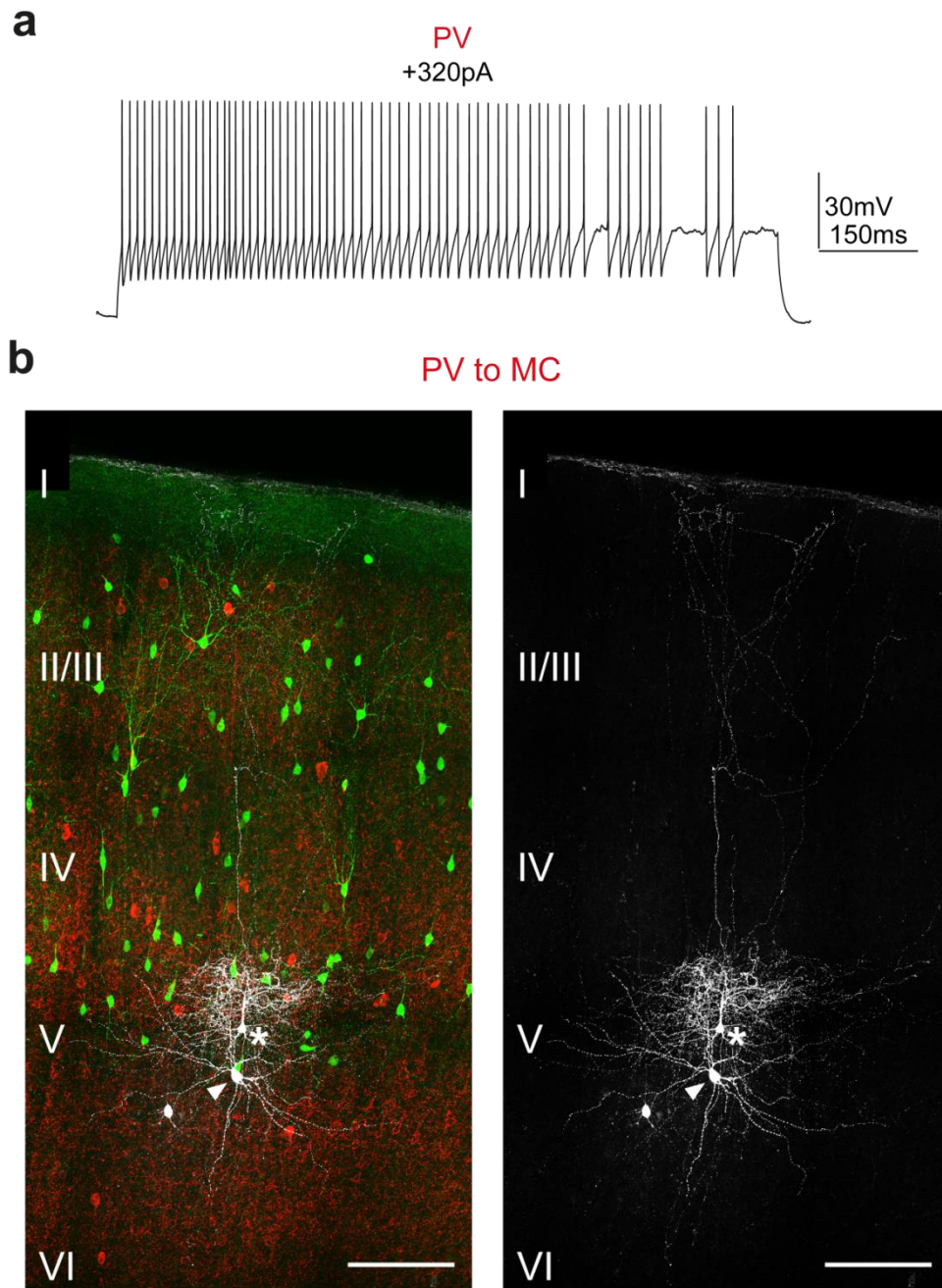


Figure 4.15: Morphology and electrophysiology of a L V PV-cell coupled to a L V MC

a) Whole cell recordings of a presynaptic PV-cell, which was connected to a recorded postsynaptic MC. During depolarizing current injections, the PV-cell shows a fast spiking pattern.

b) Staining of an acute brain slices containing a synaptically connected and morphologically recovered PV to MC pair. The connected cells are shown in white (pseudo-colored). Asterisks mark the MC soma and the arrowhead the soma of the presynaptic PV-cell. GIN-cells are labeled green and the PV-cell population is labeled red (tdTomato-fluorescence). For clarity, connected cells are shown separately as gray-scale images(right). The recorded PV-cell exhibits a multipolar dendritic morphology, as described for basket cells. Layers are labeled I-VI. Scale bars, 100 μ m

1st to the 2nd response, with an amplitude drop of $30.74 \pm 6.38\%$ ($n = 7$), and remained at this decreased amplitude level (Figure 4.16c). With an 8 and 40 Hz AP frequency the amplitude change between 1st and 2nd IPSC further increased (8 Hz: $36.00 \pm 3.31\%$, $n = 7$; 40 Hz: $35.60 \pm 5.18\%$, $n = 6$) and a tendency to further declining amplitudes of the following responses was observable (Figure 4.16b, c).

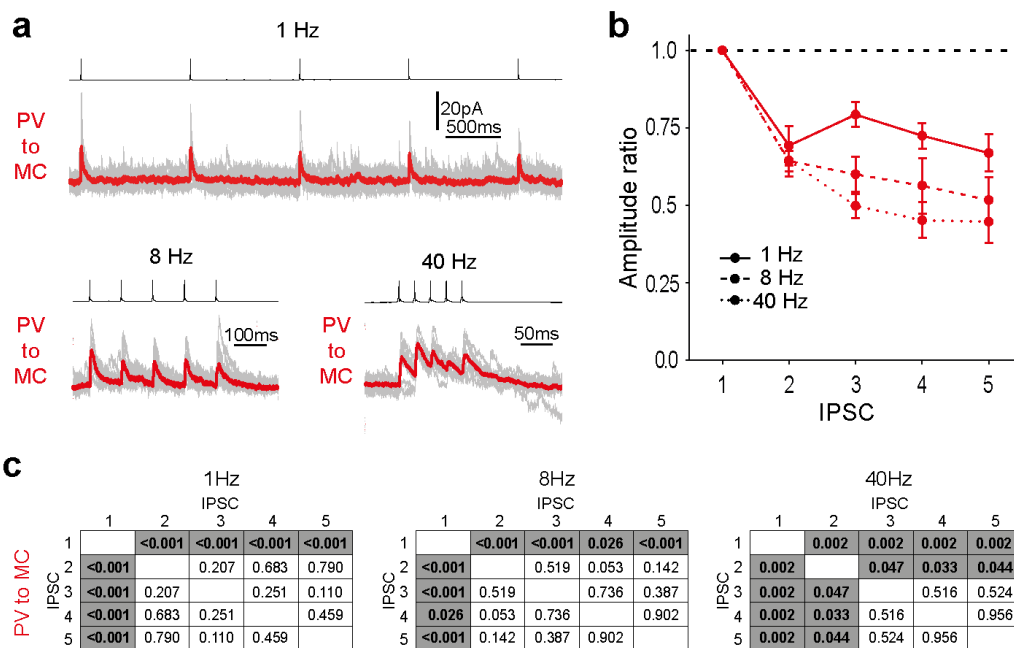


Figure 4.16: Unitary connections of L V PV-cells onto L V MCs also show reliable short-term depression

a) Individual examples of averaged IPSCs in MCs in response to trains of five spikes (1, 8 and 40 Hz) in a presynaptic PV-cell (red trace). Individual traces are shown in gray. Quantification is shown in **b**.

b) Quantitative analysis of short-term plasticity at different frequencies (1 Hz: $n = 7$, 8 Hz: $n = 7$, 40 Hz: $n = 6$). Amplitude-ratio (n^{th} response/ 1^{st} response) of consecutive IPSCs plotted versus successive IPSCs. At the population level, PV to MC responses showed synaptic depression under all stimulus conditions.

c) Tables containing p-values of the statistical analysis of normalized IPSC amplitudes for the different stimulus frequencies (1, 8, and 40 Hz). Amplitude ratios (n^{th} -response/ 1^{st} -response) were calculated and compared among each other. Significant differences ($P < 0.05$) are indicated by gray shading. Under all stimulus conditions, short-term plasticity was observed for the PV to MC connection. With a 1 and 8 Hz stimulus there is a significant difference between the 1st and the four subsequent IPSCs, which remain at a similarly depressed amplitude level. A frequency of 40 Hz induced further change in amplitude.

Finally we compared the elementary synaptic properties and short-term plasticity of PV to MC connections in L V and II/III. There was no significant difference in amplitude (L V: 37.07 ± 11.67 pA, $n = 9$; L II/III: 49.74 ± 12.97 pA, $n = 12$), latency (L V: 0.71 ± 0.06 ms; L II/III: 0.60 ± 0.07 ms), time to peak (L V: 4.66 ± 0.68 ms; L II/III: 3.58 ± 0.38 ms) and slope (L V: 7.23 ± 2.33 pA/ms; L II/III: 15.87 ± 4.61 pA/ms) (Figure 4.14d). On average a depressing short-term plasticity was caused by PV-inputs in L V as well as in L II/III.

Next, we considered if PV-cells in L II/III are responsible for the interlaminar input onto L V MCs, as shown by glutamate uncaging. However, PV-cells commonly show a local axonal arborization pattern not crossing several layers. Thus, we did not test whether L II/III PV-cells target MCs in L V. We rather assume that bipolar VIP-cells located in layer II/III project onto L V MCs, as these often exhibit a vertically distributed axonal tree covering all layers from L II/III to V.

4.5.2 Innervation of L V MCs by VIP-cells

Shown before, L II/III MCs also received local input from VIP-cells (Figure 4.12a). Therefore, we also recorded from VIP-cells close to L V MCs (distances up to 200 μ m). In this case only 5 out of 30 VIP cells were connected with MCs. Unfortunately, further quantification of synaptic properties and short-term plasticity was not possible due to the poor recording quality and the low number of connected pairs.

Nevertheless, as shown in figure 4.17a, L V VIP to MC connections showed tendencies for facilitating input with a 40 Hz stimulus, similar to VIP to MC connections in L II/III.

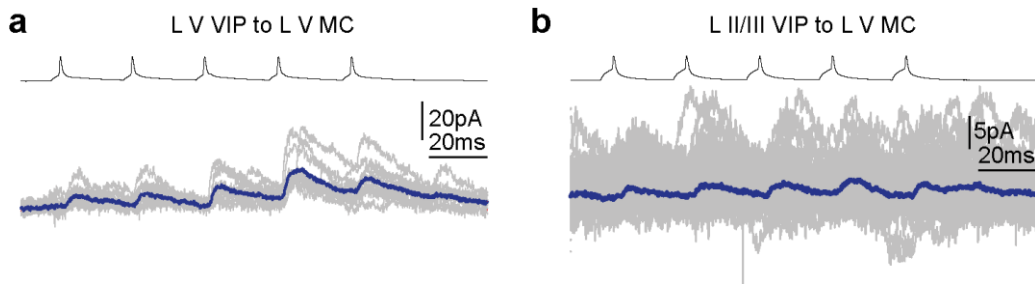


Figure 4.17: Local VIP-cells as well as L II/III VIP-cells project onto L V MCs

a, b) Individual example of averaged IPSCs in L V MCs in response to trains of five spikes (40 Hz) in presynaptic L V **(a)** or L II/III VIP-cells **(b)**. Individual traces (**a**: traces = 10, **b**: traces = 40) are shown in gray. Note the facilitation of consecutive IPSCs in **a** and the small consistent IPSCs in **b**.

Another finding of the glutamate uncaging experiments was the interlaminar inhibitory input onto L V MCs arising from L II/III. Due to specific morphological characteristics of L II/III VIP-cells, with a vertically extending axon covering several layers (Figure 2.2), they were most suitable to transmit interlaminar inhibitory input to L V MCs. As these rather distant paired recordings are a challenging task, we were only able to record from two trans laminarily connected pairs of presynaptic L II/III VIP-cells and a postsynaptic L V MCs. Hence, the synaptic properties and short-term plasticity could not be evaluated. However, these recordings exhibited non-depressive consecutive

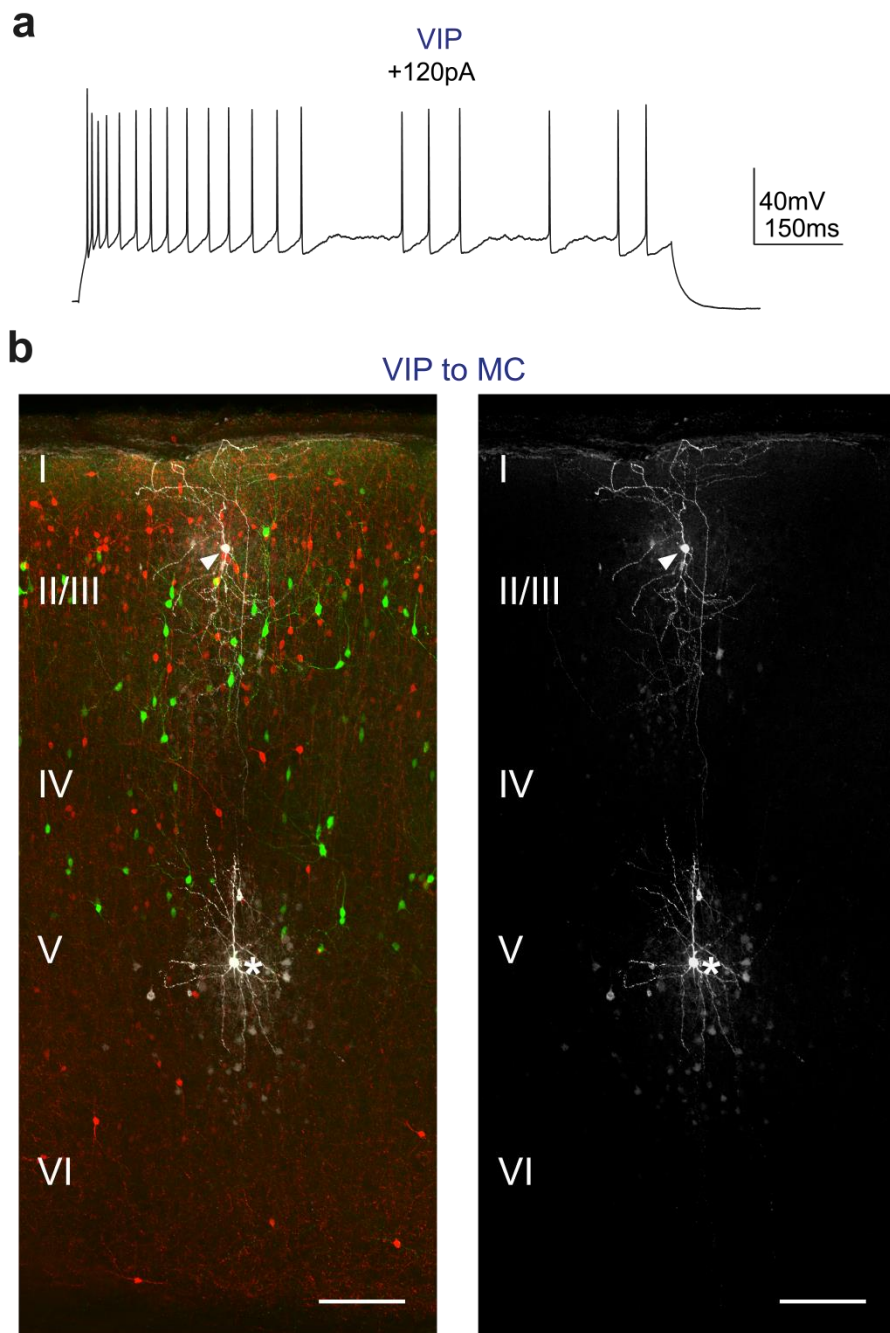


Figure 4.18: Morphology and electrophysiology of a L II/III VIP-cell coupled to a L V MC

a) Whole cell recordings of a presynaptic VIP-cell, which was connected to a recorded postsynaptic MC. During depolarizing current injections, the VIP-cell shows an irregular spiking pattern.

b) Staining of an acute brain slices containing a synaptically connected and morphologically recovered interlaminar VIP to MC pair. The connected cells are shown in white (pseudo-colored). Asterisks mark the MC soma and the arrowhead the soma of the presynaptic VIP-cell. GIN-cells are labeled green and the VIP-cell population is labeled red (tdTomato-fluorescence). For clarity, connected cells are shown separately as gray-scale images(right). The recorded VIP-cell exhibits a bipolar dendritic morphology, as described for VIP-cells. Layers are labeled I-VI. Scale bars, 100 μm

IPSCs in response to a 40 Hz spike train in the presynaptic cell, as exemplified in figure 4.17b. Additionally, one of these VIP-cells in L II/III showed electrophysiological and morphological characteristics, which were described before for this specific IN population (Figure 4.18a, b). This cell exhibited an irregular spiking pattern and a bipolar somato-dendritic configuration.

These experiments showed that locally also VIP-cells target MCs in L V. Future experiments have to verify this unitary connection, by increasing the overall number of recorded and synaptically coupled pairs and investigating the short-term plasticity for a comparison with the VIP to MC connection in L II/III. Finally, we could show that, although with a very low number, L II/III VIP-cells might be the best candidate for the interlaminar input onto L V MCs. Also this specific interlaminar connection needs to be further investigated in future experiments.

5 Discussion

How is sensory information processed in the brain? One of the many approaches to answer this question is to understand the neuronal circuitry, which forms the basis of this information processing. An extensively discussed hypothesis debates the existence of a module with a common neuroanatomical architecture, the cortical column (Mountcastle et al., 1955). This column might be slightly changed due to specific needs in processing certain information in dedicated cortical areas (DeFelipe, 1993; Meyer et al., 2013). Nevertheless, this means that the cortex consists of a multiple of this basic processing unit and that there might be certain rules for the interconnection and interaction of neuronal subtypes within the cortical column. GABAergic INs seem to play a major role in processing sensory information within the cortex and the cortical column (Lee et al., 2013; Pfeffer et al., 2013; Pi et al., 2013; Hangya et al., 2014). Only recently, the interconnectivity of these specific neurons became the focus of scientific research. These cells can be subdivided into several subclasses based on morphological, electrophysiological and molecular characteristic (Rudy et al., 2011; Staiger et al., 2015). A special IN subtype came to our attention, the SST-expressing MC, due to its capability to control the activity of cortical excitatory PCs and its probable involvement in specialized disinhibitory circuitries (Silberberg and Markram, 2007; Gentet et al., 2012). Thus, we investigated the inhibitory input of MCs in L II/III and V of mouse somatosensory cortex.

In the present study we could show that MCs in L II/III receive distinct inhibitory input from local PV- and VIP-cells. PV-cells are often reciprocally connected to MCs in this layer, whereas this was rarely observed for paired VIP-cells and MCs. Furthermore, the two identified unitary connections, PV to MC and VIP to MC, differed in elementary synaptic properties of the IPSC evoked in MCs, like latency, amplitude, time to peak and slope, but also in terms of short-term plasticity. PV-cells caused a strong depressing input, whereas VIP-cell input was weaker and facilitating. This might lead to differential inhibitory control of MCs in L II/III and hence, probably to specific types of disinhibition of local PCs.

In case of L V MCs we observed local inhibitory input from PV- and VIP-cells and interlaminar input from L II/III VIP-cells. The local PV to MC connection showed striking similarities to the PV to MC connection in L II/III in elementary synaptic properties as well as short-term plasticity. However, the local and interlaminar VIP-inputs onto L V MCs need to be investigated further. As L II/III VIP-cells display an axonal branching pattern which spans all cortical layers (Prönneke et al., 2015), these are likely presynaptic candidates for the interlaminar connection.

5.1 Technical consideration of glutamate uncaging

By means of glutamate uncaging, we could show that both L II/III and V MCs receive local inhibitory input. In case of L V MCs additional interlaminar input was observed. During uncaging experiments we used a laser energy of 120 μ J (20 mW for 6 ms). This specific energy primarily activates INs and a minor proportion of excitatory neurons, as shown by preceding calibration experiments. Thus, it might well be that some presynaptic INs were not activated during the uncaging experiments. This could lead to an underestimation of the number of inhibitory inputs. Furthermore, we repeated the laser stimulus three times per field. IPSCs were only accepted if they were detected at least two out of three times within a 10 ms time window after stimulus offset. This was done (i) to distinguish between spontaneous IPSCs and stimulus evoked IPSCs and (ii) to prevent detection of disynaptically evoked IPSCs. However, our results for the distribution of inhibitory input to L II/III MCs are in striking contrast to previous observations (Xu and Callaway, 2009). In their case, MCs in L II/III of mouse somatosensory cortex received extensive inhibition from layers II/III, IV, and V. Unfortunately they did not specify the laser intensity used during uncaging experiments. However, it seems that the same laser energy was applied to map excitatory as well as inhibitory input. Therefore, we have to assume that a large amount of excitatory cells was activated during the mapping of inhibitory input, which likely led to a large

proportion of disynaptically evoked IPSCs. To prevent detection of such inhibitory input we only accepted IPSCs occurring within 10 ms after stimulus offset. Xu and Callaway, however, analyzed IPSCs detected within a broad time window of 150 ms after stimulus onset. This will likely introduce a bias towards disynaptically evoked IPSCs. In addition, nothing is stated about stimulus repetitions. If they used a single stimulus protocol, a separation of spontaneous and stimulus evoked IPSCs was not possible. In summary, we have to point out that a fine calibration of experimental conditions is needed for localizing inhibitory input to certain cell types with glutamate uncaging.

5.2 Unique innervation of MCs by PV- and VIP-cells in S1

By means of paired recordings we could show that both PV- and VIP-cells target L II/III and V MCs. The VIP to MC connection has already been described in the primary somatosensory, auditory and visual cortex as well as the medial prefrontal cortex (Lee et al., 2013; Pfeffer et al., 2013; Pi et al., 2013; Fu et al., 2014). Pfeffer and colleagues (Pfeffer et al., 2013) also investigated the interconnection of PV-cells and SST-cells, which include MCs, in the visual cortex by means of optogenetics and paired recordings. In this publication they claim that the group of SST-cells receives inhibitory inputs exclusively from VIP-cells. Hence, to our knowledge, in the neocortex, the PV to MC connection seems to be unique for S1.

As both MCs in L II/III and V receive input from PV- as well as VIP-cells, this specific innervation of MCs seems to be a general feature for S1. At least for the PV to MC connection, previous observations suggest that this unitary connection might be, indeed, common for MCs in S1 independent of their layer-specific localization. Gibson and colleagues (Gibson et al., 1999) showed an inhibitory innervation of low-threshold spiking cells by fast-spiking ones in L IV and VI of rat somatosensory cortex. Nevertheless, one has to mention that although some of the postsynaptic cells expressed somatostatin, none of these showed an ascending axon branching in L I, the most prominent feature of MCs. Further investigations of inhibitory input to MCs in other layers of S1 are needed to answer this question. Unfortunately, within the used GIN-line, MCs were labelled almost exclusively in L II/III and V, hence, data for other layers is lacking.

Why do we observe a mismatch between the inhibitory innervation pattern of MCs between the primary somatosensory (PV and VIP to MC) and visual cortex (VIP to MC only)? One might speculate that the PV to MC connection might have been evolved as a special feature of S1 in need for processing tactile information. Or on the other hand, it might as well be that within the visual cortex the PV to MC connection was not needed for processing sensory information and, hence, might have been removed. A future comparison with other cortical areas will further increase our knowledge considering inhibitory input onto MCs and will give answers to this specific question.

5.3 Differences in axonal targeting and/or synaptic architecture can explain differential elementary synaptic properties

The two unitary connections in layer II/III, PV to MC and VIP to MC, differed substantially in IPSC amplitude, latency, time to peak and slope. What might be the reason for these differences? On the one hand, these divergent properties might be due to different subcellular targeting of MCs by presynaptic INs (Figure 5.1 a). In consideration of the cable properties of dendrites (Rall, 2011), attenuated and slowed inhibitory responses will be detected at the soma, due to the electrotonic spread, if these were elicited at distal dendritic compartments (Spruston et al., 1993). Furthermore, the transmission of inhibitory inputs along the dendrite to the somatic recording site might also account for an increase in latency of these responses. In the present sample we observed that on average the input from VIP-cells was significantly smaller in amplitude, slower in rise, and more delayed in time to peak and latency in comparison to PV-input to MCs. Therefore, one might assume that VIP-cells target MCs substantially more distal than PV-cells. This finding raised the question if these two inhibitory subtypes might target divergent areas of MCs, e.g. perisomatic respectively dendritic innervation sites. Indeed, considering the innervation pattern of cortical PCs by inhibitory INs, such a distinct separation of axonal target-sites of INs was recently described (see Staiger et al., 2015). Accordingly, VIP-cells were described to target

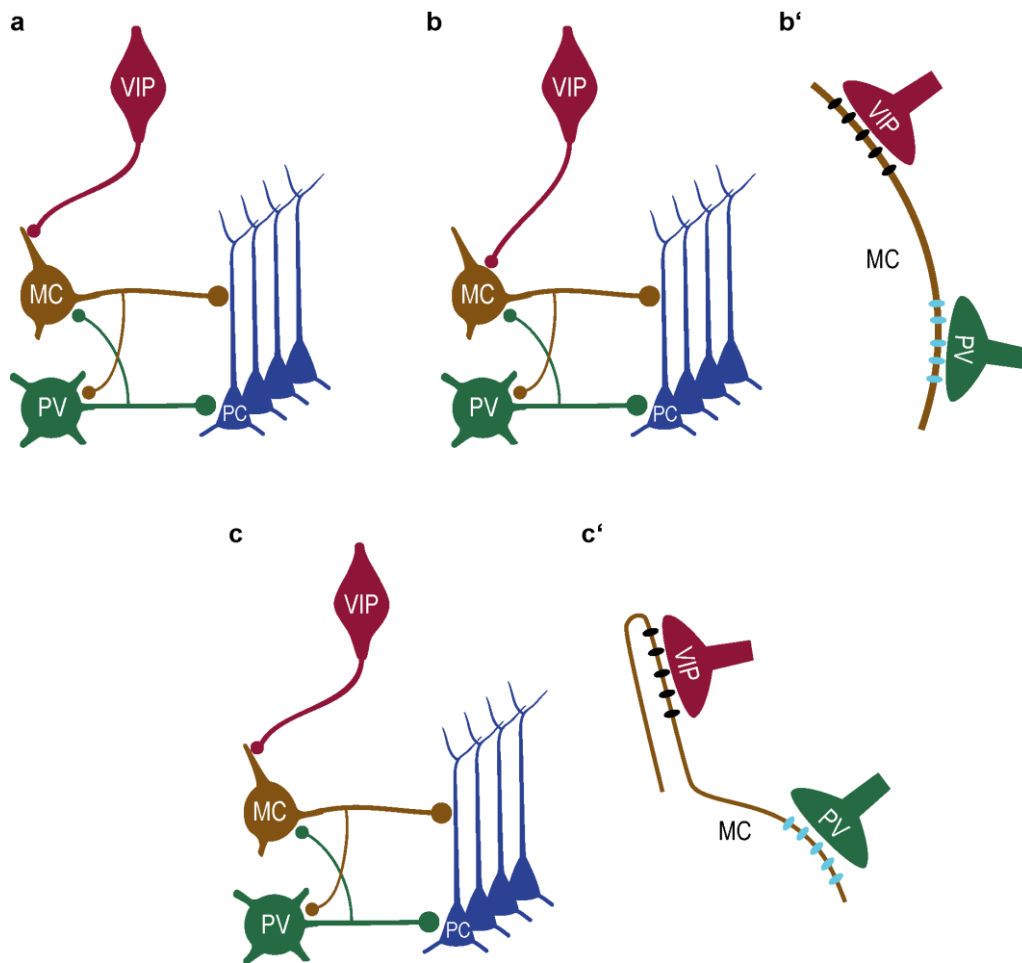


Figure 5.1: Proposed connectivities of the disinhibitory circuitry in L II/III of the primary somatosensory cortex involving VIP-cells, PV-cells, MC and PC

a-c') Shown is the projection of VIP- and PV-cells onto MCs, which in turn inhibit PCs. Only the somatodendritic configuration is depicted. Note, the reciprocal connection between PV-cells and MCs. Differences in IPSC amplitude, latency and kinetics induced in MCs by activity of VIP- respectively PV-cells, as shown in present thesis, can be explained by (i) differences in target areas, whereas VIP-cells target the dendrite and PV-cells perisomatic areas of MCs (a), (ii) by differences in subunit-composition of postsynaptic GABA_A-receptors (indicated by differently colored ellipses), while VIP- and PV-cells target the same cellular compartments, for example perisomatic areas (b, b') or (iii) by a combination of both (c, c'). In latter case, VIP- and PV-cells differ in axonal target areas as well as GABA_A-receptor subunit composition.

small and medium sized dendrites of PCs, whereas PV-cells predominantly the perisomatic regions of PCs (Hajos et al., 1988; Tamas et al., 1998; Thomson and Bannister, 2003; Kubota et al., 2015). Nevertheless, it also has been reported that a minor number of VIP-

boutons were found on the somata of PCs (Hajos et al., 1988; Peters, 1990; Kawaguchi and Kubota, 1997). If such a targeting pattern, perisomatic innervation by PV-cells and a more distal one on dendritic compartments by VIP-cells, also holds true for MCs, this specific pattern will have interesting consequences for information processing within MCs. VIP-cells might be in a position to selectively control excitatory inputs to MCs via dendritic inhibition, whereas the perisomatic inhibition by PV-cells could globally control the spiking output of MCs. However, to our knowledge there is so far no ultrastructural evidence for this specific projection pattern onto MCs or any other IN subtype. It has to be noted that on a light microscopic level a recent study claimed that VIP-cells innervate PV-cells via perisomatic innervation (Hioki et al., 2013). In this report, pre- and postsynaptic compartments of INs were labelled and determined as a functional synapse if these label were in close vicinity.

Differences in the subunit composition of GABA_A-receptors in the postsynaptic membrane of MCs (Figure 5.1b, b') might be another explanation for the divergent elementary synaptic properties of the two identified unitary connections mentioned above. These receptors exert an archetypical structure, which consists of a heteropentamer. This heteropentamer is composed of 2 α -, 2 β -, and 1 γ -subunit (Macdonald and Olsen, 1994). These subunits are present as several isoforms (Cherubini and Conti, 2001) and the postsynaptic currents mediated by GABA_A-receptors differ in amplitude and kinetics depending on the specific α - and β -subunit isoforms, which are involved in forming the

GABA_A-receptors (Gingrich et al., 1995; Bacci et al., 2003). In order to account for the present observations different GABA_A-receptors need to be distributed specifically in one postsynaptic MC. At least for cortical PCs it was described that the subunit composition of postsynaptic GABA_A-receptors is, indeed, dictated by the type of the presynaptic IN, as reviewed by Thomson and Jovanovic (Thomson and Jovanovic, 2010). It was shown that PV-expressing basket cells preferentially innervate GABA_A-receptors including α 1-, β 2/3-, and γ 2-subunits whereas cholecystinin-expressing basket cells innervate GABA_A-receptors containing α 2-, β 2/3-, and γ 2-subunits (Pawelzik et al., 1999; Thomson et al., 2000; Ali and Thomson, 2008).

Nevertheless, these two alternatives for explaining the differences in elementary synaptic properties, differential axonal targeting or differences in GABA_A-receptor subunit composition, are not mutually exclusive but might as well occur in parallel (Figure 5.1c, c') (Thomson and Jovanovic, 2010). We observed similar elementary synaptic properties of local PV-inputs to MCs in L V in comparison to the one in L II/III, thus the synaptic architecture of the PV to MC connection might be similar in both layers. Unfortunately, the sample size of connected VIP-cells and L V MCs was too small for comparing the elementary synaptic properties of inhibitory inputs to MCs in this layer.

5.4 Differential effect of short-term plasticity on MC activity

After observing differences in size and kinetics of the unitary connections in L II/III, these also differed in short-term plasticity. The PV-cell input exhibited frequency-independent depression, whereas VIP-cells input showed neither depression nor facilitation at low stimulus frequencies. But these inputs rather facilitated using a high frequency stimulus. The frequency-independent depression of PV-input, as described in the present thesis, seems to be a common feature of PV-cells (Bartos et al., 2001; Beierlein et al., 2003; Gulyas et al., 2010; Ma et al., 2012). Ma and colleagues (Ma et al., 2012), for example, investigated neuronal connections in L IV of S1 and showed a short-term depressive effect of PV-input regardless of the type of postsynaptic cell in sensory cortical areas. In this case input of fast-spiking cells onto SST-cells and regular-spiking excitatory cells was analyzed. However, it has to be noted that the X94-mouse line was used for these experiments. In this specific mouse line SST-cells in L IV are labelled and do not include MCs (Xu et al., 2013).

In contrast, there is a lack of reports describing short-term plasticity of unitary VIP-inputs in sensory cortical areas. However, recently, Pi and colleagues (Pi et al., 2013) used an optogenetic approach to drive expression of channelrhodopsin2 (ChR2) in VIP-cells in the auditory and medial prefrontal cortex via transfection with an adeno associated virus (AAV). Afterwards, larger populations of VIP-cells were activated

by light and they observed synaptic depression in different postsynaptic INs, i.e. SST- and PV-cells, at stimulus frequencies of 40 Hz. These results are in strong contrast to our finding of frequency-dependent facilitation of VIP-input onto MCs. However, Jackman and colleagues (Jackman et al., 2014) compared optogenetic to electrical stimulation of presynaptic cells and its effect on short-term plasticity. They could show that specific AAV serotypes, which were used to drive expression of ChR2, introduced an artificial depression of synaptic inputs. Therefore, it might well be that studying short-term plasticity with different approaches like optogenetics and paired recordings, respectively, may yield contradictory results. Furthermore, desensitization of the activated ChR2 and a slow recovery from this desensitization could prevent reliable triggering of spikes while using a high-frequent stimulus (Nagel et al., 2003; Olsen et al., 2012; Jackman et al., 2014). Additionally, the property of release might be increased due to broadened spikes, caused by the overall slow kinetics of ChR2, which will result in a rapid depletion of the presynaptic vesicle pool (Zhang and Oertner, 2007; Jackman et al., 2014). Both explanations could introduce an artificial depressing input and might even act complementary.

In this thesis we showed short-term depressing PV-inputs on MCs, which might be described as phasic. In comparison we observed more tonic properties considering VIP-inputs on MCs (Figure 4.13). It has to be noted, however, that even depressed PV inputs at low frequency stimulation exert a stronger influence at the soma than the corresponding VIP-inputs. Only with a 40 Hz stimulus the depressed

PV-input and the facilitated VIP-input converge to similar amplitudes. If one, however, considers the probable distal dendritic targeting of MCs by VIP-cells the true impact of these cells on dendritic input control of MCs would be much stronger. Furthermore, facilitation at high frequencies could be a dominant factor in controlling the activity in the postsynaptic cell. Indeed, VIP-cells seem to have a major impact on MCs in S1. Lee and colleagues (Lee et al., 2013) showed that, *in vivo*, VIP-cells have massive influence on the activity of SST-cells during whisking. These SST-cells, in turn, have been described to target apical dendrites of PCs, a typical feature of MCs.

These findings implicate that VIP- and PV-cells may provide different spatial and temporal windows of opportunities (Ma et al., 2012). We presented an initial weaker VIP-cell input onto MCs, which needs high frequency spiking to build up over time. This could lead to a rather long integration window in MCs in respect to VIP-input. Contrary, PV-cells exert an immediate strong but depressing inhibitory input to MCs, which keeps the time window for integration comparably short in MCs.

In case of L V MCs PV-input causes as similar depressing input, which points to a common innervation pattern of MCs by PV-cells in S1. Considering VIP-input, we observed a tendency of non-depressive and even facilitating input of local as well as interlaminar VIP-cells. Unfortunately, the overall number of connected pairs was again too low for detailed comparisons.

5.5 Disinhibition of cortical PCs depends on excitatory drive of VIP- and PV-cells

By using paired recordings we could show that MCs in L II/III of S1 receive inhibitory input from at least two sources, local VIP- and PV-cells, with divergent elementary synaptic properties and short-term plasticity. These two separate inhibitory input channels to L II/III MCs, may provide two distinct forms of PC disinhibition in S1. Considering this specific circuitry, two separate input channels to VIP- and PV-cells could, in principle, allow different sources of excitatory drive to disinhibit PCs via the distinct inhibitory control of MCs. On the other hand it might as well allow one single excitatory input to utilize two different kinds of MC inhibition, hence disinhibition of PCs. Therefore, the question arose what sources of excitatory input do drive VIP- and PV-cells. Both cell types receive local excitatory input from L II/III PCs and excitatory input forwarded by L IV excitatory cells (Porter et al., 1998; Holmgren et al., 2003; Helmstaedter et al., 2008). However, a major difference in excitatory input to these cell types includes long-range input from other cortical areas. Recently, it was described that long-range excitatory input from the primary motor cortex selectively targets VIP-cells in S1 (Lee et al., 2013). Hence, to our knowledge, inhibition of MCs mediated by VIP-cells integrates somatosensory information as well as motor information into S1, whereas PV-cells seem to be only driven by somatosensory inputs.

Furthermore, VIP- and PV-cells receive modulatory input via cholinergic afferents. These afferents derive from the basal forebrain and influence both types of MC-inhibiting INs. On the one hand, VIP-cells can be activated via nicotinic acetylcholine-receptors, whereas PV-cells are activated by muscarinic acetylcholine-receptors but rather suppressed by nicotinic ones (Porter et al., 1999; Alitto and Dan, 2012; Disney and Reynolds, 2014). Ultimately, state-dependent cholinergic modulation may thereby selectively enhance and/or suppress activity in IN inhibiting MCs (Jones, 2004; Lee et al., 2005).

5.6 Functional aspects of reciprocal PV to MC connections in L II/III of S1

Finally, we could show that PV-cells and MCs in L II/III are often reciprocally connected (Figure 5.1). The consequence of such a reciprocally connected pair would be mutual inhibition if both cells receive the same excitatory drive. But this would be a rather ineffective mechanism in respect to functionality. Hence, this raises the question if PV-cells and MCs receive divergent or a common excitatory input. To our knowledge both cell-types primarily get excitation from L II/III and L IV (Holmgren et al., 2003; Silberberg and Markram, 2007; Helmstaedter et al., 2008; Xu and Callaway, 2009), but whether PV-cells and MCs share a common or rather have a diverging excitatory drive is still unknown. Furthermore, modulatory mechanisms could

differentially affect the activity of PV-cells and MCs. Indeed, cholinergic innervation causes activation of SST-cells (Kawaguchi, 1997) whereas PV-activity is increased by muscarinic acetylcholine-receptors and decreased by nicotinic ones, depending on the activity state of the basal forebrain (Alitto and Dan, 2012). Furthermore, noradrenaline (NA) causes depolarization but not spiking in fast-spiking cells, whereas in MCs NA even caused spiking (Kawaguchi and Shindou, 1998). Hence, depending on the presence of certain neuromodulators, PV-cells and MCs can be activated differently. If a similar mechanism can be found in L V as well needs to be investigated in future experiments.

If reciprocally connected PV-cells and MCs share a common excitatory drive, temporal features of the mutual inhibitory input might allow a functional circuit. As we could show in this thesis, PV-cells exert a depressive inhibitory input on MCs. This might initially shut down MC-activity but may allow spiking shortly after, due to decreasing PV-input. How both cell-types interact during ongoing activity needs to be investigated in the future.

6 Outlook

Our results show that both PV- and VIP-cells project onto MCs in S1, independently of the laminar location of MCs. PV- and VIP-cells might target different cellular compartments of MCs, PV-cells perisomatic regions and VIP-cells distal dendrites. Correlated light- and electron-microscopy might give an answer to the specific subcellular targeting. Moreover, there might be differences in the subunit composition of GABA_A-receptors. To test for the influence of probable differences in GABA_A-receptor architecture, experiments using specific modulators, agonists and antagonists for different α -subunits have to be carried out. However, it needs to be further evaluated if the local and interlaminar VIP-input derives from distinct subpopulations of this specific IN subtype (Prönneke et al., 2015). Therefore, additional paired recordings of VIP-cells and MCs are necessary. To test for the specific function of the unitary connections onto MCs, in a next step *in vivo* experiments have to be carried out. In particular, the excitatory drive of the individual components of the circuitry, as proposed in this thesis, needs to be investigated. Especially, the activity of certain cell types during specific behavior, e.g. quiet wakefulness, arousal or active whisking, must be one of the major targets of future experiments. Another question that needs to be addressed is the consequence on cortical oscillatory states due to the activity of PV-cells and MCs. In respect thereof, it was shown that PV-cells are involved in maintaining up-states and balancing gamma- and beta-oscillations, whereas SST-cells seem to have an

opposite effect on up-state regulation (Kuki et al., 2015). Furthermore, PV- and SST-cells have an asymmetric contribution on delta-oscillations (Kuki et al., 2015). A probable functional explanation for this opposing effect might be the reciprocal connection between PV-cells and MCs.

7 Figures & Tables

Figure 2.1: The rodent whisker-to-barrel pathway (modified after Schubert et al., 2007)	5
Figure 2.2: Three non-overlapping groups of INs and the corresponding morphology of their main subtypes (modified after Rudy et al., 2011, Staiger et al., 2015)	13
Figure 2.3: Schematic of a disinhibitory circuitry (modified after Roux and Buszaki, 2015).....	16
Figure 2.4: Known connectivity of Martinotti cells in the primary somatosensory cortex and working hypothesis	21
Figure 3.1: Transgenic mice used for experiments.....	25
Figure 3.2: Acute brain slice used for electrophysiological experiments	26
Figure 3.3: Electrophysiological set-up and experimental approach for uncaging experiments (modified after Schubert et al., 2007)	28
Figure 3.4: Dendritic cable properties interfere with detection of dendritic events	33
Figure 3.5: Fitting procedure to determine the amplitude of overlapping IPSCs in response to a 40 Hz spike train	38
Figure 4.1: L II/III and V GIN cells show electrophysiological characteristics of MCs	43
Figure 4.2: Morphological characteristics of MCs in L II/III and V	46
Figure 4.3: Layer II/III GIN cells show typical morphology of Martinotti cells	47
Figure 4.4: L V GIN cells show typical morphology of Martinotti cells ..	48
Figure 4.5: GABA-evoked IPSCs can be detected in all compartments of recorded GIN-cells	50
Figure 4.6: Different laser energies are needed to activate inhibitory and excitatory neurons by glutamate uncaging	52
Figure 4.7: Mapping inhibitory input to L II/III and V MCs using glutamate uncaging	55
Figure 4.8: Distribution of inhibitory fields.....	57

Figure 4.9: Localization of presynaptic inhibitory cells to L II/III and V MCs.....	59
Figure 4.10: Connection properties of presynaptic PV- and VIP-cells and postsynaptic L II/III MCs	61
Figure 4.11: Morphology and electrophysiology of L II/III PV-MC and VIP-MC pairs	63
Figure 4.12: Unitary connections of PV- and VIP-cells onto L II/III MCs differ in their elementary synaptic properties	65
Figure 4.13: Unitary connections of PV- and VIP-cells onto L II/III MCs differ in short-term plasticity.....	68
Figure 4.14: The local unitary connection of PV-cells onto L V MCs shows similar properties than the L II/III PV to MC connection.....	70
Figure 4.15: Morphology and electrophysiology of a L V PV-cell coupled to a L V MC.....	72
Figure 4.16: Unitary connections of L V PV-cells onto L V MCs also show reliable short-term depression.....	73
Figure 4.17: Local VIP-cells as well as L II/III VIP-cells project onto L V MCs.....	75
Figure 4.18: Morphology and electrophysiology of a L II/III VIP-cell coupled to a L V MC.....	76
Figure 5.1: Proposed connectivities of the disinhibitory circuitry in L II/III of the primary somatosensory cortex involving VIP-cells, PV-cells, MC and PC	84
Table 3.1: Constant laser intensity before and after uncaging experiments.....	31
Table 4.1: Comparison of observed electrophysiological properties of L II/III and V MCs with data from literature	45

8 Abbreviations

5HT3aR: Serotonin receptor 3a

AAV: Adeno associated virus

ABC: Acidin-Biotin Complex

ACSF: Artificial cerebrospinal fluid

AP: Action potential

AP amp: Action potential amplitude at firing threshold

AP width: Action potential width at firing threshold

BSA: Bovine serum albumin

Caudalis: Caudal nucleus

ChR2: Channelrhodopsin 2

CO: Cytochrome oxidase

CR: Calretinin

DAB: Diaminobenzidine

GABA: Gamma-aminobutyric acid

GFP: Green fluorescent protein

IN: Inhibitory interneuron

Interpolaris: Interpolar nucleus

IPSC: Inhibitory postsynaptic current

L: Layer

MC: Martinotti cell

NA: Noradrenaline

Principalis: Principal nucleus

Oralis: Oral nucleus

POm: Posterior medial thalamic nucleus

PB: Phosphate buffer

PBS: Phosphate buffer saline

PC: Pyramidal cell

PV: Parvalbumin

RFP: Red fluorescent protein

Rheo: Rheobase

R_{in}: Input resistance

S1: Primary somatosensory cortex

S.D.: Standard deviation

S.E.M.: Standard error of the mean

SST: Somatostatin

Tau: Membrane time constant

V_{Hold}: Holding potential

VIP: Vasoactive intestinal polypeptide

X94: X94-cell

9 References

- Agmon A, Connors BW (1991) Thalamocortical responses of mouse somatosensory (barrel) cortex in vitro. *Neuroscience* 41:365-379.
- Ahissar E, Sosnik R, Haidarliu S (2000) Transformation from temporal to rate coding in a somatosensory thalamocortical pathway. *Nature* 406:302-306.
- Ali AB, Thomson AM (2008) Synaptic alpha 5 subunit-containing GABAA receptors mediate IPSPs elicited by dendrite-preferring cells in rat neocortex. *Cereb Cortex* 18:1260-1271.
- Alitto HJ, Dan Y (2012) Cell-type-specific modulation of neocortical activity by basal forebrain input. *Front Syst Neurosci* 6:79.
- Anderson JS, Carandini M, Ferster D (2000) Orientation tuning of input conductance, excitation, and inhibition in cat primary visual cortex. *J Neurophysiol* 84:909-926.
- Armstrong-James M, Fox K (1987) Spatiotemporal convergence and divergence in the rat S1 "barrel" cortex. *J Comp Neurol* 263:265-281.
- Armstrong-James M, Fox K, Das-Gupta A (1992) Flow of excitation within rat barrel cortex on striking a single vibrissa. *J Neurophysiol* 68:1345-1358.
- Ascoli GA et al. (2008) Petilla terminology: nomenclature of features of GABAergic interneurons of the cerebral cortex. *Nat Rev Neurosci* 9:557-568.
- Atallah BV, Scanziani M (2009) Instantaneous modulation of gamma oscillation frequency by balancing excitation with inhibition. *Neuron* 62:566-577.
- Bacci A, Rudolph U, Huguenard JR, Prince DA (2003) Major differences in inhibitory synaptic transmission onto two neocortical interneuron subclasses. *J Neurosci* 23:9664-9674.
- Bartos M, Vida I, Frotscher M, Geiger JR, Jonas P (2001) Rapid signaling at inhibitory synapses in a dentate gyrus interneuron network. *J Neurosci* 21:2687-2698.

- Beierlein M, Gibson JR, Connors BW (2003) Two dynamically distinct inhibitory networks in layer 4 of the neocortex. *J Neurophysiol* 90:2987-3000.
- Belford GR, Killackey HP (1979) Vibrissae representation in subcortical trigeminal centers of the neonatal rat. *J Comp Neurol* 183:305-321.
- Beneyto M, Abbott A, Hashimoto T, Lewis DA (2011) Lamina-specific alterations in cortical GABA(A) receptor subunit expression in schizophrenia. *Cereb Cortex* 21:999-1011.
- Bennett-Clarke CA, Leslie MJ, Chiaia NL, Rhoades RW (1993) Serotonin 1B receptors in the developing somatosensory and visual cortices are located on thalamocortical axons. *Proc Natl Acad Sci U S A* 90:153-157.
- Berger TK, Perin R, Silberberg G, Markram H (2009) Frequency-dependent disynaptic inhibition in the pyramidal network: a ubiquitous pathway in the developing rat neocortex. *J Physiol-London* 587:5411-5425.
- Berger TK, Silberberg G, Perin R, Markram H (2010) Brief Bursts Self-Inhibit and Correlate the Pyramidal Network. *PLoS Biol* 8.
- Biró ÁA, Holderith NB, Nusser Z (2006) Release probability-dependent scaling of the postsynaptic responses at single hippocampal GABAergic synapses. *The Journal of neuroscience* 26:12487-12496.
- Boylan CB, Bennett-Clarke CA, Crissman RS, Mooney RD, Rhoades RW (2000) Clorgyline treatment elevates cortical serotonin and temporarily disrupts the vibrissae-related pattern in rat somatosensory cortex. *J Comp Neurol* 427:139-149.
- Brecht M, Sakmann B (2002) Dynamic representation of whisker deflection by synaptic potentials in spiny stellate and pyramidal cells in the barrels and septa of layer 4 rat somatosensory cortex. *J Physiol* 543:49-70.
- Brecht M, Roth A, Sakmann B (2003) Dynamic receptive fields of reconstructed pyramidal cells in layers 3 and 2 of rat somatosensory barrel cortex. *J Physiol* 553:243-265.

- Brodmann K (1909) Vergleichende Lokalisationslehre der Grosshirnrinde in ihren Prinzipien dargestellt auf Grund des Zellenbaues: Barth.
- Bureau I, von Saint Paul F, Svoboda K (2006) Interdigitated paralemniscal and lemniscal pathways in the mouse barrel cortex. *PLoS Biol* 4:e382.
- Buzsaki G, Wang XJ (2012) Mechanisms of gamma oscillations. *Annu Rev Neurosci* 35:203-225.
- Cardin JA, Carlén M, Meletis K, Knoblich U, Zhang F, Deisseroth K, Tsai L-H, Moore CI (2009) Driving fast-spiking cells induces gamma rhythm and controls sensory responses. *Nature* 459:663-667.
- Cauli B, Audinat E, Lambolez B, Angulo MC, Ropert N, Tsuzuki K, Hestrin S, Rossier J (1997) Molecular and physiological diversity of cortical nonpyramidal cells. *J Neurosci* 17:3894-3906.
- Chen SX, Kim AN, Peters AJ, Komiyama T (2015) Subtype-specific plasticity of inhibitory circuits in motor cortex during motor learning. *Nat Neurosci*.
- Cherubini E, Conti F (2001) Generating diversity at GABAergic synapses. *Trends Neurosci* 24:155-162.
- Chiaia NL, Rhoades RW, Bennett-Clarke CA, Fish SE, Killackey HP (1991) Thalamic processing of vibrissal information in the rat. I. Afferent input to the medial ventral posterior and posterior nuclei. *J Comp Neurol* 314:201-216.
- Chiaia NL, Fish SE, Bauer WR, Bennett-Clarke CA, Rhoades RW (1992) Postnatal blockade of cortical activity by tetrodotoxin does not disrupt the formation of vibrissa-related patterns in the rat's somatosensory cortex. *Brain Res Dev Brain Res* 66:244-250.
- Chmielowska J, Carvell GE, Simons DJ (1989) Spatial organization of thalamocortical and corticothalamic projection systems in the rat Sml barrel cortex. *J Comp Neurol* 285:325-338.
- Citri A, Malenka RC (2008) Synaptic plasticity: multiple forms, functions, and mechanisms. *Neuropsychopharmacology* 33:18-41.
- Cobos I, Calcagnotto ME, Vilaythong AJ, Thwin MT, Noebels JL, Baraban SC, Rubenstein JLR (2005) Mice lacking Dlx1 show

subtype-specific loss of interneurons, reduced inhibition and epilepsy. *Nat Neurosci* 8:1059-1068.

Cooper NG, Steindler DA (1986) Lectins demarcate the barrel subfield in the somatosensory cortex of the early postnatal mouse. *J Comp Neurol* 249:157-169.

De No Lorente R (1949) Cerebral cortex: architecture, intracortical connections, motor projections. In: "Physiology of the Nervous System. In: London: Oxford University Press.

de Nó RL (1922) La corteza cerebral del ratón:(Primera contribución.- La corteza acústica).

DeFelipe J (1993) Neocortical neuronal diversity: chemical heterogeneity revealed by colocalization studies of classic neurotransmitters, neuropeptides, calcium-binding proteins, and cell surface molecules. *Cereb Cortex* 3:273-289.

DeFelipe J et al. (2013) New insights into the classification and nomenclature of cortical GABAergic interneurons. *Nat Rev Neurosci* 14:202-216.

Diamond M (1995) Somatosensory Thalamus of the Rat. In: *The Barrel Cortex of Rodents* (Jones E, Diamond I, eds), pp 189-219: Springer US.

Diamond M, Armstrong-James M (1992) Role of parallel sensory pathways and cortical columns in learning. *Concepts Neurosci* 3:55-78.

Disney AA, Reynolds JH (2014) Expression of m1-type muscarinic acetylcholine receptors by parvalbumin-immunoreactive neurons in the primary visual cortex: a comparative study of rat, guinea pig, ferret, macaque, and human. *J Comp Neurol* 522:986-1003.

Doischer D, Hosp JA, Yanagawa Y, Obata K, Jonas P, Vida I, Bartos M (2008) Postnatal Differentiation of Basket Cells from Slow to Fast Signaling Devices. *Journal of Neuroscience* 28:12956-12968.

Donato F, Rompani SB, Caroni P (2013) Parvalbumin-expressing basket-cell network plasticity induced by experience regulates adult learning. *Nature* 504:272-276.

Douglas RJ, Martin KA (2004) Neuronal circuits of the neocortex. *Annu Rev Neurosci* 27:419-451.

- Douglas RJ, Martin KAC, Whitteridge D (1989) A Canonical Microcircuit for Neocortex. *Neural Computation* 1:480-488.
- Ebara S, Kumamoto K, Matsuura T, Mazurkiewicz JE, Rice FL (2002) Similarities and differences in the innervation of mystacial vibrissal follicle-sinus complexes in the rat and cat: a confocal microscopic study. *J Comp Neurol* 449:103-119.
- Fagiolini M, Fritschy J-M, Löw K, Möhler H, Rudolph U, Hensch TK (2004) Specific GABAA circuits for visual cortical plasticity. *Science* 303:1681-1683.
- Fairén A, DeFelipe J, Regidor J (1984) Nonpyramidal neurons: general account. *Cereb Cortex* 1:201-253.
- Fanselow EE, Richardson KA, Connors BW (2008) Selective, state-dependent activation of somatostatin-expressing inhibitory interneurons in mouse neocortex. *J Neurophysiol* 100:2640-2652.
- Feldmeyer D, Lubke J, Silver RA, Sakmann B (2002) Synaptic connections between layer 4 spiny neurone-layer 2/3 pyramidal cell pairs in juvenile rat barrel cortex: physiology and anatomy of interlaminar signalling within a cortical column. *J Physiol-London* 538:803-822.
- Ferezou I, Cauli B, Hill EL, Rossier J, Hamel E, Lambolez B (2002) 5-HT₃ receptors mediate serotonergic fast synaptic excitation of neocortical vasoactive intestinal peptide/cholecystokinin interneurons. *J Neurosci* 22:7389-7397.
- Fioravante D, Regehr WG (2011) Short-term forms of presynaptic plasticity. *Curr Opin Neurobiol* 21:269-274.
- Fox K (2008) *Barrel cortex*: Cambridge University Press.
- Freund TF, Katona I (2007) Perisomatic inhibition. *Neuron* 56:33-42.
- Fu Y, Tucciarone JM, Espinosa JS, Sheng N, Darcy DP, Nicoll RA, Huang ZJ, Stryker MP (2014) A cortical circuit for gain control by behavioral state. *Cell* 156:1139-1152.
- Gabbott PL, Bacon SJ (1996) Local circuit neurons in the medial prefrontal cortex (areas 24a,b,c, 25 and 32) in the monkey: I. Cell morphology and morphometrics. *J Comp Neurol* 364:567-608.

- Galarreta M, Hestrin S (2002) Electrical and chemical synapses among parvalbumin fast-spiking GABAergic interneurons in adult mouse neocortex. *Proc Natl Acad Sci U S A* 99:12438-12443.
- Gentet LJ, Kremer Y, Taniguchi H, Huang ZJ, Staiger JF, Petersen CC (2012) Unique functional properties of somatostatin-expressing GABAergic neurons in mouse barrel cortex. *Nat Neurosci* 15:607-612.
- Gibson JR, Beierlein M, Connors BW (1999) Two networks of electrically coupled inhibitory neurons in neocortex. *Nature* 402:75-79.
- Gingrich KJ, Roberts WA, Kass RS (1995) Dependence of the GABA_A receptor gating kinetics on the alpha-subunit isoform: implications for structure-function relations and synaptic transmission. *J Physiol* 489 (Pt 2):529-543.
- Goldberg JH, Lacefield CO, Yuste R (2004) Global dendritic calcium spikes in mouse layer 5 low threshold spiking interneurons: implications for control of pyramidal cell bursting. *J Physiol* 558:465-478.
- Gulyas AI, Szabo GG, Ulbert I, Holderith N, Monyer H, Erdelyi F, Szabo G, Freund TF, Hajos N (2010) Parvalbumin-containing fast-spiking basket cells generate the field potential oscillations induced by cholinergic receptor activation in the hippocampus. *J Neurosci* 30:15134-15145.
- Hajos F, Zilles K, Schleicher A, Kalman M (1988) Types and spatial distribution of vasoactive intestinal polypeptide (VIP)-containing synapses in the rat visual cortex. *Anat Embryol (Berl)* 178:207-217.
- Hangya B, Pi HJ, Kvitsiani D, Ranade SP, Kepecs A (2014) From circuit motifs to computations: mapping the behavioral repertoire of cortical interneurons. *Curr Opin Neurobiol* 26:117-124.
- Harris KD, Mrsic-Flogel TD (2013) Cortical connectivity and sensory coding. *Nature* 503:51-58.
- Helmstaedter M, Staiger JF, Sakmann B, Feldmeyer D (2008) Efficient recruitment of layer 2/3 interneurons by layer 4 input in single columns of rat somatosensory cortex. *J Neurosci* 28:8273-8284.

- Hensch TK, Fagiolini M, Mataga N, Stryker MP, Baekkeskov S, Kash SF (1998) Local GABA circuit control of experience-dependent plasticity in developing visual cortex. *Science* 282:1504-1508.
- Hioki H, Okamoto S, Konno M, Kameda H, Sohn J, Kuramoto E, Fujiyama F, Kaneko T (2013) Cell type-specific inhibitory inputs to dendritic and somatic compartments of parvalbumin-expressing neocortical interneuron. *J Neurosci* 33:544-555.
- Holmgren C, Harkany T, Svennenfors B, Zilberter Y (2003) Pyramidal cell communication within local networks in layer 2/3 of rat neocortex. *J Physiol* 551:139-153.
- Horton JC, Adams DL (2005) The cortical column: a structure without a function. *Philos Trans R Soc Lond B Biol Sci* 360:837-862.
- Hu H, Gan J, Jonas P (2014) Fast-spiking, parvalbumin(+) GABAergic interneurons: From cellular design to microcircuit function. *Science* 345:529-+.
- Huang ZJ (2006) Subcellular organization of GABAergic synapses: role of ankyrins and L1 cell adhesion molecules. *Nat Neurosci* 9:163-166.
- Hubel DH, Wiesel TN (1962) Receptive fields, binocular interaction and functional architecture in the cat's visual cortex. *J Physiol* 160:106-154.
- Hubel DH, Wiesel TN (1968) Receptive fields and functional architecture of monkey striate cortex. *J Physiol* 195:215-243.
- Isaacson JS, Scanziani M (2011) How Inhibition Shapes Cortical Activity. *Neuron* 72:231-243.
- Jackman SL, Beneduce BM, Drew IR, Regehr WG (2014) Achieving high-frequency optical control of synaptic transmission. *J Neurosci* 34:7704-7714.
- Jacquin MF, Renehan WE, Rhoades RW, Panneton WM (1993) Morphology and topography of identified primary afferents in trigeminal subnuclei principalis and oralis. *J Neurophysiol* 70:1911-1936.
- Jones BE (2004) Activity, modulation and role of basal forebrain cholinergic neurons innervating the cerebral cortex. *Prog Brain Res* 145:157-169.

- Jones EG, Hendry SH (1984) Basket cells. *Cereb Cortex* 1:309-336.
- Kaas JH (1997) Topographic maps are fundamental to sensory processing. *Brain Res Bull* 44:107-112.
- Kawaguchi Y (1995) Physiological subgroups of nonpyramidal cells with specific morphological characteristics in layer II/III of rat frontal cortex. *J Neurosci* 15:2638-2655.
- Kawaguchi Y (1997) Selective cholinergic modulation of cortical GABAergic cell subtypes. *J Neurophysiol* 78:1743-1747.
- Kawaguchi Y, Kubota Y (1996) Physiological and morphological identification of somatostatin- or vasoactive intestinal polypeptide-containing cells among GABAergic cell subtypes in rat frontal cortex. *J Neurosci* 16:2701-2715.
- Kawaguchi Y, Kubota Y (1997) GABAergic cell subtypes and their synaptic connections in rat frontal cortex. *Cereb Cortex* 7:476-486.
- Kawaguchi Y, Shindou T (1998) Noradrenergic excitation and inhibition of GABAergic cell types in rat frontal cortex. *J Neurosci* 18:6963-6976.
- Kawaguchi Y, Kubota Y (1998) Neurochemical features and synaptic connections of large physiologically-identified GABAergic cells in the rat frontal cortex. *Neuroscience* 85:677-701.
- Kawaguchi Y, Kondo S (2002) Parvalbumin, somatostatin and cholecystikinin as chemical markers for specific GABAergic interneuron types in the rat frontal cortex. *J Neurocytol* 31:277-287.
- Kawaguchi Y, Katsumaru H, Kosaka T, Heizmann CW, Hama K (1987) Fast spiking cells in rat hippocampus (CA1 region) contain the calcium-binding protein parvalbumin. *Brain Res* 416:369-374.
- Kepecs A, Fishell G (2014) Interneuron cell types are fit to function. *Nature* 505:318-326.
- Killackey HP, Belford GR (1979) The formation of afferent patterns in the somatosensory cortex of the neonatal rat. *J Comp Neurol* 183:285-303.
- Killackey HP, Rhoades RW, Bennett-Clarke CA (1995) The formation of a cortical somatotopic map. *Trends Neurosci* 18:402-407.

- Kisvarday ZF (1992) GABAergic networks of basket cells in the visual cortex. *Prog Brain Res* 90:385-405.
- Klausberger T, Somogyi P (2008) Neuronal diversity and temporal dynamics: the unity of hippocampal circuit operations. *Science* 321:53-57.
- Koralek KA, Jensen KF, Killackey HP (1988) Evidence for two complementary patterns of thalamic input to the rat somatosensory cortex. *Brain Res* 463:346-351.
- Koralek KA, Olavarria J, Killackey HP (1990) Areal and laminar organization of corticocortical projections in the rat somatosensory cortex. *J Comp Neurol* 299:133-150.
- Kubota Y, Kondo S, Nomura M, Hatada S, Yamaguchi N, Mohamed AA, Karube F, Lubke J, Kawaguchi Y (2015) Functional effects of distinct innervation styles of pyramidal cells by fast spiking cortical interneurons. *Elife* 4.
- Kuki T, Fujihara K, Miwa H, Tamamaki N, Yanagawa Y, Mushiake H (2015) Contribution of parvalbumin and somatostatin-expressing GABAergic neurons to slow oscillations and the balance in beta-gamma oscillations across cortical layers. *Front Neural Circuits* 9:6.
- Laaris N, Carlson GC, Keller A (2000) Thalamic-evoked synaptic interactions in barrel cortex revealed by optical imaging. *J Neurosci* 20:1529-1537.
- Larkman A, Mason A (1990) Correlations between morphology and electrophysiology of pyramidal neurons in slices of rat visual cortex. I. Establishment of cell classes. *The Journal of neuroscience* 10:1407-1414.
- Lee MG, Hassani OK, Alonso A, Jones BE (2005) Cholinergic basal forebrain neurons burst with theta during waking and paradoxical sleep. *J Neurosci* 25:4365-4369.
- Lee S, Hjerling-Leffler J, Zaghera E, Fishell G, Rudy B (2010) The Largest Group of Superficial Neocortical GABAergic Interneurons Expresses Ionotropic Serotonin Receptors. *Journal of Neuroscience* 30:16796-16808.

- Lee S, Kruglikov I, Huang ZJ, Fishell G, Rudy B (2013) A disinhibitory circuit mediates motor integration in the somatosensory cortex. *Nat Neurosci* 16:1662-1670.
- Lemkey-Johnston N, Larramendi LMH (1968) Morphological characteristics of mouse stellate and basket cells and their neuroglial envelope: An electron microscopic study. *J Comp Neurol* 134:39-71.
- Levinson AJ, Young LT, Fitzgerald PB, Daskalakis ZJ (2007) Cortical inhibitory dysfunction in bipolar disorder - A study using transcranial magnetic stimulation. *J Clin Psychopharm* 27:493-497.
- Li LY, Ji XY, Liang F, Li YT, Xiao Z, Tao HW, Zhang LI (2014) A feedforward inhibitory circuit mediates lateral refinement of sensory representation in upper layer 2/3 of mouse primary auditory cortex. *J Neurosci* 34:13670-13683.
- Li X, Morita K, Robinson HPC, Small M (2013) Control of layer 5 pyramidal cell spiking by oscillatory inhibition in the distal apical dendrites: a computational modeling study. *J Neurophysiol* 109:2739-2756.
- Liu G (2003) Presynaptic control of quantal size: kinetic mechanisms and implications for synaptic transmission and plasticity. *Curr Opin Neurobiol* 13:324-331.
- Lu SM, Lin RC (1993) Thalamic afferents of the rat barrel cortex: a light- and electron-microscopic study using Phaseolus vulgaris leucoagglutinin as an anterograde tracer. *Somatosens Mot Res* 10:1-16.
- Lubke J, Egger V, Sakmann B, Feldmeyer D (2000) Columnar organization of dendrites and axons of single and synaptically coupled excitatory spiny neurons in layer 4 of the rat barrel cortex. *J Neurosci* 20:5300-5311.
- Luth HJ, Hedlich A, Hilbig H, Winkelmann E, Mayer B (1994) Morphological analyses of NADPH-diaphorase/nitric oxide synthase positive structures in human visual cortex. *J Neurocytol* 23:770-782.
- Ma PM (1991) The barrelettes--architectonic vibrissal representations in the brainstem trigeminal complex of the mouse. I. Normal structural organization. *J Comp Neurol* 309:161-199.

- Ma PM, Woolsey TA (1984) Cytoarchitectonic correlates of the vibrissae in the medullary trigeminal complex of the mouse. *Brain Res* 306:374-379.
- Ma Y, Hu H, Agmon A (2012) Short-term plasticity of unitary inhibitory-to-inhibitory synapses depends on the presynaptic interneuron subtype. *J Neurosci* 32:983-988.
- Ma Y, Hu H, Berrebi AS, Mathers PH, Agmon A (2006) Distinct subtypes of somatostatin-containing neocortical interneurons revealed in transgenic mice. *J Neurosci* 26:5069-5082.
- Macdonald RL, Olsen RW (1994) GABA_A receptor channels. *Annu Rev Neurosci* 17:569-602.
- Marin-Padilla M (1970) Prenatal and early postnatal ontogenesis of the human motor cortex: a golgi study. I. The sequential development of the cortical layers. *Brain Res* 23:167-183.
- Markram H, Toledo-Rodriguez M, Wang Y, Gupta A, Silberberg G, Wu C (2004) Interneurons of the neocortical inhibitory system. *Nat Rev Neurosci* 5:793-807.
- Martinotti C (1889) Contributo allo studio della corteccia cerebrale, ed all'origine centrale dei nervi. *Ann Freniatr Sci Affini* 1:14-381.
- McGarry LM, Packer AM, Fino E, Nikolenko V, Sippy T, Yuste R (2010) Quantitative classification of somatostatin-positive neocortical interneurons identifies three interneuron subtypes. *Front Neural Circuits* 4:12.
- Meyer HS, Egger R, Guest JM, Foerster R, Reissl S, Oberlaender M (2013) Cellular organization of cortical barrel columns is whisker-specific. *Proc Natl Acad Sci U S A* 110:19113-19118.
- Molyneaux BJ, Arlotta P, Menezes JRL, Macklis JD (2007) Neuronal subtype specification in the cerebral cortex. *Nat Rev Neurosci* 8:427-437.
- Mountcastle V, Berman A, Davies P (1955) Topographic organization and modality representation in first somatic area of cat's cerebral cortex by method of single unit analysis. *Am J Physiol* 183:464.
- Mountcastle VB (1957) Modality and Topographic Properties of Single Neurons of Cats Somatic Sensory Cortex. *J Neurophysiol* 20:408-434.

- Mountcastle VB, Davies PW, Berman AL (1957) Response Properties of Neurons of Cats Somatic Sensory Cortex to Peripheral Stimuli. *J Neurophysiol* 20:374-407.
- Nagel G, Szellas T, Huhn W, Kateriya S, Adeishvili N, Berthold P, Ollig D, Hegemann P, Bamberg E (2003) Channelrhodopsin-2, a directly light-gated cation-selective membrane channel. *Proc Natl Acad Sci U S A* 100:13940-13945.
- Nelson S (2002) Cortical microcircuits: diverse or canonical? *Neuron* 36:19-27.
- Okun M, Lampl I (2008) Instantaneous correlation of excitation and inhibition during ongoing and sensory-evoked activities. *Nat Neurosci* 11:535-537.
- Oliva AA, Jr., Jiang M, Lam T, Smith KL, Swann JW (2000) Novel hippocampal interneuronal subtypes identified using transgenic mice that express green fluorescent protein in GABAergic interneurons. *J Neurosci* 20:3354-3368.
- Olsen SR, Bortone DS, Adesnik H, Scanziani M (2012) Gain control by layer six in cortical circuits of vision. *Nature* 483:47-52.
- Pasternak JR, Woolsey TA (1975) The number, size and spatial distribution of neurons in lamina IV of the mouse Sml neocortex. *J Comp Neurol* 160:291-306.
- Pawelzik H, Bannister AP, Deuchars J, Ilia M, Thomson AM (1999) Modulation of bistratified cell IPSPs and basket cell IPSPs by pentobarbitone sodium, diazepam and Zn²⁺: dual recordings in slices of adult rat hippocampus. *Eur J Neurosci* 11:3552-3564.
- Peters A (1990) The axon terminals of vasoactive intestinal polypeptide (VIP)-containing bipolar cells in rat visual cortex. *J Neurocytol* 19:672-685.
- Petersen CC (2007) The functional organization of the barrel cortex. *Neuron* 56:339-355.
- Petersen CC, Sakmann B (2000) The excitatory neuronal network of rat layer 4 barrel cortex. *J Neurosci* 20:7579-7586.
- Petersen CC, Hahn TT, Mehta M, Grinvald A, Sakmann B (2003) Interaction of sensory responses with spontaneous

- depolarization in layer 2/3 barrel cortex. *Proc Natl Acad Sci U S A* 100:13638-13643.
- Pfeffer CK, Xue M, He M, Huang ZJ, Scanziani M (2013) Inhibition of inhibition in visual cortex: the logic of connections between molecularly distinct interneurons. *Nat Neurosci* 16:1068-1076.
- Pi HJ, Hangya B, Kvitsiani D, Sanders JI, Huang ZJ, Kepecs A (2013) Cortical interneurons that specialize in disinhibitory control. *Nature* 503:521-524.
- Porter JT, Johnson CK, Agmon A (2001) Diverse types of interneurons generate thalamus-evoked feedforward inhibition in the mouse barrel cortex. *J Neurosci* 21:2699-2710.
- Porter JT, Cauli B, Staiger JF, Lambolez B, Rossier J, Audinat E (1998) Properties of bipolar VIPergic interneurons and their excitation by pyramidal neurons in the rat neocortex. *Eur J Neurosci* 10:3617-3628.
- Porter JT, Cauli B, Tsuzuki K, Lambolez B, Rossier J, Audinat E (1999) Selective excitation of subtypes of neocortical interneurons by nicotinic receptors. *J Neurosci* 19:5228-5235.
- Powell EM, Campbell DB, Stanwood GD, Davis C, Noebels JL, Levitt P (2003) Genetic disruption of cortical interneuron development causes region- and GABA cell type-specific deficits, epilepsy, and behavioral dysfunction. *Journal of Neuroscience* 23:622-631.
- Prigg T, Goldreich D, Carvell GE, Simons DJ (2002) Texture discrimination and unit recordings in the rat whisker/barrel system. *Physiol Behav* 77:671-675.
- Prönneke A, Scheuer B, Wagener RJ, Möck M, Witte M, Staiger JF (2015) Characterizing VIP Neurons in the Barrel Cortex of VIPcre/tdTomato Mice Reveals Layer-Specific Differences. *Cereb Cortex*.
- Rall W (1977) *Handbook of Physiology. The Nervous System. Cellular Biology of Neurons*. Bethesda, MD: Am Physiol Soc:39-97.
- Rall W (2011) Core conductor theory and cable properties of neurons. *Comprehensive physiology*.
- Ren JQ, Aika Y, Heizmann CW, Kosaka T (1992) Quantitative-Analysis of Neurons and Glial-Cells in the Rat Somatosensory Cortex,

with Special Reference to Gabaergic Neurons and Parvalbumin-Containing Neurons. *Exp Brain Res* 92:1-14.

Rice FL, Kinnman E, Aldskogius H, Johansson O, Arvidsson J (1993) The innervation of the mystacial pad of the rat as revealed by PGP 9.5 immunofluorescence. *J Comp Neurol* 337:366-385.

Rogasch NC, Daskalakis ZJ, Fitzgerald PB (2014) Cortical Inhibition, Excitation, and Connectivity in Schizophrenia: A Review of Insights From Transcranial Magnetic Stimulation. *Schizophrenia Bull* 40:685-696.

Roux L, Buzsáki G (2015) Tasks for inhibitory interneurons in intact brain circuits. *Neuropharmacology* 88:10-23.

Rudy B, McBain CJ (2001) Kv3 channels: voltage-gated K⁺ channels designed for high-frequency repetitive firing. *Trends Neurosci* 24:517-526.

Rudy B, Fishell G, Lee S, Hjerling-Leffler J (2011) Three groups of interneurons account for nearly 100% of neocortical GABAergic neurons. *Dev Neurobiol* 71:45-61.

Ruiz-Marcos A, Valverde F (1970) Dynamic architecture of the visual cortex. *Brain Res* 19:25-39.

Schlaggar BL, De Carlos JA, O'Leary DD (1993) Acetylcholinesterase as an early marker of the differentiation of dorsal thalamus in embryonic rats. *Brain Res Dev Brain Res* 75:19-30.

Schubert D, Kotter R, Staiger JF (2007) Mapping functional connectivity in barrel-related columns reveals layer- and cell type-specific microcircuits. *Brain Struct Funct* 212:107-119.

Schubert D, Staiger JF, Cho N, Kotter R, Zilles K, Luhmann HJ (2001) Layer-specific intracolumnar and transcolumar functional connectivity of layer V pyramidal cells in rat barrel cortex. *J Neurosci* 21:3580-3592.

Silberberg G, Markram H (2007) Disynaptic inhibition between neocortical pyramidal cells mediated by Martinotti cells. *Neuron* 53:735-746.

Simons DJ (1978) Response properties of vibrissa units in rat SI somatosensory neocortex. *J Neurophysiol* 41:798-820.

- Simons DJ, Woolsey TA (1979) Functional organization in mouse barrel cortex. *Brain Res* 165:327-332.
- Sohal VS, Zhang F, Yizhar O, Deisseroth K (2009) Parvalbumin neurons and gamma rhythms enhance cortical circuit performance. *Nature* 459:698-702.
- Somogyi P (1977) A specific 'axo-axonal' interneuron in the visual cortex of the rat. *Brain Res* 136:345-350.
- Somogyi P, Kisvarday ZF, Martin KA, Whitteridge D (1983) Synaptic connections of morphologically identified and physiologically characterized large basket cells in the striate cortex of cat. *Neuroscience* 10:261-294.
- Somogyi P, Tamas G, Lujan R, Buhl EH (1998) Salient features of synaptic organisation in the cerebral cortex. *Brain Res Rev* 26:113-135.
- Spratling MW, Johnson MH (2003) Exploring the functional significance of dendritic inhibition in cortical pyramidal cells. *Neurocomputing* 52-4:389-395.
- Spruston N, Jaffe DB, Williams SH, Johnston D (1993) Voltage- and space-clamp errors associated with the measurement of electrotonically remote synaptic events. *J Neurophysiol* 70:781-802.
- Staiger JF, Masannek C, Schleicher A, Zuschratter W (2004a) Calbindin-containing interneurons are a target for VIP-immunoreactive synapses in rat primary somatosensory cortex. *J Comp Neurol* 468:179-189.
- Staiger JF, Möck M, Proenneke A, Witte M (2015) What types of neocortical GABAergic neurons do really exist? *e-Neuroforum* 6:49-56.
- Staiger JF, Flagmeyer I, Schubert D, Zilles K, Kotter R, Luhmann HJ (2004b) Functional diversity of layer IV spiny neurons in rat somatosensory cortex: quantitative morphology of electrophysiologically characterized and biocytin labeled cells. *Cereb Cortex* 14:690-701.
- Swadlow HA (2003) Fast-spike interneurons and feedforward inhibition in awake sensory neocortex. *Cereb Cortex* 13:25-32.

- Szentagothai J (1975) The 'module-concept' in cerebral cortex architecture. *Brain Res* 95:475-496.
- Szentagothai J, Arbib MA (1974) Conceptual models of neural organization. *Neurosci Res Program Bull*.
- Tai C, Abe Y, Westenbroek RE, Scheuer T, Catterall WA (2014) Impaired excitability of somatostatin- and parvalbumin-expressing cortical interneurons in a mouse model of Dravet syndrome. *Proc Natl Acad Sci U S A* 111:E3139-3148.
- Tamas G, Somogyi P, Buhl EH (1998) Differentially interconnected networks of GABAergic interneurons in the visual cortex of the cat. *J Neurosci* 18:4255-4270.
- Taub AH, Katz Y, Lampl I (2013) Cortical balance of excitation and inhibition is regulated by the rate of synaptic activity. *J Neurosci* 33:14359-14368.
- Thomson AM, Bannister AP (2003) Interlaminar connections in the neocortex. *Cereb Cortex* 13:5-14.
- Thomson AM, Jovanovic JN (2010) Mechanisms underlying synapse-specific clustering of GABA(A) receptors. *Eur J Neurosci* 31:2193-2203.
- Thomson AM, West DC, Deuchars J (1995) Properties of single axon excitatory postsynaptic potentials elicited in spiny interneurons by action potentials in pyramidal neurons in slices of rat neocortex. *Neuroscience* 69:727-738.
- Thomson AM, Bannister AP, Hughes DI, Pawelzik H (2000) Differential sensitivity to Zolpidem of IPSPs activated by morphologically identified CA1 interneurons in slices of rat hippocampus. *Eur J Neurosci* 12:425-436.
- Valverde F (1976) Aspects of cortical organization related to the geometry of neurons with intra-cortical axons. *J Neurocytol* 5:509-529.
- Van Der Loos H (1976) Barreloids in mouse somatosensory thalamus. *Neurosci Lett* 2:1-6.
- Vogt BA, Peters A (1981) Form and distribution of neurons in rat cingulate cortex: areas 32, 24, and 29. *J Comp Neurol* 195:603-625.

- Wang Y, Gupta A, Toledo-Rodriguez M, Wu CZ, Markram H (2002) Anatomical, physiological, molecular and circuit properties of nest basket cells in the developing somatosensory cortex. *Cereb Cortex* 12:395-410.
- Wang Y, Toledo-Rodriguez M, Gupta A, Wu C, Silberberg G, Luo J, Markram H (2004) Anatomical, physiological and molecular properties of Martinotti cells in the somatosensory cortex of the juvenile rat. *J Physiol* 561:65-90.
- Wehr M, Zador AM (2003) Balanced inhibition underlies tuning and sharpens spike timing in auditory cortex. *Nature* 426:442-446.
- Welker C (1971) Microelectrode delineation of fine grain somatotopic organization of (Sml) cerebral neocortex in albino rat. *Brain Res* 26:259-275.
- Welker C, Woolsey TA (1974) Structure of layer IV in the somatosensory neocortex of the rat: description and comparison with the mouse. *J Comp Neurol* 158:437-453.
- Wilent WB, Contreras D (2004) Synaptic responses to whisker deflections in rat barrel cortex as a function of cortical layer and stimulus intensity. *J Neurosci* 24:3985-3998.
- Williams SR, Mitchell SJ (2008) Direct measurement of somatic voltage clamp errors in central neurons. *Nat Neurosci* 11:790-798.
- Woodruff AR, Anderson SA, Yuste R (2010) The enigmatic function of chandelier cells. *Front Neurosci* 4:201.
- Woolsey TA, Van der Loos H (1970) The structural organization of layer IV in the somatosensory region (SI) of mouse cerebral cortex. The description of a cortical field composed of discrete cytoarchitectonic units. *Brain Res* 17:205-242.
- Woolsey TA, Welker C, Schwartz RH (1975) Comparative anatomical studies of the SmL face cortex with special reference to the occurrence of "barrels" in layer IV. *J Comp Neurol* 164:79-94.
- Xiang ZX, Huguenard JR, Prince DA (2002) Synaptic inhibition of pyramidal cells evoked by different interneuronal subtypes in layer V of rat visual cortex. *J Neurophysiol* 88:740-750.

- Xu H, Jeong HY, Tremblay R, Rudy B (2013) Neocortical somatostatin-expressing GABAergic interneurons disinhibit the thalamorecipient layer 4. *Neuron* 77:155-167.
- Xu X, Callaway EM (2009) Laminar specificity of functional input to distinct types of inhibitory cortical neurons. *J Neurosci* 29:70-85.
- Xu X, Roby KD, Callaway EM (2006) Mouse cortical inhibitory neuron type that coexpresses somatostatin and calretinin. *J Comp Neurol* 499:144-160.
- y Cajal SR (1891) *Sur la structure de l'écorce cérébrale de quelques mammifères*: Typ. de Joseph van In & Cie.; Aug. Peeters, lib.
- y Cajal SR (1911) *Histologie de systeme nerveux de l'homme et des vertebres tomme II*.
- Zhang YP, Oertner TG (2007) Optical induction of synaptic plasticity using a light-sensitive channel. *Nat Methods* 4:139-141.
- Zhang ZW, Deschenes M (1997) Intracortical axonal projections of lamina VI cells of the primary somatosensory cortex in the rat: A single-cell labeling study. *Journal of Neuroscience* 17:6365-6379.
- Zilles K, Wree A (1995) Cortex: areal and laminar structure. *The rat nervous system* 1:375-415.

10 Curriculum Vitae

Personal Data

Name: Florian Walker
Date of birth: March 22nd 1984
Place of birth: Papenburg
Address: Sültebecksbreite 13, 37075, Göttingen, Germany
E-mail: walker_florian@hotmail.com

Education

since 2013 **PhD-thesis,**
GGNB Graduate school “Sensory and Motor Neuroscience”,
Department of Neuroanatomy,
University medical center Göttingen, Germany
Supervisor: Prof. J. Staiger

2012-2013 **Research assistant,**
Department of Neuroanatomy,
University medical center Göttingen, Germany

2010-2012 **Phd-thesis** (cancelled),
Ludwig-Maximilians-Universität Munich, Germany
Supervisor: Prof. A. Herz

2010 **Diploma Thesis:** „Vergleichende neuroanatomische und elektrophysiologische Untersuchungen an den Mushroom-Sensillen bodenbewohnender Stabschrecken (Insecta: Phasmatodea)“,
Department of Neurobiology,
Georg-August-Universität Göttingen, Germany,
Supervisor: Prof. R. Heinrich,

	Grade: “mit Auszeichnung”
2004-2010	Study of biology, Georg-August-Universität Göttingen, Germany
2003-2004	Civilian service: Krankenhaus Bethanien, Hamburg, Germany
1996-2003	Gymnasium Papenburg, Germany 2003: allgemeine Hochschulreife Grade: 3.3
1994-1996	Orientierungstufe Papenburg, Germany
1990-1994	Grundschule: Kirchschole Papenburg, Germany

Organization & Representation

2015	Organization SFB 889 retreat 2015, Goslar, Germany
2014-2015	Student representative of the GGNB Graduate School “Sensory and Motor Neuroscience”
2014	Organization Barrel conference 2014, Göttingen, Germany

Stipends & Travel Grants

2014	GGNB Travel Grant for FENS meeting 2014, Milano, Italy
2014	GGNB Bridging fund – PhD-stipend
2014	Janelia Farms Travel Grant for Janelia Farms Conference “How to read a map” 2014, Ashburn, USA

Prizes & Invitations

- 2015 **Invitation to the Young Investigator Orals, 11th**
Göttingen Meeting of the German Neuroscience
Society, Göttingen, Germany
- 2014 **Poster prize** for 2nd-best poster at Barrels conference
2014, Göttingen, Germany
- 2014 **Poster prize** for best poster at Janelia Farms
conference “How to read a map”, Ashburn, USA
-

Teaching experiences

- 2015 **Method course “Sensory Systems”,**
MSc/PhD/MD-PhD Program “Neurosciences”,
Georg-August-Universität Göttingen, International
Max Planck Research School
- 2014 **Supervision Laboratory work (6 weeks)** of Mr.
Joris Brehmer
- 2013 **Method course “Sensory Systems”,**
MSc/PhD/MD-PhD Program “Neurosciences”,
Georg-August-Universität Göttingen, International
Max Planck Research School
- 2008-2009 **Tutor & Practical course “Biology for medical
students”**
- 2008 **Practical course “Vertiefungspraktikum
Neurowissenschaften und Verhalten, Kursteil:
Streckrezeptor der Wanderheuschrecke“**
Bachelor study program „Biology“, Georg-August-
Universität Göttingen
-

Conferences & Retreats

- 2015 **SFB 889 retreat**, Dresden, Germany
Oral presentation
- 2015 **11th Göttingen Meeting of the German
Neuroscience Society**, Göttingen, Germany
Oral presentation
- 2014 **SFB 889 retreat**, Goslar, Germany
Oral presentation
- 2014 **FENS meeting 2014**, Milano, Italy
Poster presentation
- 2014 **Barrels meeting 2014**, Göttingen, Germany
Poster presentation
- 2014 **Janelia Farms Spring Conference “How to read a
map” 2014**, Ashburn, USA
Chair, Oral & Poster presentation
- 2013 **NeuroDoWo 2014**, Göttingen, Germany
Poster presentation
- 2013 **10th Göttingen Meeting of the German
Neuroscience Society**, Göttingen, Germany
Poster presentation
- 2011 **9th Göttingen Meeting of the German
Neuroscience Society**, Göttingen, Germany
Poster presentation
- 2010 **103th Meeting of the German Zoological Society**,
Hamburg, Germany
Poster presentation
-

Qualifications & Experience

Whole-cell patch clamp recording incl. focal photolysis of caged compounds and pharmacology

Histochemical & immunohistochemical stainings

Experiences in PCR, Protein purification, Cloning, Genotyping and other molecular techniques

FELASA B certificate on laboratory animal science

Advanced experience in Microsoft office applications (Excell, Word, Powerpoint), Adobe Illustrator, Adobe InDesign, Signal 5.0, SigmaPlot, Origin

Minor experience in Adobe Photoshop, CorelDraw, R, Matlab

Languages

English (fluent)

French (beginner)

Activities & Interests

Member of the Göttingen Underwaterrugby team, Member & Assistant trainer of the Göttingen scuba diving club "USC Seegurke e.V.", Member of the german lifesaving society "DLRG Ortsgruppe Papenburg"

11 Publications related to this thesis

“Temporally distinct inhibitory control of Martinotti cells by PV- and VIP-cells”

Authors: F. Walker, M. Möck, M. Feyerabend, J. Guy, R.J. Wagener, D. Schubert, J.F. Staiger & M. Witte (in review)

12 Acknowledgments

Wissenschaftliche Erkenntnis entsteht selten durch das Werk eines Einzelnen sondern ist fast immer die Leistung einer größeren Gemeinschaft. Daher möchte ich diese Gelegenheit nutzen um mich bei allen zu bedanken, die mir während meines Studiums und meiner Promotion zur Seite standen.

Als erstes gilt mein Dank meinem Betreuer Prof. Jochen Staiger, der es mir ermöglicht hat an diesem Thema zu arbeiten und ohne dessen konstante Unterstützung diese Dissertation nicht möglich gewesen wäre.

Ein besonderer Dank gilt Dr. Mirko Witte. Nicht nur, dass er mir alles in Bezug auf elektrophysiologische Versuche beigebracht hat, er hatte auch immer ein offenes Ohr und war immer zur Stelle um mir bei meinen Problemen weiterzuhelfen. Es hat immer viel Freude bereitet mit ihm über Wissenschaft zu diskutieren als auch über andere Themen des Alltags.

Des Weiteren möchte ich mich bei allen Mitarbeitern des Instituts für Neuroanatomie bedanken, den Postdocs, meinen Mitdoktoranden und insbesondere den technischen Assistenten, ohne deren Einsatz der wissenschaftliche Betrieb nicht funktioniert hätte. Ich habe mit jedem unglaublich gerne zusammen gearbeitet und hatte eine Menge Spaß.

Auch die restlichen Mitglieder meines Promotionskomitees, Prof. Swen Hülsmann und Prof. Tobias Moser, standen mir immer mit Rat und Tat zur Seite und für ihre Anmerkungen und Kommentare bin ich sehr dankbar.

Während meines Studiums habe ich unglaublich viele Freunde gewonnen, die zum Teil wie Familie für mich geworden sind. Es sind zu viele um sie alle bei Namen zu nennen, aber es war eine großartige Zeit und ich werde nie vergessen was ich alles mit Euch erlebt habe.

Besonders erwähnen möchte ich Fenja Schmalkuche, die mit mir in den letzten Jahren alles gemeinsam durchgestanden hat.

Mein größter Dank gilt jedoch meiner Familie, meinen Eltern, meinem Bruder, meinen Großeltern, Tanten, Onkel, Cousins und Cousinen. Insbesondere meine Eltern waren immer für mich da und haben immer an mich geglaubt. Ohne Sie wäre ich nicht das was ich heute bin und dafür bin ich Ihnen unendlich dankbar.